

1979

The crystal and molecular structure of some high coordination rare earth compounds, the magnetic and structural properties of some rare earth-transition metal compounds, and use of radial distribution functions structural analysis

Charles Curtis Fuller
Iowa State University

Follow this and additional works at: <https://lib.dr.iastate.edu/rtd>

 Part of the [Physical Chemistry Commons](#)

Recommended Citation

Fuller, Charles Curtis, "The crystal and molecular structure of some high coordination rare earth compounds, the magnetic and structural properties of some rare earth-transition metal compounds, and use of radial distribution functions structural analysis " (1979). *Retrospective Theses and Dissertations*. 6643.

<https://lib.dr.iastate.edu/rtd/6643>

This Dissertation is brought to you for free and open access by the Iowa State University Capstones, Theses and Dissertations at Iowa State University Digital Repository. It has been accepted for inclusion in Retrospective Theses and Dissertations by an authorized administrator of Iowa State University Digital Repository. For more information, please contact digirep@iastate.edu.

INFORMATION TO USERS

This was produced from a copy of a document sent to us for microfilming. While the most advanced technological means to photograph and reproduce this document have been used, the quality is heavily dependent upon the quality of the material submitted.

The following explanation of techniques is provided to help you understand markings or notations which may appear on this reproduction.

1. The sign or "target" for pages apparently lacking from the document photographed is "Missing Page(s)". If it was possible to obtain the missing page(s) or section, they are spliced into the film along with adjacent pages. This may have necessitated cutting through an image and duplicating adjacent pages to assure you of complete continuity.
2. When an image on the film is obliterated with a round black mark it is an indication that the film inspector noticed either blurred copy because of movement during exposure, or duplicate copy. Unless we meant to delete copyrighted materials that should not have been filmed, you will find a good image of the page in the adjacent frame.
3. When a map, drawing or chart, etc., is part of the material being photographed the photographer has followed a definite method in "sectioning" the material. It is customary to begin filming at the upper left hand corner of a large sheet and to continue from left to right in equal sections with small overlaps. If necessary, sectioning is continued again—beginning below the first row and continuing on until complete.
4. For any illustrations that cannot be reproduced satisfactorily by xerography, photographic prints can be purchased at additional cost and tipped into your xerographic copy. Requests can be made to our Dissertations Customer Services Department.
5. Some pages in any document may have indistinct print. In all cases we have filmed the best available copy.

University
Microfilms
International

300 N. ZEEB ROAD, ANN ARBOR, MI 48106
18 BEDFORD ROW, LONDON WC1R 4EJ, ENGLAND

7924241

FULLER, CHARLES CURTIS

THE CRYSTAL AND MOLECULAR STRUCTURE OF SOME
HIGH COORDINATION RARE EARTH COMPOUNDS, THE
MAGNETIC AND STRUCTURAL PROPERTIES OF SOME
RARE-EARTH - TRANSITION METAL COMPOUNDS, AND
USE OF RADIAL DISTRIBUTION FUNCTIONS IN
STRUCTURAL ANALYSIS.

IOWA STATE UNIVERSITY, PH.D., 1979

University
Microfilms
International 300 N. ZEEB ROAD, ANN ARBOR, MI 48106

The crystal and molecular structure of some high coordination
rare earth compounds, the magnetic and structural
properties of some rare earth-transition metal
compounds, and use of radial distribution
functions in structural analysis

by

Charles Curtis Fuller

A Dissertation Submitted to the
Graduate Faculty in Partial Fulfillment of
The Requirements for the Degree of
DOCTOR OF PHILOSOPHY

Department: Chemistry
Major: Physical Chemistry

Approved:

Members of the Committee:

Signature was redacted for privacy.

Signature was redacted for privacy.

In Charge of Major Work

Signature was redacted for privacy.

For the Major Department

Signature was redacted for privacy.

For the Graduate College

Iowa State University
Ames, Iowa

1979

TABLE OF CONTENTS

	Page
CHAPTER I. THE CRYSTAL AND MOLECULAR STRUCTURE OF THE DECACOORDINATE COMPOUND HYDROXYETHYLENE- DIAMINETRIACETODIAQUOLANTHANUM(III) TRIHYDRATE	1
Introduction	1
Experimental Section	3
Crystal Data	3
Collection and Reduction of X-ray Intensity Data	3
Refinement of Structure	4
Description and Discussion	5
CHAPTER II. THE CRYSTAL AND MOLECULAR STRUCTURE OF THE DECACOORDINATE COMPOUND TRIS(NITRATO)- TETRAAQUOPRASEODYMIUM(III) DIHYDRATE, $\text{Pr}(\text{NO}_3)_3(\text{H}_2\text{O})_4 \cdot 2\text{H}_2\text{O}$	23
Introduction	23
Experimental Section	24
Crystal Data	24
Intensity Data, Structure Determination and Refinement	24
Description and Discussion	26
CHAPTER III. A DISCUSSION OF DECACOORDINATION	33
CHAPTER IV. THE STRUCTURAL AND MAGNETIC PROPERTIES OF SOME RARE EARTH INTERMETALLIC COMPOUNDS OF STOICHIOMETRY RM_4Al_8	45
Introduction	45
Description	51
Compounds of Stoichiometry RM_4Al_8	66
Introduction	66

	Page
Sample Preparation	68
Discussion	74
X-ray Diffraction	74
Magnetic Susceptibility	86
Theoretical	86
Experimental	89
Results	91
Neutron Diffraction Data	102
Conclusion and Future Work	113
CHAPTER V. USE OF RADIAL DISTRIBUTION FUNCTIONS IN STRUCTURAL ANALYSIS	115
Introduction	115
Theoretical	115
Experimental	126
Sample Preparation	126
Diffraction Experiments	127
Analysis of Diffraction Data	128
Analysis of Results	151
RDF-Patterson Superposition Studies	153
Conclusions	155
BIBLIOGRAPHY	158
ACKNOWLEDGEMENTS	164
APPENDIX. THE CRYSTAL AND MOLECULAR STRUCTURE OF THE COMPOUND BIS(O-TRICYANOETHLENEOATE)BIS (2',2',N,N'BISPYRIDYLAMINE) COPPER(II)	166

	Page
Abstract	166
Introduction	166
Experimental Section	167
Crystal Data	167
Collection and Reduction of X-ray Intensity Data	168
Solution and Refinement of Structure	169
Description and Discussion	170

CHAPTER I.

THE CRYSTAL AND MOLECULAR STRUCTURE OF THE DECACOORDINATE COMPOUND
HYDROXYETHYLETHYLENEDIAMINETRIACETODIAQUOLANTHANUM(III)
TRIHYDRATE

Introduction

The physical properties of the rare earths are inescapably tied to the electronic structure of those elements. Due to the well-shielded valence electrons of that series which exist concurrently with an effectively constant external electronic structure, a unique collection of chemical, metallurgical, and magnetic properties is found for the rare earths. Of particular interest here are the chemical properties of the rare earths, including especially their structural properties, which include high coordination number and the types of ligands with which they form stable compounds. Chapter III of this thesis will directly address the high coordination of rare earths, in particular, decacoordination, whereas Chapters I and II will discuss the crystal and molecular structures of two rare earths chelate species. As mentioned by Moeller et al., appreciably stable complex species, other than the hydrated cations themselves, are obtained only when the most strongly chelating ligands are used, and, in particular, when these ligands contain highly electronegative donor atoms (e.g., oxygen).¹ Such is the case for the ligands discussed in both Chapters I and II.

In their review article, Moeller et al. have shown that the thermodynamic properties which are used to describe the separation of rare earths (i.e., separation constants, ΔH , ΔS) can be related to structure.¹ Powell and Burkholder have demonstrated that the Gd-Eu and Eu-Sm separation factors in cation-exchange elution with ammonium ethylenediaminetetraacetate (EDTA) can be augmented by increasing the temperature from 25° to 92°, and have shown that similar enhancements should occur in the cases of Ho-Dy and Dy-Tb pairs when hydroxyethylethylenediaminetriacetate (HEDTA) is the eluant.² The stabilities of the four heaviest HEDTA chelate species (Tm-Lu) are not affected by this increase in temperature, whereas the stabilities of the remaining lanthanide HEDTA species vary significantly with temperature. This difference may be explained by the assumption that the HEDTA ligand always forms pentadentate bonds to the four smaller lanthanides (Lu^{3+} through Er^{3+}) and hexadentate bonds to those lanthanides larger than Eu^{3+} at temperatures approaching 0°, with the remaining coordination sites being occupied by water molecules.

A program of solution of the crystal and molecular structures of selected members of the series of lanthanide HEDTA compounds has been undertaken in this laboratory in order to provide further information on the coordination of the HEDTA ligand to the lanthanides. In particular, the decacoordinate geometries arising in the case of the lanthanides (lanthanum, cerium, and praseodymium) have been

discussed.^{3,4,5} In this chapter, the crystal and molecular structure of LaHEDTA will be considered.

Experimental Section

Crystal Data

Well-formed white rhombohedral crystals of LaHEDTA were supplied by J. E. Powell of this laboratory and were used without further purification. A crystal of approximate dimensions 0.4 x 0.4 x 0.2 mm was mounted on a glass fiber. Preliminary precession photographs indicated that the compound crystallized in the triclinic crystal system. Final unit cell parameters, obtained from a least squares fit of $\pm 2\theta$ values for fourteen independent reflections (Mo K α radiation, $\lambda = 0.70954 \text{ \AA}$) at 30° , yielded $a = 9.476(2)$, $b = 10.947(3)$, $c = 9.391(2) \text{ \AA}$, $\alpha = 108.18(2)$, $\beta = 104.66(3)$, $\gamma = 79.31(3)^\circ$. A calculated density of $1.90 \text{ g}\cdot\text{cm}^{-3}$ for two molecules per unit cell ($P\bar{1}$, space group) is in excellent agreement with the observed density of $1.88 \pm 0.02 \text{ g}\cdot\text{cm}^{-3}$, determined by the flotation method.

Collection and Reduction of X-ray Intensity Data

Data were collected at room temperature using a technique and apparatus described by Rohrbaugh and Jacobson.⁶ Within a 2θ sphere of 40° ($\sin\theta/\lambda = 0.481 \text{ \AA}^{-1}$) all data in the hkl , $hk\bar{l}$, $h\bar{k}l$, and $h\bar{k}\bar{l}$ octants were measured. The intensity data were corrected for absorption and Lorentz-polarization effects. The minimum and maximum

transmission factors were 0.38 and 0.62, respectively ($\mu = 25.1 \text{ cm}^{-1}$). The estimated error in each intensity was calculated by

$$\sigma_I^2 = C_T + C_B + (0.03C_T)^2 + (0.03C_B)^2 + (0.03C_N/A)^2$$

Where C_T , C_B , C_N and A are the total count, background count, net count and absorption factor, respectively, and the factor 0.03 represents an estimate of nonstatistical errors. The estimated deviations in the structure factors were calculated by the finite difference method.⁷ Of the 1815 independent reflections, 1637 were considered observed ($> 2\sigma_{F_o}$).

Refinement of Structure

The position of lanthanum atom was obtained from the analysis of a three dimensional Patterson function. The remaining nonhydrogen atoms were found by successive structure factor⁸ and electron density map calculations.⁹ The hydrogen positions in the HEDTA ligands were calculated except for those in the associated water molecules. In addition to the positional parameters, the anisotropic thermal parameters for all nonhydrogen atoms were refined by a full matrix least squares procedure, minimizing the function $\sum \omega (|F_o| - |F_c|)^2$, where $\omega = 1/\sigma_F^2$, to a final conventional residual $R = \sum ||F_o| - |F_c|| / \sum |F_o| = 6.4\%$, and a corresponding weighted residual of 6.7%. The scattering factors for the nonhydrogen atoms were those of Hanson et al.,¹⁰ modified for the real and imaginary parts of anomalous dispersion.¹¹ For hydrogen the scattering factors of Stewart et al. were used.¹²

The final positional parameters are listed in Table I.1.a; the anisotropic temperature factors are listed in Table I.1.b. A listing of structure factor amplitudes is given in the supplemental material of Fuller et al.³ The standard deviations were calculated using the local program DAPT, a distances, angles, inter-planar angles, and torsional angles program written by Fusao Takusagawa.¹³ Bond lengths and bond angles are listed in Tables I.2.a and I.3.a, respectively.

Description and Discussion

Original characterization of this lanthanum complex indicated an approximate formula $\text{La}(\text{HEDTA}) \cdot 4\frac{1}{2}\text{H}_2\text{O}$. However, refinement of the crystal structure showed that this compound crystallizes as a centrosymmetric dimer, with five water molecules associated with each lanthanum moiety. The lanthanum ions of hydroxyethylethylenediaminetriacetodiaquolanthanum(III) trihydrate are ten coordinate, as seen in Figure I.1.¹⁴ Eight of the coordination sites are satisfied by the HEDTA ligand. Of these eight sites, five are solely from one group (N1, N2, O3, O5, and the hydroxyethyl oxygen O1), two by a sharing of a carboxymethyl oxygen between the two lanthanum atoms (O6), and one carboxymethyl oxygen from the HEDTA ligand primarily coordinated to the other lanthanum atom (O7). The remaining two sites are filled by water molecules (Ow1 and Ow2). Three water molecules of hydration (Ow3, Ow4, and Ow5) are associated with each moiety. A unit cell diagram is shown in Figure I.2.

Table I.1.a. Final positional^a parameters for LaHEDTA^b

Atom	X	Y	Z
La	5684(1)	2958(0)	3854(1)
O1	6340(9)	1560(7)	1338(10)
O2	9059(9)	4694(9)	2471(11)
O3	7149(9)	4357(7)	3201(9)
O4	7097(8)	-750(8)	5426(9)
O5	6220(8)	738(7)	4189(9)
O6	5956(8)	5988(7)	8442(9)
O7	6186(8)	4939(6)	6112(9)
Ow1	3466(8)	1705(7)	2362(9)
Ow2	4026(8)	3072(7)	5710(8)
Ow3	4487(10)	1237(8)	8613(9)
Ow4	2333(10)	3338(8)	8714(9)
Ow5	9083(10)	7279(12)	9334(12)
N1	8681(9)	2130(8)	3926(10)
N2	8321(10)	2689(9)	6731(10)
C1	9399(13)	1779(12)	5362(13)
C2	8890(12)	2727(12)	6739(13)
C3	8742(15)	944(12)	2596(15)
C4	7811(14)	1144(14)	1118(16)
C5	9434(13)	3145(13)	3814(17)
C6	8470(13)	4122(11)	3067(17)
C7	7144(14)	1442(10)	6911(13)
C8	6820(11)	400(10)	5391(13)
C9	6865(14)	3768(10)	7990(12)
C10	6320(11)	4979(11)	7500(14)

^aThe positional parameters are presented in fractional coordinates ($\times 10^4$ for the nonhydrogen atoms, $\times 10^3$ for the hydrogen atoms).

^bIn this and succeeding tables, estimated standard deviations are given in parentheses for the least significant figures.

Table I.1.a. Continued

Atom	X	Y	Z
H1	1051(19)	166(13)	546(14)
H2	907(15)	94(16)	515(14)
H3	897(16)	362(16)	666(15)
H4	952(16)	251(13)	769(16)
H5	974(19)	68(13)	244(14)
H6	820(15)	19(14)	281(14)
H7	808(14)	194(15)	89(14)
H8	801(15)	36(16)	26(17)
H9	568(17)	120(13)	23(19)
H10	973(15)	371(14)	494(17)
H11	1014(17)	258(14)	309(15)
H12	637(17)	145(13)	741(15)
H13	798(18)	115(14)	758(16)
H14	765(17)	385(13)	886(17)
H15	606(17)	331(14)	819(14)

Table I.1.b. Thermal parameters for LaHEDTA ^a

Atom	β_{11}	β_{22}	β_{33}	β_{12}	β_{13}	β_{23}
La	41(1)	20(1)	106(2)	5(1)	21(1)	14(1)
O1	92(12)	75(9)	117(12)	14(8)	42(9)	5(8)
O2	104(12)	116(10)	257(17)	-10(9)	57(11)	110(12)
O3	84(13)	57(8)	193(14)	9(7)	48(9)	48(8)
O4	96(11)	54(10)	180(13)	-4(8)	35(9)	47(8)
O5	80(10)	38(7)	135(12)	-2(7)	20(9)	22(8)
O6	105(11)	36(9)	142(12)	10(7)	22(9)	15(9)
O7	85(10)	42(7)	112(13)	5(6)	21(8)	19(7)
Ow1	96(11)	74(8)	162(12)	-23(8)	1(9)	36(8)
Ow2	89(10)	59(8)	153(11)	-6(7)	61(8)	20(7)
Ow3	152(13)	69(8)	144(12)	11(8)	25(10)	-5(8)
Ow4	137(13)	76(9)	167(13)	-5(8)	28(10)	25(9)
Ow5	95(13)	193(15)	240(17)	-18(11)	18(12)	103(13)
N1	47(10)	38(9)	149(15)	0(7)	29(10)	23(9)
N2	84(13)	26(9)	139(14)	-3(8)	30(10)	19(9)
C1	53(17)	49(13)	153(20)	7(11)	18(13)	33(12)
C2	37(15)	64(13)	133(19)	3(11)	4(13)	44(13)
C3	73(17)	81(15)	176(22)	15(12)	52(16)	16(14)
C4	97(19)	73(14)	162(22)	17(13)	60(16)	17(15)
C5	77(15)	97(15)	174(23)	-8(13)	35(16)	60(16)
C6	70(19)	59(12)	145(18)	-1(12)	24(14)	34(12)
C7	73(15)	45(12)	122(17)	3(10)	26(15)	24(12)
C8	49(14)	27(13)	161(21)	8(9)	31(13)	37(12)
C9	101(16)	28(11)	81(16)	2(11)	-1(14)	1(11)
C10	55(14)	34(13)	124(21)	3(10)	2(12)	17(13)

^aThe β_{ij} are reported as fractional coordinates ($\times 10^6$), and are defined as follows:

$$T = \exp\{-h^2\beta_{11} + k^2\beta_{22} + l^2\beta_{33} + 2hk\beta_{12} + 2hl\beta_{13} + 2kl\beta_{23}\}.$$

Isotropic temperature factors of $\beta = 2.0$ were assigned to all hydrogen atoms.

Table I.2.a. Selected bonding distances (\AA) for LaHEDTA

La-N1	2.750(8)	C1-C2	1.508(16)
-N2	2.819(9)	C3-C4	1.500(19)
	av 2.785 \pm 0.035	C5-C6	1.501(19)
La-O1	2.534(8)	C7-C8	1.525(14)
-O3	2.520(10)	C9-C10	1.497(17)
-O5	2.490(8)		av 1.506 \pm 0.010
-O7	2.534(6)	01-C4	1.430(16)
	av 2.520 \pm 0.018	02-C6	1.234(19)
La-O7'	2.629(6)	04-C8	1.246(14)
La-O6'	2.745(8)		av 1.240 \pm 0.006
La-Ow1	2.543(7)	03-C6	1.260(15)
-Ow2	2.563(9)	05-C8	1.262(15)
	av 2.553 \pm 0.010	06-C10	av 1.261 \pm 0.001
N1-C1	1.480(16)		1.235(12)
-C3	1.498(14)	07-C10	1.265(16)
-C5	1.470(19)		
N2-C2	1.493(16)		
-C7	1.471(16)		
-C9	1.476(13)		
	av 1.481 \pm 0.011		

Table I.2.b. Distances describing polyhedral geometry of LaHEDTA

O6'-O7'	2.176(11)	Ow2-O5	3.185(10)
O6'-Ow1	3.027(13)	Ow2-Ow1	2.987(10)
O6'-O1	3.114(10)	Ow2-O7'	3.114(12)
O6'-O3	2.988(10)	O5-N1	3.109(13)
N2-N1	3.065(14)	O5-O1	3.112(14)
N2-O7	2.675(11)	O5-Ow1	2.952(10)
N2-Ow2	3.016(11)	N1-O1	2.839(11)
N2-O5	2.781(10)	N1-O3	2.782(12)
O7-O7'	2.668(10)	Ow1-O1	3.072(13)
O7-O3	2.945(13)	O1-O3	3.142(10)
O7-Ow2	3.031(12)	O3-O7'	3.289(12)
O7-N1	3.883(10)	O7'-Ow1	3.548(10)

Table I.3.a. Bond angles for LaHEDTA ($^{\circ}$)

Bond Angles around the La ³⁺ Cation			
06'-La-07'	47.6(2) ^a	N1-La-07	93.1(2)
N2-La-07	39.5(2) ^a	06'-La-07	102.8(2)
07-La-07'	62.2(2)	N2-La-03	103.2(3)
N1-La-03	62.4(3)	06'-La-Ow2	108.5(2)
N2-La-05	62.7(3) ^a	N2-La-07'	116.5(2)
N1-La-01	63.9(2)	N1-La-06'	119.4(3)
N1-La-N2	65.9(3) ^a	01-La-07'	119.5(3)
N2-La-Ow2	67.5(2) ^a	05-La-07	121.4(2)
03-La-06'	68.6(2) ^a	N2-La-Ow1	122.4(3)
06'-La-Ow1	69.1(2) ^a	N2-La-01	122.6(2)
Ow1-La-Ow2	70.6(2)	N1-La-Ow1	128.6(2)
03-La-07	70.9(3)	N1-La-Ow2	132.0(2)
05-La-Ow1	71.2(2)	03-La-05	133.3(2)
N1-La-05	71.6(3)	03-La-Ow1	133.8(3)
01-La-06	71.9(2) ^a	05-La-06'	134.5(2)
07-La-Ow2	72.5(2)	07-La-Ow1	136.8(4)
07'-La-Ow2	73.3(3)	N1-La-07'	139.8(3)
01-La-Ow1	73.8(3)	01-La-Ow2	141.1(2)
01-La-03	76.4(3)	03-La-Ow2	141.4(2)
01-La-05	76.5(3)	01-La-07	146.3(3)
05-La-Ow2	77.7(3)	05-La-07'	147.7(6)
03-La-07'	79.0(2)	N2-La-06'	162.3(2)
07'-La-Ow1	85.9(2)		
Tetrahedral Angles			
La-N1-C3	105.6(6)	La-N1-C1	110.6(7)
La-N2-C2	106.4(7)	La-N2-C9	110.8(6)
La-N2-C7	110.1(6)	La-N1-C5	111.1(6)
		av	109.1 ± 2.2
C1-N1-C5	108.8(9)	C7-N2-C9	110.4(10)
C1-N1-C3	109.0(9)	C3-N1-C5	111.6(11)
C2-N2-C9	109.2(8)	av	109.8 ± 1.0
C2-N2-C7	109.8(9)		
C10-C9-N2	111.5(10)	C8-C7-N2	113.3(10)
C2-C1-N1	112.2(9)	C6-C5-N1	115.4(10)
C4-C3-N1	113.0(10)	av	113.1 ± 1.2
C1-C2-N2	113.2(9)		
C3-C4-O1	107.7(12)		

^aθ angles as defined by Al-Karaghoulis and Wood³⁴

Table I.3.a. Continued

Trigonal Angles			
C5-C6-O2	117.3(11)	C9-C10-O6	119.6(12)
C7-C8-O4	117.3(10)		av 118.1 \pm 1.1
C5-C6-O3	117.0(13)	C9-C10-O7	119.3(9)
C7-C8-O5	119.0(10)		av 118.4 \pm 1.0
O6-C10-O7	121.0(11)	O2-C6-O3	125.4(11)
O4-C8-O5	123.5(9)		av 123.3 \pm 1.8
Other Angles			
La-O1-C4	124.1(7)	La-O7-C10	125.0(7)
La-O3-C6	127.7(8)		av 126.3 \pm 1.8
La-O5-C8	128.4(6)		
La'-O7-La	117.8(3)	La-O6-C10	91.6(8)
La'-O7-C10	96.8(6)		

Table I.3.b. Angles describing polyhedral geometry

01-06'-0w1	60.0(3)	0w2-05-N1	103.1(3)
0w1-06'-07'	84.3(4)	05-N1-07	76.7(2)
07'-06'-03	77.3(3)	N1-07-0w2	90.1(2)
03-06'-01	61.9(2)	07-0w2-05	89.6(2)
0w2-N2-05	66.5(3)	0w1-01-03	98.5(3)
05-N2-N1	64.0(3)	01-03-07'	87.9(3)
N1-N2-07	84.8(4)	03-07'-0w1	87.0(2)
07-N2-0w2	64.0(3)	07'-0w1-01	84.5(3)
01-N1-03	68.0(3)	06'-01-0w1	58.6(3)
03-N1-07	49.1(2)	0w1-01-05	57.0(3)
07-N1-N2	43.3(2)	05-01-N1	62.8(3)
N2-N1-05	53.5(3)	N1-01-03	55.2(2)
05-N1-01	62.9(3)	03-01-06'	57.1(2)
03-07-07'	71.5(3)	06'-03-01	61.0(2)
07'-07-0w2	65.9(3)	01-03-N1	56.9(2)
0w2-07-N2	63.4(3)	N1-03-07	85.3(4)
N2-07-N1	51.8(3)	07-03-07'	50.3(2)
N1-07-03	45.6(2)	07'-03-06'	40.2(2)
07-0w2-N2	52.5(3)	03-07'-07	58.1(3)
N2-0w2-05	53.2(2)	07-07'-0w2	62.7(3)
05-0w2-0w1	57.0(2)	0w2-07'-0w1	52.8(2)
0w1-0w2-07'	71.1(3)	0w1-07'-06'	58.1(3)
07'-0w2-07	51.4(2)	06'-07'-03	62.4(3)
0w2-05-N2	60.3(2)	07'-0w1-06'	37.6(2)
N2-05-N1	62.4(3)	06'-0w1-01	61.4(3)
N1-05-01	54.3(3)	01-0w1-05	62.2(3)
01-05-0w1	60.8(3)	05-0w1-0w2	64.9(2)
0w1-05-0w2	58.1(2)	0w2-0w1-07'	56.1(2)

Table I.3.c. Ring angle sums (degrees)^a

Complex	a	b	c	d	e
LaHEDTA	514.3	533.6	508.3	533.3	526.1
LaEDTA	518.7	532.5	511.7	527.8	531.0
CeHEDTA	513.0	533.5	512.8	533.6	522.2
PrHEDTA	513.5	537.8	505.8	534.9	526.7

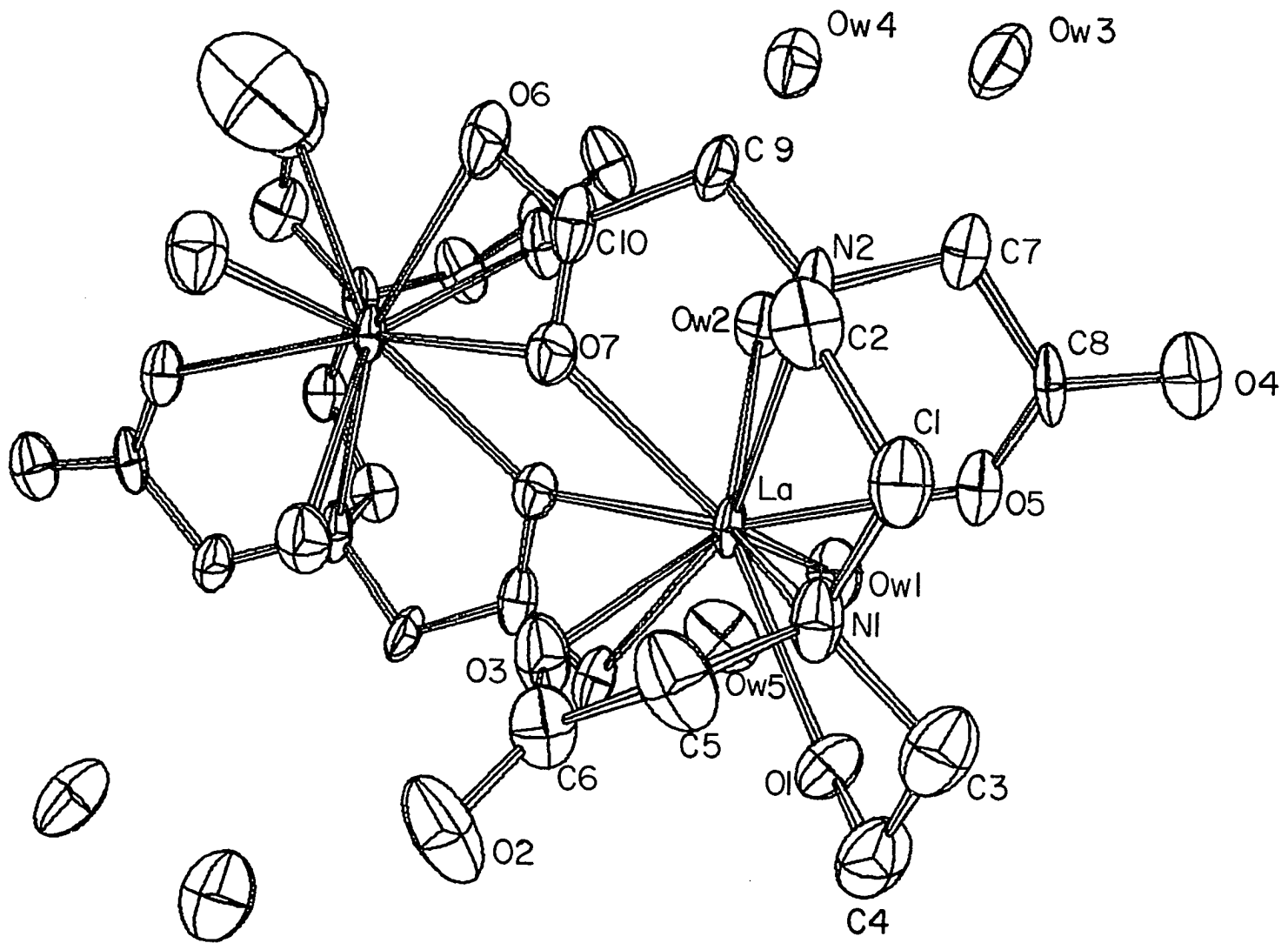
^aRings are defined as follows (lists in parentheses refer to LaEDTA):

a = R-N1-C3-C4-01 (R-N1-C5-C6-02)
 b = R-N1-C5-C6-03 (R-N1-C3-C4-01)
 c = R-N1-C1-C2-N2 (R-N1-C1-C2-N2)
 d = R-N2-C7-C8-05 (R-N2-C7-C8-03)
 e = R-N2-C9-C10-07 (R-N2-C9-C10-04)

Table I.3.d. Ruffling parameters for LaHEDTA

ring members	ϕ_1	ϕ_2	type
La-03-C6-C5-N1	18	12	a λ
La-01-C4-C3-N1	37	-20	e λ
La-N1-C1-C2-N2	30	38	
La-N2-C7-C8-05	21	-4	e λ
La-N2-C9-C10-07	23	-16	a λ

Figure I.1. OR TEP picture of LaHEDTA



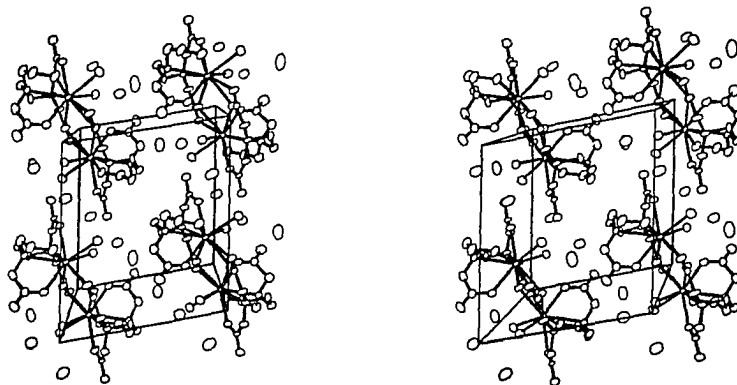


Figure I.2. Unit cell drawing for LaHEDTA

Three of the lanthanum-oxygen (HEDTA) distances are equal (2.53 Å), cf. Table I.2.a, and one (La-05) is slightly shorter (2.490 Å). The bond distances between the lanthanum atom and the bridging oxygen atoms are significantly longer, however, being 2.629 Å and 2.745 Å. These two long distances seem to be dictated by distortion from the ideal geometry imposed by dimerization and by the fact that bridging oxygen atoms frequently have longer associated bonds. The bond angles associated with these bridging atoms are also indicative of this distortion, particularly the angles C10-06-La' (91.6) and C10-07-La' (96.8°), where the prime indicates the atom related by the inversion operation.

The carboxymethyl groups are planar as expected. For the non-bridging groups, the distances C-Oc average 1.261 Å, slightly longer than the C-Ou average distance of 1.240 Å (cf. Table I.2.a), where Oc = a coordinated oxygen atom and Ou = an uncoordinated oxygen atom. The average angles are: C-C-Oc, 118.4; C-C-Ou, 118.1; and Oc-C-Ou, 123.3° (cf. Table I.3.a).

There are many similarities between the structure of LaHEDTA and that of LaEDTA, reported by Lind, Lee, and Hoard,¹⁵ as would be expected, since the HEDTA ligand differs from the EDTA ligand only in that one of the carboxymethyl groups of EDTA has been replaced by a hydroxyethyl group. One of the questions we sought to answer in this investigation was whether the hydroxyethyl group is coordinated in

LaHEDTA, as is the corresponding carboxymethyl group in the EDTA complex. Moeller and Horwitz had suggested that while spectral data could not be used to determine whether this group was coordinated, dehydration studies, the generally poor coordinating properties of this group, and similarities between HEDTA and EDTA materials suggest that it is not.¹⁶ However, our structural result shows that the hydroxy oxygen (O1) is indeed coordinated, being at a distance of 2.534 Å from the lanthanum.

While the EDTA complex does not crystallize as a centrosymmetric dimer, the configuration of the ethylenediamine and glycinate rings, and thus the geometry about the lanthanum atom in the LaEDTA complex, is very similar to that in the LaHEDTA complex. As shown by Lind et al.,¹⁵ ruffling of the five membered rings can be viewed as a consequence of the coordination of the ligand to the lanthanum atom, and the degree of ruffling can be estimated by the sum of those interior bond angles, since this sum always decreases from the maximum value of 540° as the ring increasingly distorts from the planar configuration.

Alternatively, one may use the ruffling parameters ϕ_1 and ϕ_2 as defined by Lee,¹⁷ or the distances of the member atoms of the least squares plane drawn through those member atoms. For LaHEDTA, such information is given in Tables I.3.c, I.3.d, and I.4, respectively. The ring La-N1-C1-C2-N2 would be expected to be particularly distorted due to the small N1-La-N2 angle of 65.9° (65.3°, where the values in parentheses, here and below, refer to LaEDTA), and the two

Table I.4. Equations of least squares planes for LaHEDTA^{a,b}

Atom	Dist. from Plane, Å	Atom	Dist. from Plane, Å
Plane I Fitting O1-O3-O7'-Ow1			
$-0.16848X + 0.48007Y - 0.86089Z = 1.00472$			
O1	0.172	Ow1	-0.152
O3	-0.160	La	-1.144
O7'	0.140	O6'	1.538
Plane II Fitting N1-O7-Ow2-O5			
$0.25170X - 0.39413Y + 0.88391Z = 1.14232$			
N1	-0.065	O5	0.080
O7	0.065	La	-1.147
Ow2	-0.080	N2	1.677
Plane III Fitting La-N1-C5-C6-O3			
$-0.02778X - 0.29529Y - 0.95500Z = 1.53327$			
La	0.030	C6	0.112
N1	0.105	O3	-0.029
C5	-0.159		
Plane IV Fitting La-N1-C3-C4-O1			
$-0.41488X - 0.89104Y + 0.18413Z = 1.24778$			
La	0.057	C4	-0.215
N1	-0.223	O1	0.036
C3	0.344		

^aPlanes are defined as $c_1X + c_2Y + c_3Z = d$, where X, Y, and Z are cartesian coordinates which are related to the triclinic cell coordinates (x,y,z) by the transformations $X = xa \sin\gamma + zc (\cos\beta - \cos\alpha\cos\gamma)\sin\gamma$, $Y = xa \cos\gamma + yb + zc \cos\alpha$, and $Z = zc(1 - \cos^2\alpha - \cos^2\beta - \cos^2\gamma + 2 \cos\alpha \cos\beta \cos\gamma)^{1/2}/\sin\gamma$.

^bThe dihedral angle between plane I and plane II is 6.98°.

Table I.4. Continued

Atom Dist. from Plane, Å		Atom Dist. from Plane, Å	
Plane V Fitting La-N1-C1-C2-N2			
$-0.33674X - 0.92429Y - 0.17967Z = 1.79778$			
La	-0.026	C2	-0.350
N1	-0.092	N2	0.190
C1	0.278		
Plane VI Fitting La-N2-C7-C8-O5			
$0.96308X - 0.09211Y - 0.25295Z = 0.99406$			
La	-0.078	C8	0.056
N2	0.163	O5	0.054
C7	-0.195		
Plane VII Fitting La-N2-C9-C10-O7			
$0.98331X + 0.15927Y - 0.08788Z = 0.44993$			
La	-0.168	C10	-0.104
N2	0.248	O7	0.242
C9	-0.218		

approximately tetrahedral angles at C1 and C2, 112.2 and 113.2° (112.9 and 115.2°), respectively. Inspection of Tables I.3.c and I.4 show this to be the case. The ring La-N1-C3-C4-O1 would also be expected to be quite ruffled, for much the same reasons, and once again inspection of the tables shows this to be the case. The angles N-La-Oc are also small relative to 108°, the angle expected for a regular pentagon, averaging 62.1° (60.0°). Correspondingly, the angles La-Oc-C have opened up to an average of 125.0° (127.0°), although a similar opening has not occurred for the angles La-N-C, which average 109.4° (110.9°).

As will be discussed in Chapter III, Muettterties and Guggenberger have suggested that the dihedral angles of a particular coordination geometry can be a useful description of that geometry.¹⁸ Table I.5 gives the dihedral angles for LaHEDTA.

LaHEDTA is, of course, a decacoordinate complex. The various qualitative and quantitative aspects of ten coordination will be extensively covered in Chapter III of this thesis, using LaHEDTA as one of the prime examples.

Table I.5. Dihedral angles (degrees) for LaHEDTA^a

atom 1	atom 2	dihedral angle, deg	angle type
O6'	O3	53.80 ^b	A1 ^c
O6'	Ow1	58.13	A1
N2	N1	68.42	A1
N2	Ow2	55.73	A1
O6'	O7'	75.24	A2
O6'	O1	52.95	A2
N2	O7	66.73	A2
N2	O5	53.64	A2
O3	O7'	22.42	B1
Ow1	O1	46.66	B1
O7	Ow2	32.01	B1
O5	N1	40.75	B1
O7'	Ow1	18.17	B2
O1	O3	27.58	B2
N1	O7	8.91	B2
Ow2	O5	31.60	B2
O7	O7'	59.35	C1
O5	O1	36.98	C1
O3	O7	52.92	C2
O7'	Ow2	52.56	C2
Ow1	O5	53.90	C2
O1	N1	61.18	C2
Ow2	Ow1	60.15	C3
N1	O3	67.69	C3

^aThere are three general classes of dihedral angles for both the BSAP and BD geometries: (A) between two faces sharing an edge defined by a capping atom and an atom on the "square"; (B) between two faces sharing an edge defined by two atoms, both on the same "square"; and (C) between two faces sharing an edge defined by two atoms, which are on each of the two "squares." The nonplanarity of the "squares" of the BD geometry introduces a subclass to each of these classes.

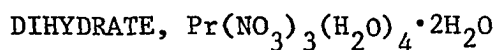
^bThe given atoms define the edge shared by the two adjacent triangle faces for which the dihedral angle is reported.

^cIf the BD geometry is classed (incorrectly) as BSAP, A, B, and C angles of 59.03 ± 8.32 , 26.26 ± 14.50 , and $60.44 \pm 9.25^\circ$, respectively, result.

CHAPTER II.

THE CRYSTAL AND MOLECULAR STRUCTURE OF THE DECACOORDINATE

COMPOUND TRIS(NITRATO)TETRAAQUOPRASEODYMIUM(III)



Introduction

The work reported in the previous chapter grew out of rare earth separation studies of Powell and Burkholder, who described the use of the HEDTA ligand in ion extraction of single rare earths.² In similar fashion, O'Brien and Bautista have also described the thermodynamics of the extraction of rare earths from their aqueous nitrate solutions, via di(2-ethylhexyl) phosphoric acid carried in organic solution.¹⁹ Thus, interest has developed in the crystal and molecular structures of rare earth nitrate crystals derived from aqueous solution.

A crystal and molecular structure determination of tris(nitrato)-tetraaquo-praseodymium(III) dihydrate was initially carried out by Volodina, Rumanova, and Belov in 1961.²⁰ However, that determination was based on data gathered using film techniques and no crystallographic discrepancy factor or thermal parameters were given. Since we desired more accurate distances and angles for comparison with other rare earth complexes, we decided to redetermine this crystal and

molecular structure using a four circle automated diffractometer and counter techniques.²¹

Experimental Section

Crystal Data

Crystal Data. (From single crystal diffractometry, Mo K α , $\lambda = 0.70954 \text{ \AA}$) $a = 9.234(26)$, $b = 11.770(36)$, $c = 6.778(20) \text{ \AA}$, $\alpha = 91.17(8)$, $\beta = 110.72(5)$, $\gamma = 69.48(12)^\circ$, $Z = 2$, space group $P\bar{1}$, $\mu = 17.2 \text{ cm}^{-1}$ (no correction made).

Intensity Data, Structure Determination and Refinement

Data were collected using the technique and apparatus described in the previous chapter, and by Rohrbaugh and Jacobson.⁶ Four octants of data within a 2θ sphere of 45° were taken. Of 1858 measured intensities, 1770 had $F_o > 3\sigma_{F_o}$, and were retained.⁷

The structure was solved independently from the earlier investigation; the heavy atom was first located by analyzing a three dimensional Patterson function and the remaining atoms were found by subsequent structure factor and electron density map calculations. The structure was refined by a full matrix least squares procedure to convergence at $R = 5.2\%$, using anisotropic thermal parameters for all atoms. It was not possible to identify hydrogen positions.

The final positional parameters for this compound are listed in Table II.1, with the anisotropic thermal parameters being listed in

Table II.1. Final positional^a parameters for $\text{Pr}(\text{NO}_3)_3(\text{H}_2\text{O})_4 \cdot 2\text{H}_2\text{O}$

Atom	X	Y	Z
Pr	987(0) ^b	2251(0)	1972(0)
N1	3279(7)	3234(5)	814(10)
N2	-2256(7)	3133(6)	-1765(9)
N3	3326(7)	-18(5)	768(9)
O1	1896(7)	3284(5)	-560(8)
O2	3652(7)	2728(5)	2628(9)
O3	4190(7)	3646(6)	406(11)
O4	-1496(7)	2035(5)	-1018(9)
O5	-1567(8)	3848(5)	-884(9)
O6	-3564(6)	3478(6)	-3280(9)
O7	1940(6)	692(4)	-532(7)
O8	3768(7)	230(5)	2633(8)
O9	4196(7)	-913(5)	229(10)
Ow1	-1040(7)	2795(5)	3720(10)
Ow2	573(6)	4328(4)	3029(8)
Ow3	538(6)	404(4)	2841(8)
Ow4	2698(7)	1761(6)	5814(8)
Ow5	-2792(6)	1387(5)	4079(9)
Ow6	2980(7)	4852(5)	6223(10)

^aThe positional parameters are presented as fractional coordinates ($\times 10^4$).

^bIn this and succeeding tables, estimated standard deviations are given in parentheses for the least significant figures.

Table II.2. Selected interatomic distances are listed in Table II.3, and selected interatomic angles are given in Table II.4, with standard deviations being calculated from the inverse matrix of the final least squares cycle.²² An illustration of this molecule is given in Figure II.1.

Description and Discussion

Tris(nitrato)tetraaquopraseodymium(III) dihydrate crystallizes as a decacoordinate complex, with six of its ten coordination sites taken by the three bidentate nitrate groups; the remaining four sites are taken by waters of hydration, and there are two additional, non-coordinated, water molecules.

The nitrate groups are planar. Defining Oc and Ou as in the previous chapter, it can be noted that the average N-Oc value is 1.255 Å, longer than the average N-Ou value of 1.216 Å (cf. Table II.3). In addition, the angles Oc-N-Oc' average to 116.3°, a smaller value than 121.9°, the value for the angles Oc-N-Ou (Table II.4). This behavior is not unexpected for such a ligand.

Table II.5 gives a listing of dihedral angles about the coordination sphere, in a manner similar to that for LaHEDTA in the previous chapter. As in that case, this table shall be discussed further in Chapter III.

Table II.2. Final thermal parameters^a for $\text{Pr}(\text{NO}_3)_3(\text{H}_2\text{O})_4 \cdot 2\text{H}_2\text{O}$

	β_{11}	β_{22}	β_{33}	β_{12}	β_{13}	β_{23}
Pr	77(1)	48(1)	96(2)	-19(0)	35(1)	-10(0)
N1	112(10)	70(5)	228(19)	-26(6)	82(12)	-7(8)
N2	86(9)	86(6)	144(14)	-22(6)	35(10)	-20(8)
N3	103(9)	61(5)	169(16)	-18(6)	59(10)	-26(7)
O1	160(10)	90(5)	196(14)	-51(5)	62(10)	-3(6)
O2	112(8)	117(6)	226(15)	-35(5)	51(9)	37(8)
O3	152(10)	106(6)	368(19)	-57(6)	121(11)	15(8)
O4	126(8)	70(5)	283(16)	-22(5)	-6(10)	-30(7)
O5	178(10)	73(4)	260(16)	-36(6)	6(11)	19(7)
O6	92(8)	124(6)	213(15)	-11(5)	-0(10)	-12(8)
O7	113(8)	80(4)	129(11)	-12(5)	32(8)	-11(6)
O8	129(8)	113(5)	175(14)	-28(5)	38(9)	-45(7)
O9	141(9)	95(5)	293(17)	-16(6)	85(10)	-44(8)
Ow1	163(10)	73(4)	379(18)	-45(5)	180(11)	-44(7)
Ow2	137(8)	59(4)	240(14)	-37(4)	80(9)	-29(6)
Ow3	137(8)	56(4)	229(14)	-34(4)	47(9)	-1(6)
Ow4	128(8)	122(5)	130(11)	-29(5)	39(8)	5(6)
Ow5	128(8)	85(5)	241(15)	-36(5)	64(9)	4(7)
O26	131(9)	87(5)	327(18)	-37(5)	105(10)	-46(7)

^aThe β_{ij} are reported $\times 10^4$, and are defined as follows:

$$T = \exp\{-h^2\beta_{11} + k^2\beta_{22} + l^2\beta_{33} + 2hk\beta_{12} + 2hl\beta_{13} + 2kl\beta_{23}\}.$$

Table II.3. Selected interatomic distances (\AA) for $\text{Pr}(\text{NO}_3)_3(\text{H}_2\text{O})_4 \cdot 2\text{H}_2\text{O}^a$

Pr-01	2.635(7)	[2.481]	N1-01	1.268(9)	[1.187]
Pr-02	2.598(9)	[2.589]	N1-02	1.254(9)	[1.470]
Pr-04	2.555(8)	[2.625]	N2-04	1.248(9)	[1.282]
Pr-05	2.580(8)	[2.511]	N2-05	1.248(9)	[1.132]
Pr-07	2.617(7)	[2.465]	N3-07	1.263(8)	[1.322]
Pr-08	2.720(9)	[2.616]	N3-08	1.246(9)	[1.171]
Ave.	2.618	[2.548	Ave.	1.255	[1.261]
	$\pm .052$	$\pm .065]$		$\pm .008$	$\pm .114]$
Pr-Ow1	2.452(7)	[2.223]	N1-03	1.215(9)	[1.329]
Pr-Ow2	2.470(8)	[2.484]	N2-06	1.214(9)	[1.335]
Pr-Ow3	2.471(8)	[2.466]	N3-09	1.219(9)	[1.385]
Pr-Ow4	2.474(8)	[2.433]	Ave.	1.216	[1.350]
Ave.	2.467	[2.402		$\pm .002$	$\pm .025]$
	$\pm .009$	$\pm .105]$			

^aIn this and the following table, the numbers given in brackets refer to the work of Volodina, Rumanova, and Belov.²⁰

Table II.4. Selected interatomic angles (degrees) for $\text{Pr}(\text{NO}_3)_3(\text{H}_2\text{O})_4 \cdot 2\text{H}_2\text{O}$

07-Pr-08	47.3(2)	{49.1}	02-Pr-05	110.9(3)	{116.1}
01-Pr-02	48.1(2)	{51.4}	05-Pr-Ow3	114.3(3)	{110.9}
04-Pr-05	48.6(2)	{49.0}	04-Pr-Ow2	115.5(2)	{118.4}
02-Pr-08	66.1(3)	{65.3}	07-Pr-Ow4	117.2(3)	{118.8}
04-Pr-07	68.4(3)	{66.0}	01-Pr-Ow4	119.8(3)	{118.1}
01-Pr-05	69.0(3)	{71.7}	08-Pr-Ow1	131.2(2)	{133.8}
05-Pr-Ow2	69.4(3)	{71.3}	02-Pr-Ow1	132.3(2)	{129.0}
08-Pr-Ow3	69.6(3)	{71.3}	08-Pr-Ow2	132.5(2)	{129.9}
04-Pr-Ow3	69.7(2)	{66.4}	02-Pr-Ow3	132.9(2)	{132.3}
02-Pr-Ow2	70.1(2)	{67.0}	Ow2-Pr-Ow3	139.1(2)	{140.0}
08-Pr-Ow4	70.3(2)	{70.6}	07-Pr-Ow1	139.3(2)	{137.0}
Ow1-Pr-Ow3	70.5(2)	{71.7}	01-Pr-Ow1	139.7(2)	{136.5}
Ow1-Pr-Ow2	70.6(2)	{70.8}	02-Pr-04	141.6(2)	{147.7}
01-Pr-07	70.7(3)	{74.4}	05-Pr-08	144.5(2)	{146.1}
02-Pr-Ow4	71.9(2)	{67.1}	05-Pr-Ow4	144.6(2)	{143.0}
07-Pr-Ow3	74.4(2)	{72.2}	01-Pr-Ow3	145.0(2)	{146.5}
Ow1-Pr-Ow4	75.3(3)	{77.0}	04-Pr-Ow4	145.3(2)	{143.9}
01-Pr-Ow2	75.8(2)	{73.3}	07-Pr-Ow2	146.5(2)	{147.8}
05-Pr-Ow1	78.6(3)	{74.1}			
Ow3-Pr-Ow4	78.8(2)	{80.8}	01-N1-02	115.7(6)	{111.3}
Ow2-Pr-Ow4	79.5(3)	{77.7}	04-N2-05	115.8(6)	{124.2}
04-Pr-Ow1	80.5(3)	{78.7}	07-N3-08	117.3(5)	{115.9}
02-Pr-07	87.1(2)	{92.8}	Ave.	116.3	{117.1}
01-Pr-08	88.2(3)	{88.5}		$\pm .7$	± 5.3
01-Pr-04	94.7(3)	{97.9}			
05-Pr-07	98.2(3)	{98.2}	02-N1-03	121.9(7)	{124.6}
04-Pr-08	110.2(3)	{110.0}	03-N1-01	122.4(6)	{122.5}
			05-N2-06	122.1(6)	{119.8}
			06-N2-04	122.1(7)	{115.1}
			08-N3-09	121.1(6)	{123.3}
			09-N3-07	121.6(6)	{120.7}
			Ave.	121.9	{121.0}
				$\pm .4$	± 3.1

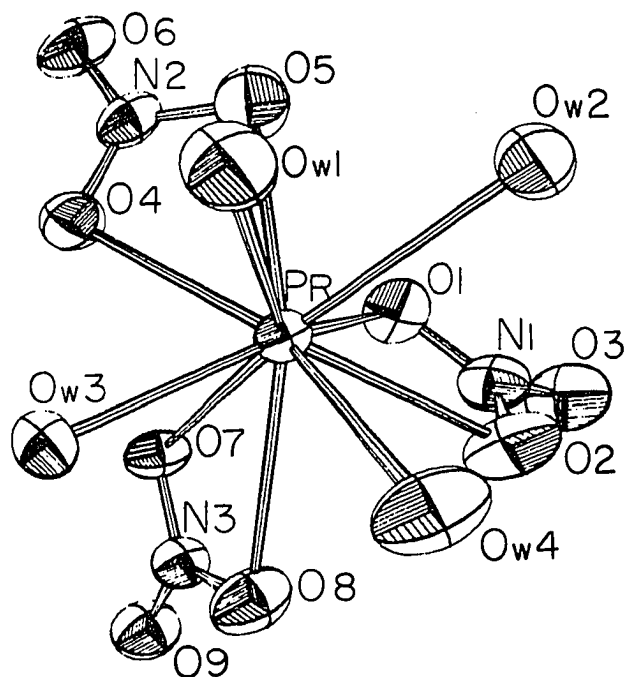


Figure II.1. ORTEP drawing of $\text{Pr}(\text{NO}_3)_3(\text{H}_2\text{O})_4 \cdot 2\text{H}_2\text{O}$

Table II.5. Dihedral angles^a (degrees) for $\text{Pr}(\text{NO}_3)_3(\text{H}_2\text{O})_4 \cdot 2\text{H}_2\text{O}$

Atom 1	Atom 2	Dihedral Angle	Angle Type
08	02	74.44	A1
08	0w4	52.94	A1
05	0w2	53.56	A1
05	04	79.42	A1
08	02	61.41	A2
08	0w3	49.65	A2
05	01	64.26	A2
05	0w1	38.84	A2
04	01	3.66	B1
0w2	0w1	54.92	B1
02	07	2.31	B1
0w4	0w3	39.47	B1
0w3	07	29.72	B2
0w4	02	47.18	B2
0w1	04	34.14	B2
0w2	01	31.81	B2
01	02	72.25	C1
0w1	0w3	56.15	C1
01	07	64.24	C2
0w3	04	53.23	C2
0w4	0w1	52.25	C2
0w2	02	47.78	C2
04	07	63.94	C3
0w4	0w2	41.94	C3

^aAngles defined as in Table I.5.

For the most part, the results of this determination are found to be in substantial agreement with the earlier Russian work. However, as can be seen from Tables II.3 and II.4, the variations in chemically equivalent distances and angles are now much less than observed previously. Most specifically, the egregious numbers in the Russian work (such as N1-02, 1.470 Å) are replaced with more realistic values.

Finally, this compound is found to be virtually isostructural with the decacoordinate compound tris(bicarbonato)tetraaquoholmium(III) dihydrate, reported by Rohrbaugh and Jacobson in 1974.⁶ As mentioned before, decacoordination will be discussed at length in Chapter III.

CHAPTER III.

A DISCUSSION OF DECACOORDINATION

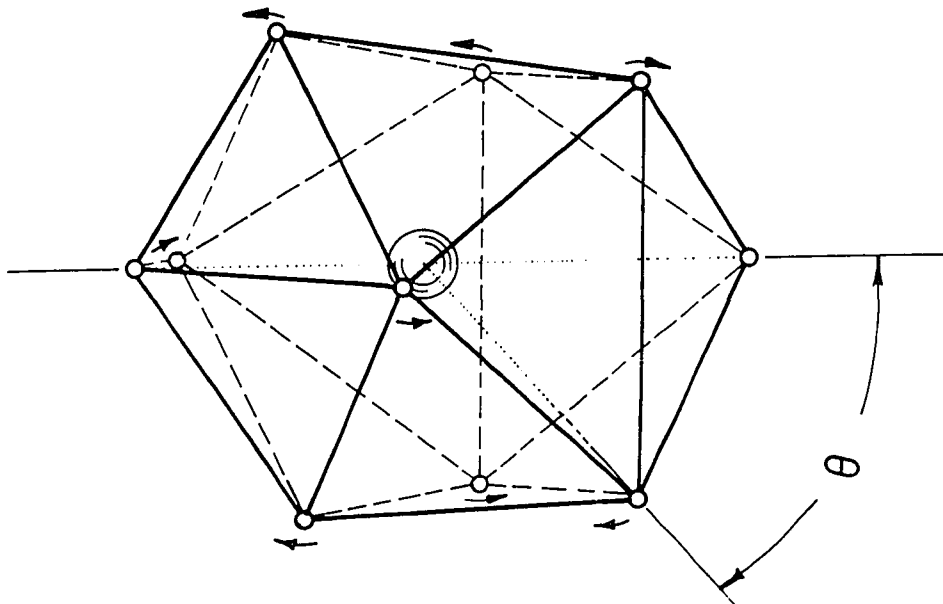
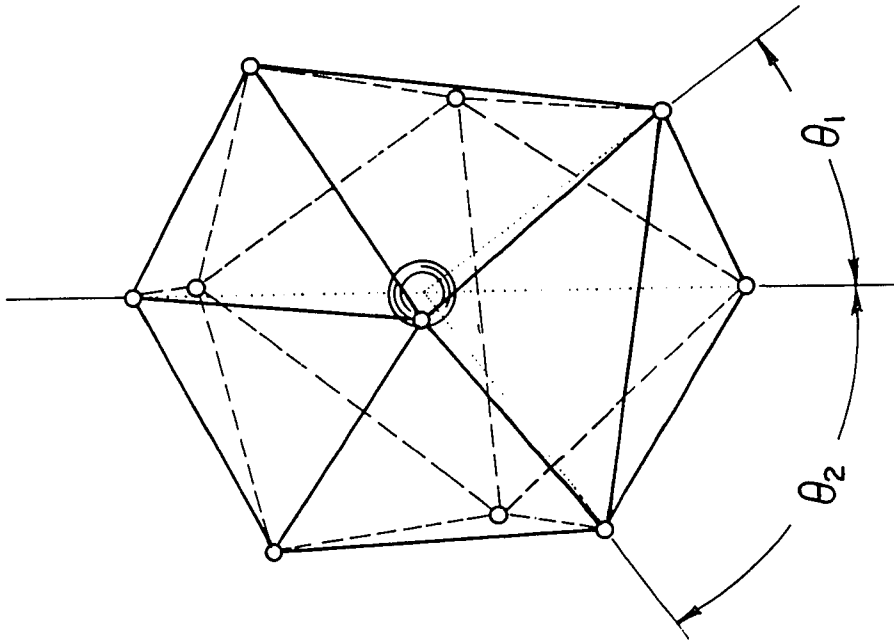
There have been numerous articles recently on rare earth compounds exhibiting large coordination numbers, and considerable controversy has arisen over the preferred geometry in such cases. As mentioned in the review article by S. P. Sinha,²³ the bonds between a lanthanide ion and its ligands can be regarded as being largely electrostatic in nature. He goes on to point out that the structure of lanthanide complexes is something of a compromise between three things: (1), preservation of spherical symmetry about the central atom; (2), minimization of ligand-ligand and metal-metal repulsions; and (3), steric requirements of the ligand.

In this chapter, the geometries of decacoordinate lanthanides will be discussed. It will be seen that the third category mentioned by Sinha (ligand steric requirements) will be of major importance here, for this discussion will feature the structures of lanthanum, cerium, and praseodymium HEDTA,³⁻⁵ lanthanum EDTA,¹⁵ praseodymium nitrate,²¹ and holmium bicarbonate.⁶ It should be pointed out that an attempt is not being made to give an exhaustive treatment of decacoordination, but rather the above mentioned examples have been chosen to demonstrate how ligand characteristics can affect the overall geometry of the complex. Comparison of the HEDTA compounds,

one with another, shows the effects of changing the central rare earth atom without changing the ligand; comparison of the two lanthanum compounds illustrates the effect of a small change in the ligand on the structure; the praseodymium nitrate and holmium bicarbonate compounds are isostructural, but not only have differing cations, but have differing ligands as well. Consideration of this series of compounds furnishes a round of comparison and contrast.

Muetterties and Wright have suggested that two geometries for decacoordination are the bicapped square antiprism (BSAP) and the bicapped dodecahedron (BD).²⁵ Sinha comments that a third geometry is also plausible, a pentagonal bipyramid,²³⁻²⁴ but as this is a 7-coordinate geometry, some question must arise as to what he actually meant. For the purposes of this thesis, only the BSAP and BD geometries will be considered. These two geometries, shown in Figure III.1, are closely related. The ten coordinate BSAP geometry obviously derives from the eight coordinate square antiprism by placing a capping atom above each square face of that latter figure. The BD geometry can also be seen to be a result of capping the two "squares" of the parent eight coordinate dodecahedron, although the BD geometry differs from the BSAP one in that the two "squares" of the parent geometry are not planar and are slightly closer together for the dodecahedral paradigm (see below): a dodecahedron may be seen as resulting from a "bend" in the square faces of a square antiprism, and narrowing of certain of its angles.²⁶

Figure III.1. Idealized decacoordinate geometries: left, the bicapped dodecahedron, showing the θ angle of Al-Karaghoulis and Wood;²⁷ right, the bicapped square antiprism, showing the θ_1 and θ_2 angles defined herein. Arrows on left figure indicate how the BD geometry may be changed to produce the BSAP geometry



Al-Karaghoulis and Wood have described the BSAP and BD geometries by θ angles,²⁷ but unfortunately these angles do not refer to the same thing in both cases. In the case of the BSAP geometry the θ angle is defined as in Figure III.1, and for the ideal figure should be 64.8° . However, for the BD geometry the angles θ_a , θ_b , and θ_c defined by Al-Karaghoulis and Wood do not refer to the angles formed by the capping atom and a member of the "square," and two more angles have to be defined (see Figure III.1), namely θ_1 (60.8°) and θ_2 (74.3°), angles which average 67.6° . Al-Karaghoulis and Wood note that the geometry based on the square antiprism is favored energetically.²⁷ The same conclusion has been reached by R. B. King,²⁸ and also by Lin and Williams for the case of "soft sphere ligands."²⁹

On the experimental side, the literature seems to be somewhat divided. Some ten coordinate compounds whose structures have been accurately determined have been classified as BSAP,^{3-6,20,21,27,30,31} others as BD,³²⁻³⁵ and a good number are either not specified, or else closely conforms to neither of the above idealized geometries.³⁶⁻⁴³ In point of fact, only small distortions are required to convert from one geometry to another. Ideally one would prefer a ten coordinate compound where all the ligands and/or bonding sites are identical, and it is interesting to note that $B_{10}H_{10}^{2-}$, while lacking a central atom, does have the BSAP geometry.⁴⁴ If more than one type of ligand or bonding site is allowed, the distortions introduced can make it even more difficult to refer confidently to one

idealized geometry or the other. With this in mind, a comparison of the two geometries, using the compounds LaHEDTA,³ LaEDTA,¹⁵ CeHEDTA,⁴ PrHEDTA,⁵ $\text{Pr}(\text{NO}_3)_3(\text{H}_2\text{O})_4 \cdot 2\text{H}_2\text{O}$ ²¹ (hereinafter called "PrNitrate"), and $\text{Ho}(\text{HCO}_3)_3(\text{H}_2\text{O})_4 \cdot 2\text{H}_2\text{O}$ ⁶ ("HoBicarb"), will serve to point out some aspects of ten coordination.

As mentioned in Chapter I, the structures of LaEDTA and LaHEDTA are very similar, and the various HEDTA complexes (La, Ce, and Pr) are isostructural, although it should be mentioned that PrHEDTA crystallizes in a monoclinic, rather than triclinic, space group, and that there are only four associated water molecules in that case, as opposed to five for LaHEDTA and CeHEDTA. In similar fashion, PrNitrate and HoBicarb are isostructural, with small bidentate ligands occupying six of the ten coordination sites.

As discussed in Chapter I, characteristic of LaHEDTA and its analogs are five membered rings involving the central atom and the ligand (cf. Tables I.3.c, I.3.d, and I.4). These five membered rings form a more relaxed environment than that formed by the four membered rings of PrNitrate and HoBicarb, defined by the holmium atom and the bicarbonate groups in HoBicarb, and the praseodymium atom and the nitrate groups in PrNitrate, have an average "bite" of 2.15 and 2.13 Å, respectively, as compared to the 2.78 Å N-O bite and 3.06 Å N-N bite of the lanthanum compounds. (2.75 and 2.98 Å for CeHEDTA, 2.76 and 3.06 Å for PrHEDTA). Thus, HoBicarb and PrNitrate

demonstrate a more distorted configuration than the other compounds, and provide further contrast in the discussion of decacoordination.

As can be seen from Table III.1, if one makes the assumption of BSAP geometry, the average θ angles for these various compounds vary from 64.0 to 64.4°; assuming BD geometry gives average θ_1 and θ_2 ranges of 57.9 to 62.4°, and 66.2 to 70.8°, respectively. The averaged θ angles seem to indicate the BSAP geometry is followed in all cases, but the deviations from the BD geometry are not large. However, large departures from ideality in individual angles occur in all six structures. HoBicarb is the most distorted, with individual θ angles of 47.1 and 50.4°, LaEDTA is the least distorted, and the HEDTA compounds are intermediate, with one angle which averages to 47.9°, that angle being the one defined by the only four membered ring of those compounds (as discussed further, below). It thus seems to be difficult to decide on either geometry due to θ arguments, alone.

Another indicator of the molecular geometry is the separation of the least squares planes passing through the "squares" of the two configurations. If χ is defined as (average plane separation) / (average bond length), $\chi = 0.76 \pm 0.08$ for the BD geometry, and 0.85 ± 0.00 for the BSAP geometry. For all compounds, the χ values seem to indicate the BSAP geometry, as can be seen in Table III.2. It must be stressed, however, that there are large statistical errors

Table III.1.a. Key for subsequent tables

For all tables in this chapter, the following letters have been used to describe these compounds:

A	LaHEDTA
B	LaEDTA
C	CeHEDTA
D	PrHEDTA
E	PrNitrate
F	HoBicarb

Table III.1.b. Theta parameters (Degrees)

	θ_1	θ_2	θ
A	60.4+8.7	67.8+1.2	64.1+7.2
B	62.4+3.5	66.2+1.1	64.3+3.2
C	60.4+8.0	67.7+1.7	64.0+6.8
D	59.9+7.4	68.1+0.9	64.0+6.7
E	57.9+12.1	70.8+4.7	64.4+11.2
F	58.9+10.2	69.2+4.8	64.1+9.5

BSAP: $\theta = 64.8$

BD: $\theta_1 = 60.8$

$\theta_2 = 74.3$ (Average of θ_1 and $\theta_2 = 67.5$)

Table III.2. χ (Plane separation parameter)

A	0.88+0.10
B	0.85+0.10
C	0.87+0.22
D	0.87+0.09
E	0.87+0.15
F	0.87+0.09

$\chi = 0.76+0.08$ for BD

$\chi = 0.85+0.00$ for BSAP

involved in these sets of numbers, so once again it is difficult to say conclusively which geometry is obeyed.

A real molecule may be described by the dihedral angles formed between adjacent faces of its coordination polyhedron. An advantage of this description is that it is frequently possible to relate a "nondescript" geometry to a limiting idealized geometry, perhaps emphasizing or denying its status as a combination of two such idealized geometries. Unfortunately, Muetterties and Guggenberger limit themselves to coordination numbers four through eight in their development of this reference technique.¹⁸ It was thus necessary to extend their treatment to include molecules of coordination number ten.

In the case of decacoordination, there are three general classes of dihedral angles for both the BSAP and BD geometries: A) between two faces sharing an edge defined by a capping atom and an atom on the "square"; B) between the two faces sharing an edge defined by two atoms, both on the same "square," and C) between two faces sharing an edge defined by two atoms, one on each of the two "squares." The nonplanarity of the two "squares" of the BD geometry introduces a subclass to each of these classes. Table III.3 shows the dihedral angles, as just defined, for the various compounds discussed herein: Table III.3.a gives the dihedral angles assuming BD geometry; Table III.3.b lists similar data for the BSAP geometry. These tabulations

Table III.3. Dihedral angles (Degrees)^a

(a) Dihedral angles assuming BD geometry

	A1	A2	B1	B2	C1	C2	C3
A	59+6	62+7	35+9	22+9	48+11	55+4	64+4
B	61+4	60+1.5	25+10	30+5	50.2+.6	58+5	59+7
C	60+7	62+9	36+8	20+9	48+12	55+4	65+4
D	60+5	65+9	36+9	20+9	48+13	56+4	64+3
E	65+12	54+10	25+23	36+7	64+8	54+6	53+11
F	66+11	58+8	24+21	33+6	63+6	53+6	54+9
BD	67.34	50.71	40.77	11.7	72.22	61.63	46.28

(b) Dihedral angles assuming BSAP geometry

	A	B	C
A	61+8	29+11	56+8
B	60+3	28+8	56+6
C	61+8	28+12	56+9
D	62+8	28+12	56+9
E	59+12	30+18	56+9
F	61+11	29+16	56+8
BSAP	56.36	30.80	56.19
BD as BSAP	59+8	26+14	60+9

^aThe various classes of dihedral angles are defined in Chapter I.

Table III.4. Capping angles (Degrees)

A	162.3(2)
B	169.5(2)
C	163.6(4)
D	163.8(2)
E	144.5(2)
F	147.7(3)

Capping angles = 180° for both geometries.

tend to indicate the BSAP geometry once again, but with the by now familiar caveat "Look to the Errors."

Finally, for both the BSAP and BD geometries, the angle formed by (capping atom₁) - (central atom) - (capping atom₂) should be 180°. In the highly distorted HoBicarb and PrNitrate compounds, this angle is 147.7 and 144.5°, respectively; in LaEDTA it is 169.5°; and in La, Ce, and Pr HEDTA it is 162.3, 163.6, and 163.8°, respectively (cf. Table III.4). The better value for LaEDTA as opposed to all others can be explained by noting that for LaEDTA the capping atoms are a nitrogen and a water oxygen, whereas in the HEDTA compounds, the capping atoms are a nitrogen and one of the bridging carboxymethyl oxygens. Presumably the capping water in LaEDTA is better able to assume an idealized position than its counterpart in the HEDTA complexes, which are members of the only four membered ring found in those structures, rings with bites that average significantly less than the bites of the five membered rings.

In summary, these various compounds seem best to approximate the BSAP geometry, but they do depart significantly from ideality. However, it does seem that the more relaxed five membered rings of the HEDTA and EDTA compounds allow these molecules to coordinate in a more idealized geometry than the more highly distorted HoBicarb and PrNitrate.

CHAPTER IV.

THE STRUCTURAL AND MAGNETIC PROPERTIES OF SOME RARE EARTH
INTERMETALLIC COMPOUNDS OF STOICHIOMETRY RM_4Al_8

Introduction

Considerable attention has been given to rare earth-transition metal complexes of stoichiometry RM_5 . This so-called Haucke phase is exemplified by $LaNi_5$, with its interesting hydrogen storage capabilities, and by $SmCo_5$. The excellent permanent magnetic properties of this latter compound have sparked interest in other rare earth intermetallics. Thus is the genesis of this chapter of this thesis. An overview of compounds related to the RM_5 phase in general, and of the RM_{12} compounds in particular, will first be given, and work done by the author on RM_4Al_8 compounds, a class strongly analogous to those of stoichiometry RM_{12} , will then be discussed.

It should be noted that for stylistic reasons the words "alloy" and "compound" are used interchangeably in this chapter, although they are not strictly synonymous. In similar fashion, an undifferentiated reference to "metal atoms" should be taken to mean "3d transition metal atoms," even though both aluminum and the rare earths are certainly metallic in nature.

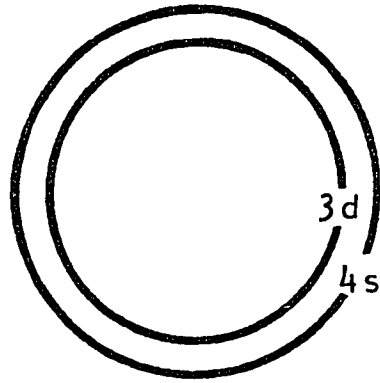
There is a rich variety of magnetic behavior in alloys made from the rare earth elements and the 3d transition metals. This great

range of properties is due in large part to characteristics basic to the two types of atoms. As one goes across the series of third row transition elements, one encounters greatly divergent physical, metallurgical and chemical properties, whereas for the lanthanides, instead of divergence of properties, one finds a series whose similarity, one to another, is unlike that found anywhere else on the periodic chart.

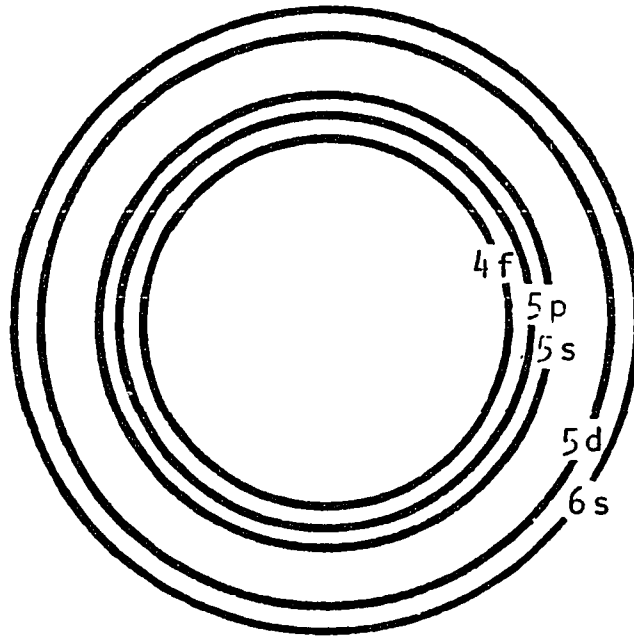
Behavioral differences between these two series exist when magnetism is considered, as well. In the transition metals correlations between the 3d electrons are strong and give rise to important short range magnetic interactions. For the rare earths the magnetic interactions are weaker and occur through the conduction electrons.⁴⁵ However, the rare earths show the largest known magnetic moments, magnetic anisotropies, and magnetoelastic effects. By alloying the rare earths and 3d transition metals, one can get a wide range of magnetic properties. Indeed, aspects of this wide range of magnetic properties are frequently predictable to the extent that it is often possible to produce magnetic materials with predetermined characteristics.⁴⁶

All of this behavior may be explained in large part by a rather straightforward representation of the electronic nature of the two types of elements. If one will allow the "freshman chemistry" approach of using shell models (see Figure IV.1), the important qualitative differences of these two elemental classes can be seen at

Figure IV.1. Shell models showing (simplistic) electronic models of the 3d and 4f elements



3d elements



4f elements

once. In the metallic states of the transition metals (eg., Fe, Co, Ni), the electrons of the external 4s shell form the conduction band, leaving the 3d electrons unshielded. Thus, the chemical properties of the transition metals differ greatly from one element to its neighbors, and the magnetic properties of these elements are not those of atoms with well-shielded electrons. The case of the rare earths is quite different. Here, the 5d and 6s shells form the conduction band, with the 4f electrons well-shielded by the full 5p and 5s shells: the external electronic structures of these atoms remain constant throughout the series (with a few exceptions), and the shell whose filling characterizes the series is well shielded, at once giving great similarity in chemical properties and the possibility of richly varied magnetic behavior.⁴⁷

Phase diagrams for the rare earth-transition metal systems show many stable alloys because of the differences in chemical properties and the atomic sizes of the two components. These various magnetic compounds show a wide range of properties, as mentioned above, but in general one can think of two classes of compounds: those based on the RM_5 stoichiometry, for which the transition metals play the dominant role in determination of magnetic properties; and the rare earth rich compounds based on trigonal prismatic subunits whose arrangements show low symmetry, and whose magnetic properties are determined by the rare earths, at least to a greater extent than in the first class. The second class of compounds are quite important, but as the

emphasis of this thesis lies with the RM_5 based compounds, they will not be discussed at length here. The interested reader is urged to read the papers by Barbara et al.,⁴⁵ and Lemaire.⁴⁸

One of the most widely studied series of magnetic rare earth-intermetallics are those with the RM_5 stoichiometry, itself. Based on the hexagonal $CaCu_5$ Haucke phase,⁴⁹ with $R =$ a lanthanide or Y, and $M =$ Fe, Co, or Ni, these compounds have short M-M distances, sometimes even shorter than in the pure metals. These short distances, further discussed below, give rise to strong positive magnetic interactions, and the transition metals determine the overall magnetic properties. In addition the uniaxial symmetry of the hexagonal unit cell of this phase, along with the magnetocrystalline anisotropy of the 3d transition and 4f rare earth atoms, allows the existence of an easy axis of magnetization (e.g. in $SmCo_5$ the 6-fold axis of the hexagonal unit cell).⁴⁷

With magnetic rare earths, the coupling between the rare earth and transition metal spins is always antiparallel. Its sign depends neither on the surroundings, nor on the interatomic distances, nor on the conduction electron concentration.⁵⁰ In fact as in metallic transition elements,⁵¹⁻⁵³ the strong correlations between 3d electrons impose a negative polarization⁵⁴ of conduction electrons in the whole crystal. This polarization being already established by the 3d electrons, the positive contact interaction of Ruderman-Kittel type between the conduction electrons and those in the 4f shell gives rise

to an antiparallel coupling between the spins of rare earth and Fe, Co, or Ni atoms.

The Curie temperatures of the RCo_5 (and analogous R_2Co_{17}) alloys are the highest of any of the R-M alloys. In these compounds, the magnetic moment of cobalt is close to that of pure cobalt.⁵⁵ Because of the antiparallel coupling between the rare earth and cobalt spins, only the compounds with light rare earths are ferromagnetic, showing a large spontaneous magnetization at room temperature. The permanent magnetic properties of these compounds are due to their strong uniaxial anisotropy.⁵⁶

This group of magnetic compounds, itself rich and important, can readily be expanded to include other analogous compounds that are derived from the RM_5 structure by simple ordered substitutions. A wide variety of such compounds exists (e.g., RM_2 , RM_3 , R_2M_7 , R_2M_{17} , and RM_{12}), but of special interest in this thesis is the phase RM_{12} . This is the most transition metal rich of all of the R-M alloys, and can be produced by simple substitutions of pairs of metal atoms for individual rare earth atoms.

Description

The RM_x series is structurally related to $CaCu_5$. That structure, described by Haucke in 1940,⁴⁹ is in the hexagonal space group $P6/mmm$, and is shown in Figure IV.2.

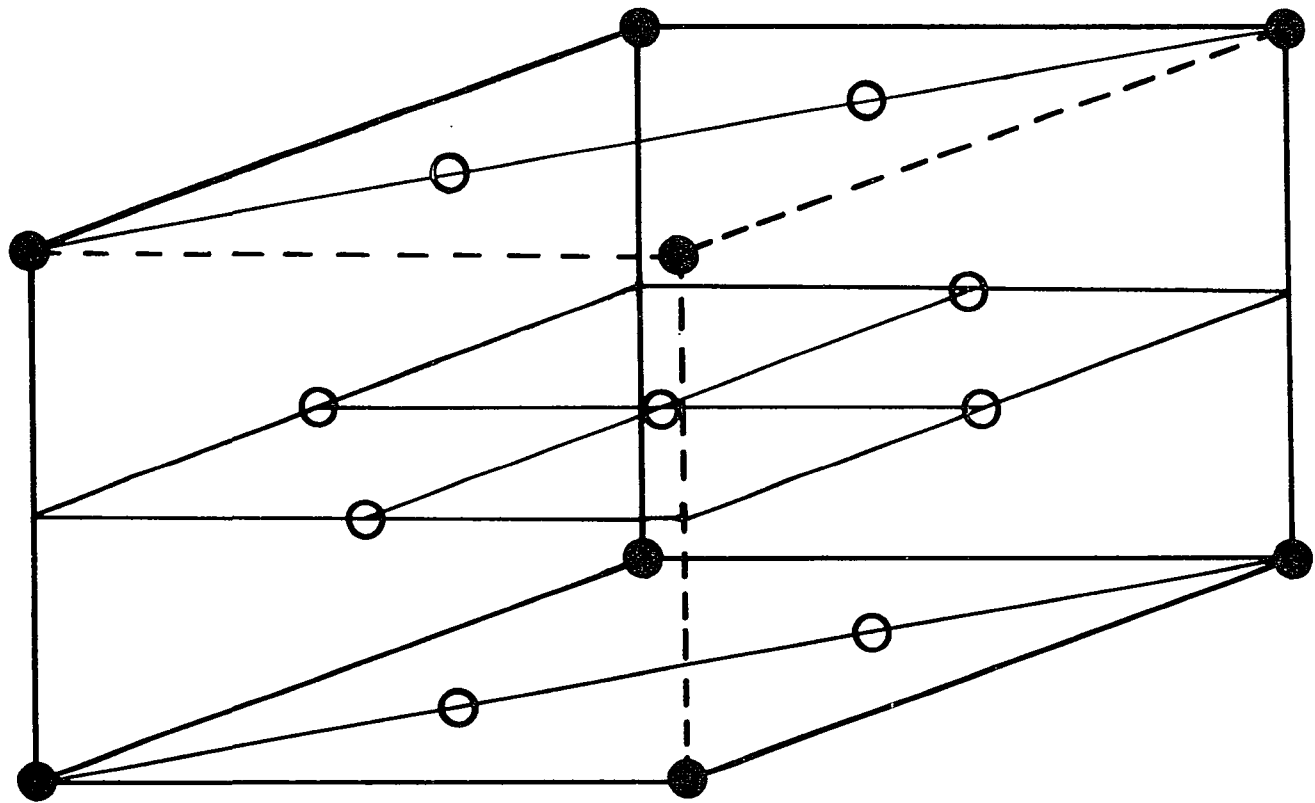


Figure IV.2. CaCu_5 structure

Description of the analogous RM_5 phases is a simple matter: substitute a rare earth atom ($R = Y$, or the lanthanides) for a calcium in site 1a, two transition metal atoms ($M = M_I = Ni, Co, Fe, \dots$) for copper in sites 2c, and three more metal atoms ($M = M_{II}$) for copper in sites 3g. (cf. Table IV.1).⁵⁷

One of the remarkable things about the RM_5 phase is that the metal-metal distances can be quite short. This is demonstrated in Table IV.2, using $GdCo_5$ as an example. Remembering that the shortest interatomic distance in metallic cobalt is 2.49 \AA , it is remarkable that Co-Co distances of 2.451 and 2.485 \AA exist in $GdCo_5$.

As mentioned above, many stable R-M phases exist. Of these, the one richest in transition metal is the RM_{12} phase; this phase may be easily derived from the RM_5 Haucke phase by simple, ordered, substitutions. As seen in Figure IV.3, the RM_{12} phase (described as $ThMn_{12}$ by Florio, Rundle, and Snow in 1952)⁵⁸ may be produced by substituting "dumbbells" (pairs) of M atoms for alternating rare earth atoms. One can also represent the transformation from the RM_5 to the RM_{12} phase algebraically: $2RM_5 - R + 2M = RM_{12}$.

The RM_{12} phase belongs to the tetragonal space group $I4/mmm$. The relationship between unit cells of the hexagonal RM_5 structure and the tetragonal RM_{12} structure may be seen in Figure IV.4; the atomic positions for RM_{12} are given in Table IV.3.

Table IV.1. Atomic positions in the CaCu_5 structure

Atoms	Site	Positions
Ca (R)	1a	(0,0,0)
2Cu_I (Ni, Co, ...)	2c	(1/3, 2/3, 0), (2/3, 1/3, 0)
3Cu_{II} (Ni, Co, ...)	3g	(1/2, 0, 1/2), (0, 1/2, 1/2), (1/2, 1/2, 1/2)

Table IV.2. Shortest interatomic distances in the RM_5 structure

Shortest Distances Between Atoms ^a	Values for GdCo_5 (Å)	Number of Occurrences Per Unit Cell
R-R = c	3.973	1
$\text{R-M}_I = a/\sqrt{3}$	2.873	6
$\text{R-M}_{II} = \sqrt{a^2 + c^2}/2$	3.184	10
$\text{M}_I\text{-M}_I = a/\sqrt{3}$	2.873	1
$\text{M}_I\text{-M}_{II} = \sqrt{a^2/3 + c^2}/2$	2.451	12
$\text{M}_{II}\text{-M}_{II} = a/2$	2.485	4

^aThe shortest interatomic distance in metallic cobalt is 2.49 Å.⁵⁷

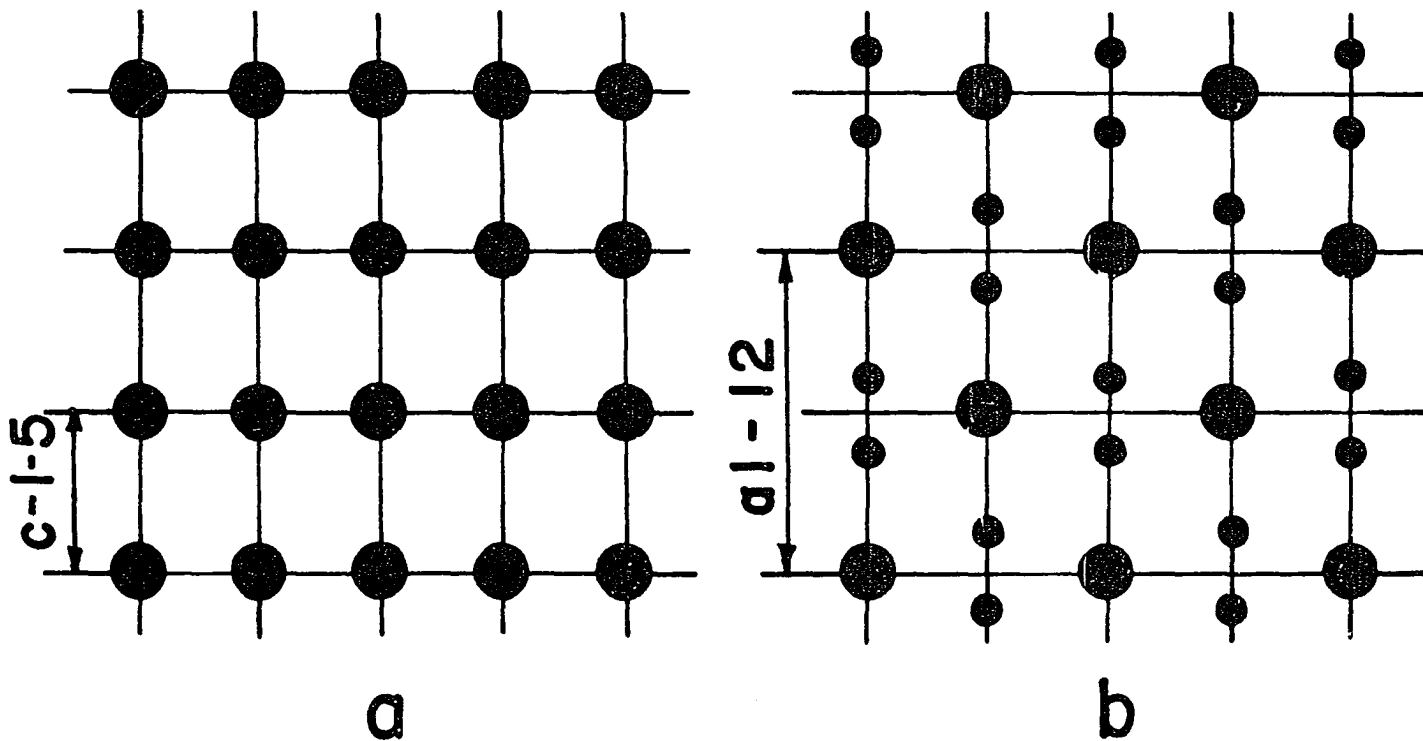
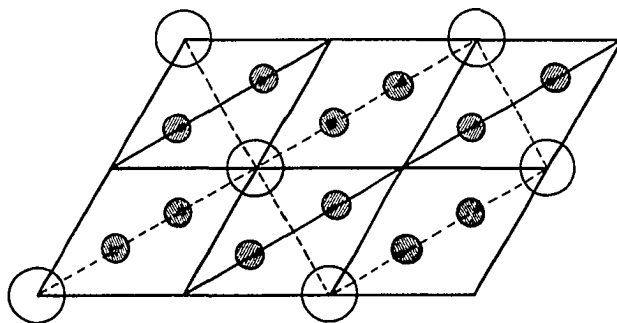
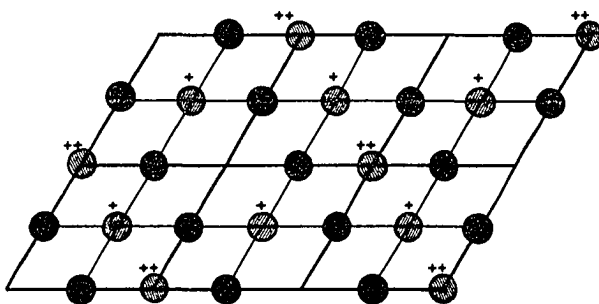


Figure IV.3. Figure showing how RM_{12} phase may be produced by substituting "dumbbells" of transition metals for individual rare earths

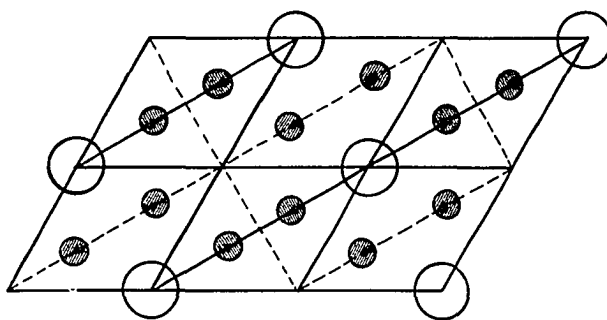
Figure IV.4. Relationship between unit cells of the hexagonal RM_5 structure and the tetragonal RM_{12} structure







$Z_{RM5} = 0$
 $Y_{RM12} = 0$



$1/2 \leq Z_{RM5} < 1$
 $1/4 \leq Y_{RM12} < 1/2$



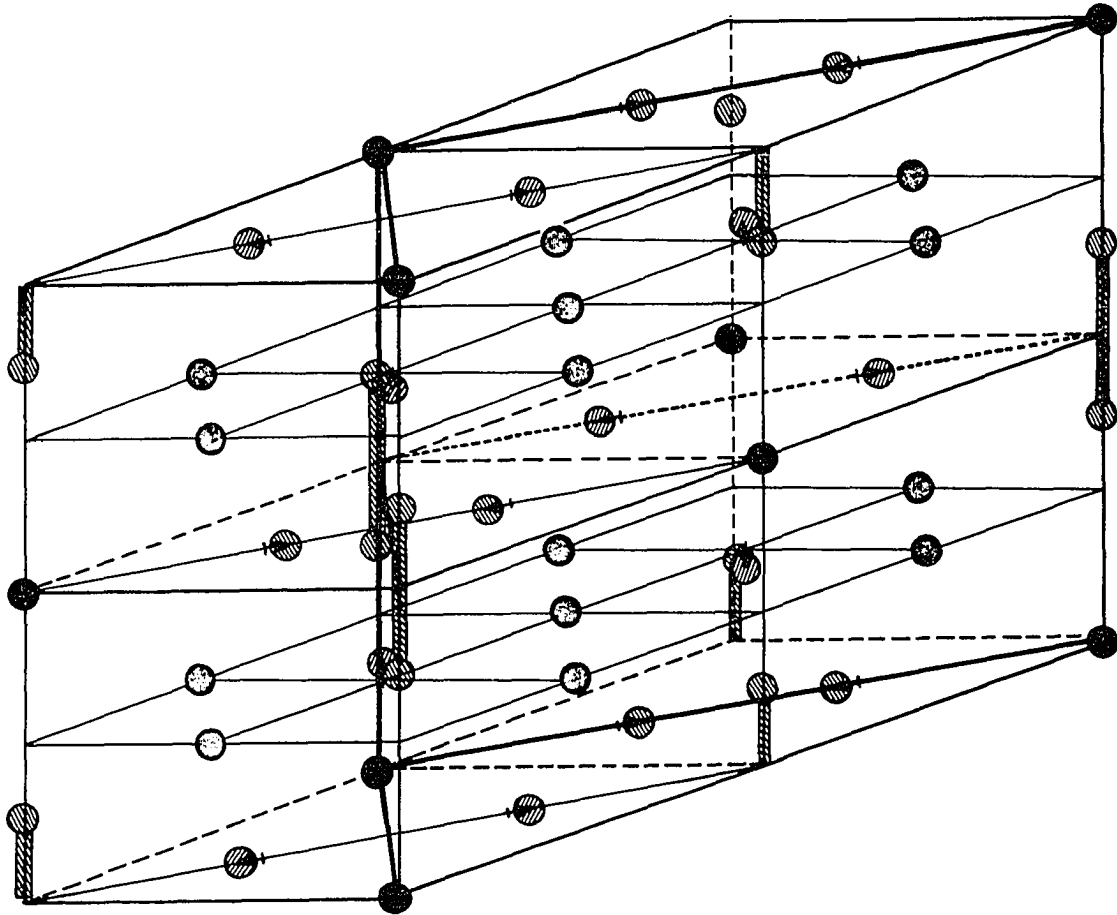
$Z_{RM5} = 1$
 $Y_{RM12} = 1/2$

-  RARE EARTH 2(a) site
-  Mn, Fe, or Cu 8(j) site
-  Al 8(i) site
-  Al 8(f) site

Although the transformation from RM_5 to RM_{12} is rather straightforward, two important complications should be mentioned: deformations arise due to the substitution of pairs of transition metal atoms for single rare earth atoms; and ordering is not perfect due to errors in substitution of the rare earths by transition metal pairs.

As can be seen from Figure IV.5, two important deformations occur when a "dumbbell" of transition metal atoms replaces a rare earth. These shifts from the original positions are indicated by the letters x and y in Table IV.3. Using YMn_{12} as an example, $x = 0.36$ and $y = 0.277$ ($x = 0.333$, $y = 0.250$ for the undeformed case). With an a parameter of 8.591 \AA for YMn_{12} , these parameters represent shifts of 0.23 \AA in both cases. However, with such a small shift, the basic crystallographic structure (and hence the magnetocrystalline character) remains essentially the same.

Errors in ordering of the substitutions present greater problems to studies of the RM_{12} alloys: instead of alternating rare earths being replaced, the period of replacement can be greater than two, at least occasionally, thus leading to superlattice effects.⁵⁹ This becomes a serious problem when the resultant stoichiometry drops from the expected value of RM_{12} : using the Ce-Mg system as an example, a stable phase exists from $CeMg_{10.5}$ ⁶⁰ to $CeMg_{12}$.⁶¹ Fortunately, this problem can be alleviated by use of a slight excess of the transition metal. In the case of the manganese compounds, where evaporation of



- RARE EARTH 2(a) site
- Mn, Fe, or Cu 8(j) site
- ▨ Al 8(i) site
- ▧ Al 8(f) site

Figure IV.5. RM_4Al_8 structure

manganese in preparation is also a problem, starting compositions of $\text{RMn}_{12.5}$ are used.

Unfortunately, the RCo_{12} phase directly analogous to RCo_5 does not exist,⁶² and so to better understand the metal rich RM_{12} phase three other types of compounds have been studied: RMn_{12} , RZn_{12} , and $\text{RM}_4\text{Al}_{18}$. This work began with a study of the RMn_{12} compounds. This series of compounds is closely related to RCo_5 , for both the rare earth and manganese atoms are magnetic. However, this leads to complex magnetocrystalline behavior, and the magnetic structures were not readily discernible.⁶³⁻⁶⁴ Thus, the RZn_{12} series was investigated, for in that case the zinc atoms are not magnetic, affording a simplification of the problem.⁶⁵

The magnetic and structural behavior of the RMn_{12} and RZn_{12} compounds has been discussed at length elsewhere,^{57,59,62,64-67} and thus will not be discussed to any great extent here. However, two interesting features will be mentioned, for they are of importance to understanding the behavior of the $\text{RM}_4\text{Al}_{18}$ compounds, discussed in the remainder of this chapter.

In the case of the RMn_{12} compounds, two ordering temperatures are found, as can be seen in Table IV.4. This is unusual behavior for most rare earth intermetallics, but it arises as a result of the centrosymmetric magnetic structure of the manganese atoms. Reference to Figure IV.6 shows how this happens. In general, transition metal atoms have higher ordering temperatures than the rare earths, and thus

Table IV.3. Atomic positions in the RM_{12} structure

Atoms	Site	Positions
R	2a	(0,0,0), (1/2,1/2,1/2)
M_I	8i	(x,0,0), (-x,0,0), (0,x,0), (0,-x,0), (1/2+x,0,1/2), (1/2-x,0,1/2), (1/2,1/2+x,1/2), (1/2,1/2-x,1/2)
M_{II}	8j	(y,1/2,0), (-y,1/2,0), (1/2,y,0), (1/2,y,0), (1/2+y,0,1/2), (1/2-y,0,1/2), (0,1/2+y,1/2), (0,1/2-y,1/2)
M_{III}	8f	(1/4,1/4,1/4), (3/4,3/4,1/4), (1/4,3/4,1/4), (3/4,1/4,1/4), (3/4,3/4,3/4), (1/4,1/4,3/4), (3/4,1/4,3/4), (1/4,3/4,3/4)

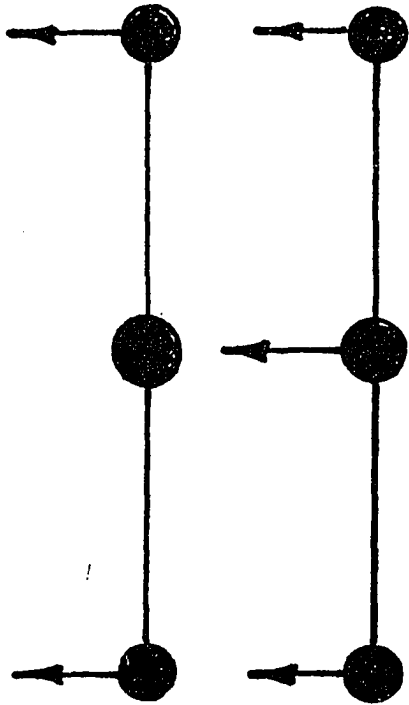
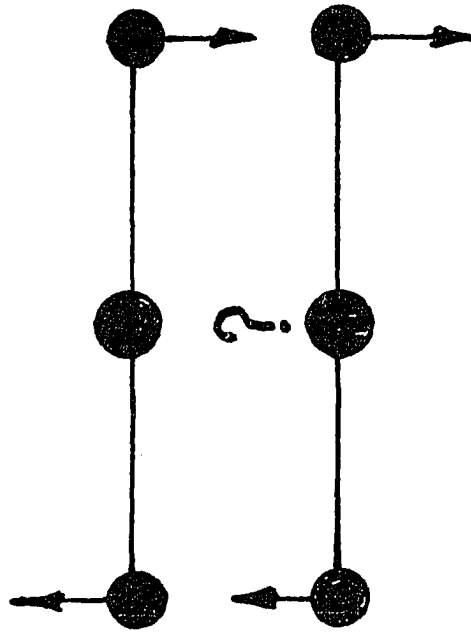
Table IV.4. Ordering temperatures for RMn_{12} compounds⁶⁴

Rare Earth	T_N^a	T_R^b
Y	120	
Gd		4.6
Tb	110	4.4
Dy		2.2
Ho	95	1.6
Er	87	1.9
Tm		<1.2

$^a T_N$ is the ordering temperature of the manganese atoms.

$^b T_R$ is the ordering temperature of the rare earth atoms.

Figure IV.6. Ordering of alloys: (a) (upper left) ferromagnetic ordering of transition metal atoms; (b) (lower left) induced ordering of rare earth atoms; (c) (upper right) antiferromagnetic ordering of transition metal atoms; (d) (lower right) ambiguous environment of rare earth atoms



as one lowers the temperature from above the ordering temperature of any atom in the particular compound being considered, to a temperature below such an ordering point, the transition metal atoms order before the rare earth atoms do. This ordering is depicted in Figure IV.6.1a, and if ferromagnetic ordering occurs, that generally precipitates ordering of the rare earth atoms at that same temperature (cf. Figure IV.6.b). However, if the transition metal atoms order antiferromagnetically, as in Figure IV.6.c, this creates an ambivalent ordering environment for the rare earth atoms. Thus, as there are equal forces "up" and "down," the net result is that the rare earth atoms are not ordered until the temperature is lowered to approximately liquid helium temperature.

In some of the RZn_{12} compounds, another peculiar ordering phenomenon occurs, that of the so-called "antiphase" structure. The derivation of this antiphase structure from the more common helimagnetic structure is depicted in Figure IV.7. That figure shows the parent helimagnetic structure; conditions such as strong magnetocrystalline anisotropy can restrict the direction of magnetization to one direction (or its reverse) only, and this can result in a modulated structure, as shown in Figure IV.7.b. For certain kinds of ions (Kramers ions) this structure is not thermodynamically allowed as the temperature approaches absolute zero. In that case, an additional transition is encountered, one in which the magnitude of the individual magnetic

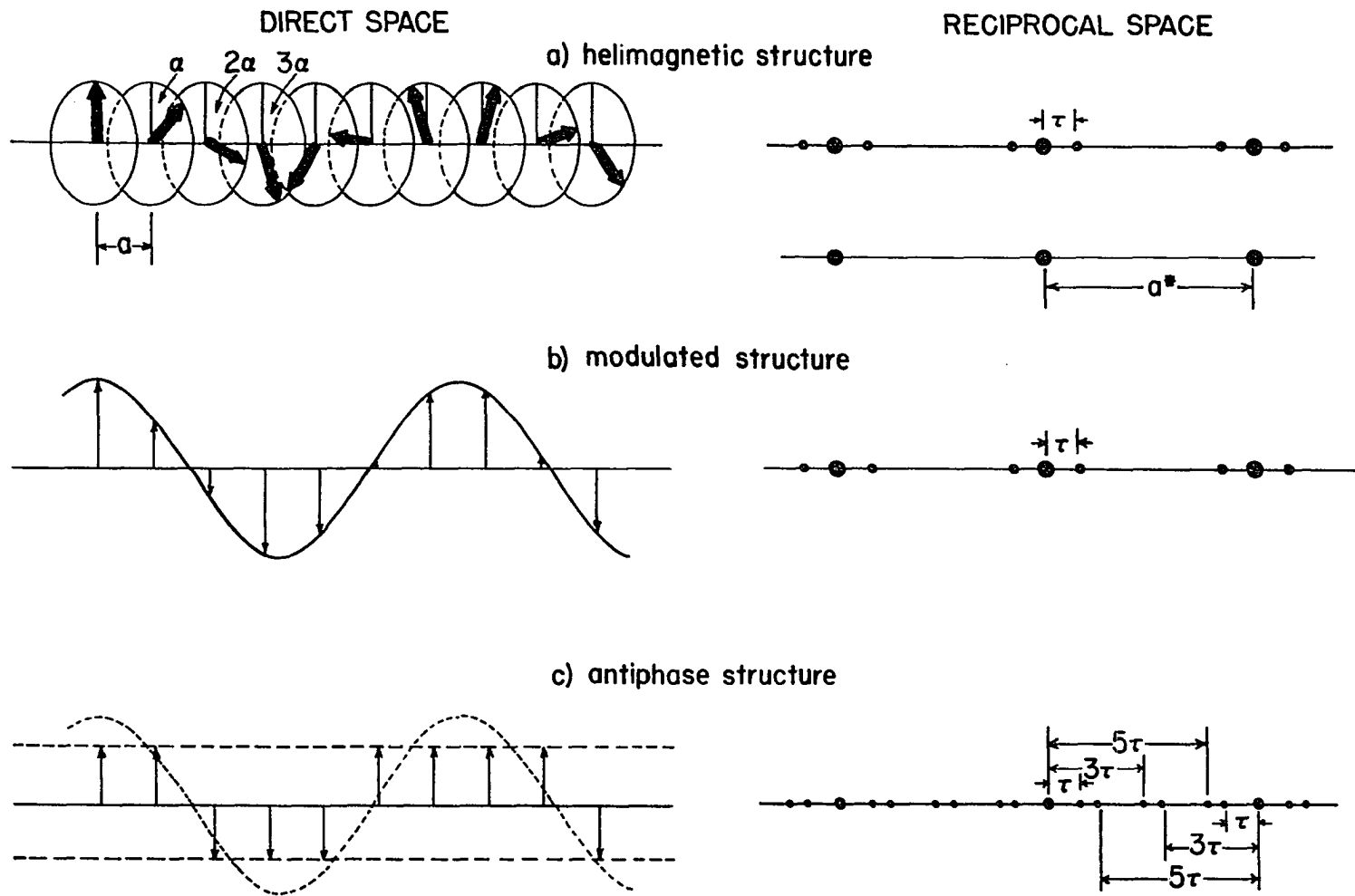


Figure IV.7. Rare earth magnetic structures

moments take on a common, average, value, but their directions remain unchanged. This results in the antiphase structure, as shown in Figure IV.7.c. This behavior is seen for TbZn_{12} .

Compounds of Stoichiometry RM_4Al_8

Introduction

As discussed above, interest in the RMn_{12} and RZn_{12} compounds grew out of initial interest in the compounds of stoichiometry RM_5 . These RMn_{12} and RZn_{12} alloys have been extensively discussed in the theses of Deportes⁵⁷ and Kebe.⁶⁶ No further comment on them will be made here, other than to say that they served in turn as the kernels from which interest in the RM_4Al_8 compounds grew.

There has been some interest previously in these compounds. For example, in the older literature, Zarechnyuk and Kripyakevich have described the crystal structures of the ternary cerium-transition metal-aluminum system,⁶³ and Zarechnyuk et al. have given the results of a series of structural investigations of the yttrium-copper-aluminum system.⁶⁸ More recently, Buschow, van Vucht, and van den Hoogenhof have given the unit cell constants of many RM_4Al_8 alloys,⁶⁹ and van der Kraan and Buschow have discussed some of the magnetic properties of the RFe_4Al_8 system.⁷⁰

In describing the cerium-transition metal-aluminum ternary systems, Zarechnyuk and Kripyakevich lay the groundwork for all other RM_4Al_8 studies. In particular, they point out that CeMn_4Al_8 is

isostructural with ThMn_{12} ,⁵⁸ as is CeFe_4Al_8 and CeCu_4Al_8 . Just as importantly, they point out that neither CeNi_4Al_8 nor CeCo_4Al_8 exist with the ThMn_{12} structure or superlattice. Other stable ternary compounds exist, such as $\text{Ce}_2\text{Mn}_7\text{Al}_{10}$, $\text{Ce}_2\text{Co}_{15}\text{Al}_2$, $\text{Ce}_2\text{Cu}_{6.5}\text{Al}_{10.5}$, and $\text{Ce}_2\text{Cu}_{7.3}\text{Al}_{9.7}$, all of which are isostructural with $\text{Th}_2\text{Zn}_{17}$.⁷¹⁻⁷³

As mentioned above, Zarechnyuk et al. describe the yttrium-copper-aluminum system. In addition to stating that $\text{Y}_2\text{Cu}_9\text{Al}_8$ is a stable compound, they mention that both $\text{Y}_2\text{Cu}_9\text{Al}_8$ and YCu_4Al_8 can be thought of as being solid solutions of YCu_4 (or YCu_5) in aluminum. Indeed, this seems rather profound in that YCu_4Al_8 contains some 62 atomic percent aluminum.

Whereas the papers by Zarechnyuk and authors describe systems of only one rare earth each (cerium and yttrium), the papers by Buschow are not so restricted, listing instead more complete information on several members of entire rare earth-transition metal systems. The paper by Buschow, van Vucht, and van den Hoogenhof lists the structural parameters of several RM_4Al_8 alloys, including cases where $\text{M} = \text{Cr}$ and $\text{R} = \text{Th}$. They note that attempts to make vanadium compounds with La, Gd, Y, and Th failed, as did an attempt to make LaCu_4Al_8 . The paper by van der Kraan and Buschow describes the magnetic properties of RFe_4Al_8 compounds. The result of their work will be described later, but at present it should be noted that all such compounds are isostructural.

Thus a program of study of some RM_4Al_8 alloys was begun. As implied above, these compounds do not exist when $M = V, Co, \text{ or } Ni$, but they do exist when $M = Cr, Mn, Fe, \text{ and } Cu$, and $R = Y$, the lanthanides, or Th . The RCu_4Al_8 compounds are true ternary compounds in which only the rare earth atoms are magnetic, and are thus analogous to the RZn_{12} compounds. RMn_4Al_8 and RFe_4Al_8 are also true ternary compounds, but there the manganese and iron atoms are magnetic. In a way analogous to the RMn_{12} compounds, the RMn_4Al_8 and RFe_4Al_8 compounds in fact represent a midpoint in complexity between the RZn_{12} and RMn_{12} compounds. The chromium alloys will not be considered here.

The next section of this chapter describes sample preparation, and following sections describe the results of X-ray and neutron diffraction experiments, as well as magnetic susceptibility work.

Sample Preparation

Samples were prepared using weighed amounts of metallic ingots. The purity of these materials was 99.9% for the rare earths, and 99.99% for the aluminum and transition metals used. These purities seemed adequate for the studies undertaken. Melting was usually done in induction furnaces. In general, the metals to be alloyed were placed in an alumina crucible, and the samples were melted at temperatures around $1000^\circ C$. This was done either in a vacuum, or, because of the high vapor pressures of many of the materials, especially in

the molten state, in a helium or argon atmosphere. In all cases, the samples were subjected to rapid quenching, thus forcing crystallization at a temperature below the peritectic transformation temperature of the compound being prepared.⁴⁸ Frequently this rapid quenching and the contraction which occurred upon cooling and solidification resulted in cavities being formed inside the sample; dendritic single crystals of approximate dimensions 0.5x0.5x3.0 mm commonly grew from the walls of the cavities, as well.

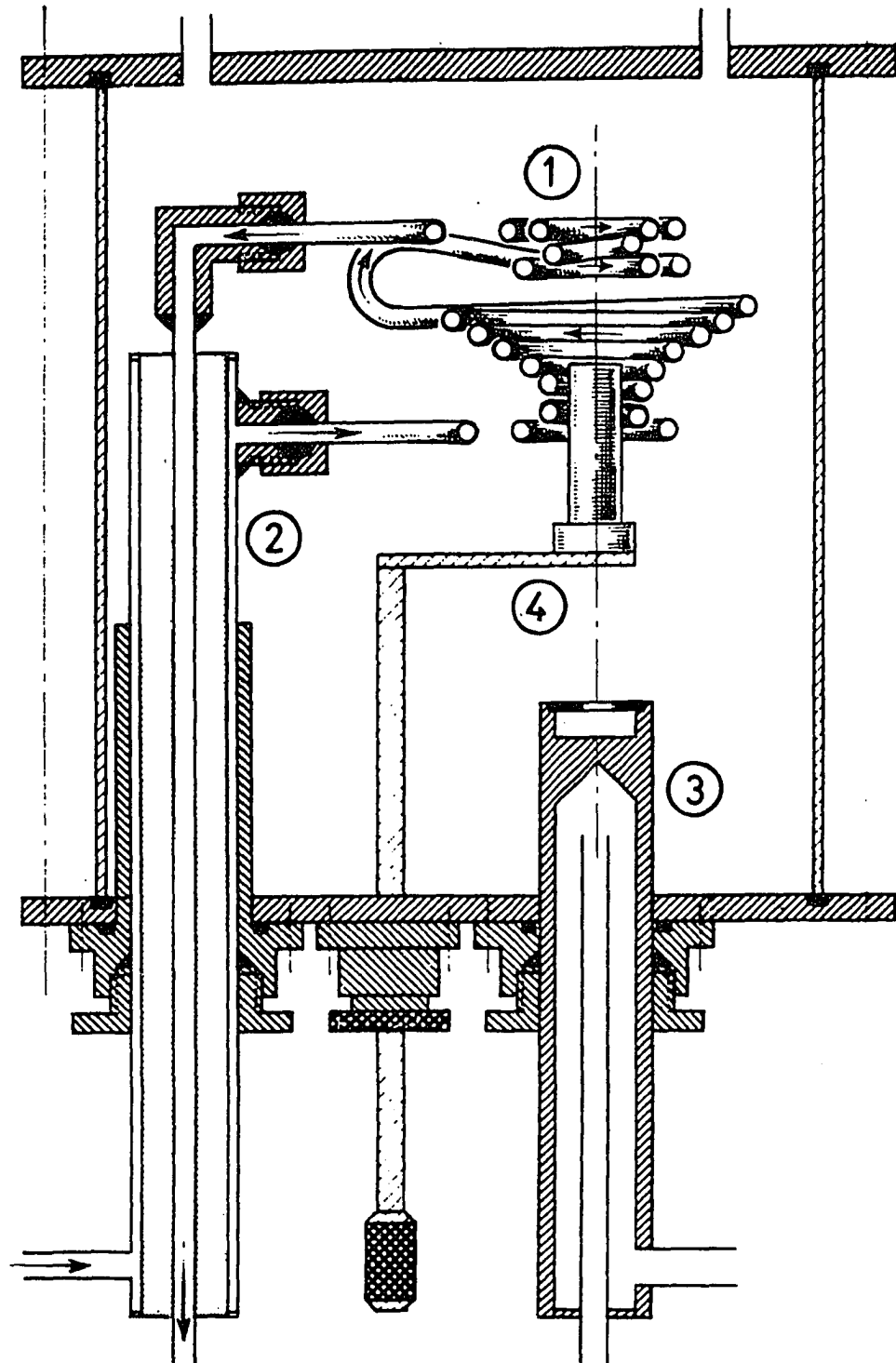
After rapid quenching, the samples were broken into powders. In general, this was readily accomplished by the technique of striking the pellet shaped sample with a hammer, for the samples were quite brittle. However, in the case of the RCu_4Al_8 alloys, the samples were very hard and plastically deformed upon striking, making the process of obtaining a powder somewhat more arduous. As the plastic deformation of the sample inferred considerable strain, the copper compounds were subsequently annealed at approximately 800° C for periods of two or three days. (The manganese and iron samples were also occasionally annealed, but this step seemed less critical for them.)

It is frequently difficult to directly react transition elements and the rare earths, due to the great differences in their melting points and the high vapor pressure of certain transition metals at elevated temperatures. In the case of the RCu_4Al_8 and RFe_4Al_8 alloys, this was not a problem. In the case of the RMn_4Al_8 compounds, however, the high vapor pressure of manganese necessitated addition of a slight

excess of manganese, to give a starting stoichiometry of approximately $\text{RMn}_{4.3}\text{Al}_8$. Subsequent analysis showed that this produced the desired material.

In addition to the alumina crucibles generally used in this study, other sample holders made from materials such as boron nitride, copper, or silver, can be used. In the case of certain rare earth intermetallics (eg. RCO_2), contamination by materials derived from the sample holder results in gross changes of physical properties.⁴⁸ In other cases, it is desirable to rapidly quench the sample, to avoid freezing it out in the wrong phase. For these reasons levitation furnaces are sometimes used. An alternative form of sample melting, levitation furnaces, shown schematically in Figure IV.8, are similar to conventional induction furnaces in that they make use of a high strength high frequency current, and this flows through a cone shaped coil, thus producing a nonuniform induction field in the sample which creates forces which counterbalance the action of gravity; in short, the sample is levitated, touching no crucible. Levitation furnaces have been used with success on many such compounds, for they are uniquely suited for the lessening of contamination problems and/or providing rapid quenching. A more complete discussion of levitation furnaces may be found in Remy Lemaire's 1966 article.⁴⁸ In the case of the aluminum-rich RM_4Al_8 compounds, aluminum contamination was no problem, but occasional use was made of the levitation furnace technique to effect rapid quenching.

Figure IV.8. Levitation furnace: (1) induction coil; (2) co-axial feeder; (3) mould; (4) retractable support



As mentioned above, the disparate melting points of the constituents of the RM_4Al_8 compounds were not a great problem. Typical behavior upon heating would be that the aluminum would first melt, followed quickly by the transition metal (manganese, iron, or copper). As the temperature rose, reaction between the aluminum-3d metal melt and the solid rare earth ingot would occur exothermically at the surface of the rare earth. Eventually, as the temperature rose, a sudden flash of light from the sample would indicate that final reaction had occurred. As the temperatures that were sustainable in the induction furnaces were well-below those of the melting points of many of the rare earths, this process must be viewed as a continuation of the solid phase-liquid phase reaction described above. Undoubtedly, the exothermicity of the process greatly aided its completion.

After suitable preparation of the samples, x-ray powder diffraction patterns were made to verify production of the desired material, and also to provide information about the unit cell dimensions. After suitable amounts of the alloys were produced, two types of studies were carried out: neutron diffraction experiments, and magnetic susceptibility measurements. The techniques and results of these experiments will be considered in the following section.

Discussion

X-ray Diffraction

Portions of all samples were ground to fine powders and prepared for standard powder diffraction experiments, using Debye-Scherrer film cameras and Cr K α radiation.

As the RM_4Al_8 alloys crystallize in the tetragonal space group I4/mmm, they obey the selection rule $h+k+l=2n+1$, extinct. In the case of the RMn_4Al_8 and RFe_4Al_8 alloys (but not the RCu_4Al_8 alloys) an additional indexing feature is present, for as the c/a ratio for these compounds is $1/\sqrt{3}$, the selection rule $h^2+k^2+3l^2=2n+1$, extinct, is followed, and all those reflections for which $h^2+k^2+3l^2$ have the same value are degenerate. Table IV.5 lists all allowed reflections for the space group I4/mmm, grouped by $h^2+k^2+3l^2$.

Tables IV.7 and IV.6 give samples of indexing of the RM_4Al_8 compounds: Table IV.6 gives the pattern for $TbMn_4Al_8$, a pattern typical not only of the analogous manganese alloys, but also the iron ones, as well; Table IV.7 gives the pattern for $TbCu_4Al_8$, a pattern typical of all the copper alloys. It should be noted that in this latter class extraneous lines frequently were present (e.g., at $2\theta = 34.15$ or 45.10°). It is generally accepted that film powder techniques are sensitive to impurities amounting to some two percent or more: these extra lines probably represent the presence of small amounts of some RCu_xAl_y phase other than that desired, RCu_4Al_8 . However, in no case

Table IV.5. Allowed reflections for the I 4/mmm space group

$h^2+k^2+3l^2$ ^a	hkl	$h^2+k^2+3l^2$	hkl	$h^2+k^2+3l^2$	hkl
2	110	36	600	64	800
4	200		303		651
	101	38	512		642
6	Absent	40	620		613
8	220		611	66	404
	211	42	323		334
10	310	44	Absent	68	820
12	301		541		741
14	112		442		811
16	400	46	413		743
	321	48	532	70	424
	202		631	72	732
18	330		602		660
20	420	50	004	74	633
	411		550		750
	222	52	710	76	514
22	312		114		831
24	Absent		640		802
			701		703
26	510		622	78	105
28	431		433		Absent
	501	54	503	80	840
	402		204		822
	103	56	Absent		723
30	332		721		444
32	440		523	82	215
	521	58	224		910
	422		730	84	534
	213	60	314		901
34	530	62	Absent		662
			552		604
			712		305

^aFor the RMn_4Al_8 and RFe_4Al_8 compounds, the ratio of the axes $a/c = \sqrt{3.0}$. Thus, the selection rule becomes $h^2+k^2+3l^2=2n+1$, extinct.

Table IV.5. Continued

$h^2+k^2+3l^2$	hkl	$h^2+k^2+3l^2$	hkl
86	752	94	912
88	761	96	Absent
	921	98	770
	653		554
	624		714
	325	100	860
90	930		1000
92	851		941
	842		833
	743		644
	813		435
	415		505

Table IV.6. Indexing for RCu_4Al_8 Powder Patterns. TbCu_4Al_8

n^a	hkl	I_{obs}	d_{obs}^b	$2\theta_{\text{obs}}$	d_{calc}	$2\theta_{\text{calc}}$	Δ^c
	110	w	42.0	21.00	42.8	21.424	(+.8)
	101	w	60.0	30.00	60.0	30.024	(0)
	200	w	60.0	30.00	61.0	30.481	(+1.0)
	-	vwv	68.3	34.15	-	-	-
	211	vst	86.3	43.15	86.6	43.313	(+.3)
	220	vst	86.3	43.15	87.3	43.648	(+1.0)
	-	vwv	90.2	45.10	-	-	-
	310	m	97.4	48.70	98.2	49.119	(+.8)
	-	vwv	103.7	51.85	-	-	-
	002	vw	106.0	53.00	106.0	53.024	(0)
	301	m	106.7	53.35	107.8	53.885	(+1.1)
1	112	w	114.6	57.30	115.7	57.834	+1.1
	-	w	116.2	58.10	-	-	-
2	202	vvst	123.4	61.70	124.8	62.402	+1.4
3	321	100%	125.4	62.70	126.4	63.179	+1.0
4	400	100%	125.4	62.70	126.9	63.436	+1.5
	-	vvvw	130.1	65.05	-	-	-
	-	vvvw	131.8	65.90	-	-	-
5	330	vw	133.9	66.95	135.6	67.785	+1.7
	-	vvvw	135.9	67.95	-	-	-
6	222	m	140.3	70.15	142.1	71.030	+1.8

^aNumber of reflection as used in lattice constant refinement program.¹³

$$d = 2x2\theta, 2\theta < 90^\circ; 2x(180-2\theta), 2\theta > 90^\circ.$$

^c $\Delta = d_{\text{calc}} - d_{\text{obs}}$. Note that the sense of Δ changes at $2\theta = 90^\circ$. Numbers in parentheses are for reflections not used in lattice refinement.

Table IV.6. Continued

n	hkl	I _{obs}	d _{obs}	2 θ _{obs}	d _{calc}	2 θ _{calc}	Δ
7	411	w-m	142.3	71.15	143.5	71.759	+1.2
8	420	w-m	142.3	71.15	144.0	72.002	+1.7
9	312	w-m	148.3	74.15	150.3	75.169	+2.0
10	510	vw	166.2	83.10	168.3	84.164	+2.1
	103	Unobs	-	-	172.1	86.057	-
	402	Unobs	-	-	174.4	87.211	-
11	431	w	176.6	88.30	171.8	85.902	-4.8
	501						
12	332	w	177.1	91.45	177.7	91.171	+6
13	213	w	171.2	94.40	172.0	93.982	+8
14	422	st	169.0	95.50	169.7	95.137	+7
	521	Unobs	-	-	168.3	95.831	-
15	440	m	167.0	96.50	167.9	96.063	+9
16	530	w	159.0	100.50	159.9	100.063	+9
17	303	w	155.2	102.40	156.0	101.984	+8
	600	Unobs	-	-	151.8	104.112	-
18	512	w	143.6	108.20	145.5	107.268	+1.9
19	323	m-st	138.8	110.60	139.5	110.234	+7
20	611	m-st	134.6	112.70	135.6	112.210	+1.0
21	620	m-st	134.6	112.70	135.1	112.459	+5
	413	Unobs	-	-	122.1	118.951	-
	442	Unobs	-	-	119.5	120.275	-
	541	Unobs	-	-	117.5	121.079	-
22	532	m	109.8	125.10	110.0	124.978	+2
23	004	m	107.0	126.50	107.1	126.450	+1
	-	w	104.4	127.80	-	-	-
24	602	vvst	100.3	129.85	100.1	129.968	-2
25	631	vst	97.9	131.05	98.2	130.876	+3
	114	Unobs	-	-	96.9	131.546	-
	204	Unobs	-	-	85.8	137.082	-
26	550	w	86.6	136.70	86.6	136.681	0
	710						
27	433	w-m	81.2	139.40	81.0	139.505	-2
	503						
28	622	w	77.7	141.15	77.4	141.311	-3
	701	Unobs	-	-	75.1	142.431	-
	640	Unobs	-	-	74.4	142.811	-
29	224	w	59.7	150.15	59.0	150.520	-7
30	523	w	52.9	153.55	52.0	153.984	-9
	721	w-diff	43.0	158.50	42.9	158.565	(-1)
	314	w-diff	43.0	158.50	40.0	159.990	(-1.0)

Table IV.7. Indexing for RMn_4Al_8 powder patterns. TbMn_4Al_8

n^a	$h^2+k^2+3l^2$	hkl	I_{obs}	d_{obs}^b	$2\theta_{\text{obs}}$	d_{calc}	$2\theta_{\text{calc}}$	Δ^c
	2	110	w	42.1	21.05	42.2	21.113	(+.1)
	4	200	w	60.3	30.15	60.1	30.033	(-.2)
	4	101	w	60.3	30.15	60.1	30.032	(-.2)
	8	220	st	86.0	43.00	86.0	42.990	(0)
	8	211	st	86.0	43.00	86.0	42.989	(0)
	10	310	w-m	96.8	48.40	96.7	48.368	(-.1)
	12	301	m	106.7	53.35	106.7	53.329	(0)
	12	002	m	106.7	53.35	106.7	53.327	(0)
1	14	112	w	115.9	57.95	116.0	57.987	+1
2	16	400	100%	124.6	62.30	124.8	62.422	+2
3	16	202	100%	124.6	62.30	124.8	62.421	+2
4	18	330	w	133.2	66.60	133.4	66.683	+2
5	20	420	m	141.3	70.65	141.6	70.811	+3
6	20	222	m	141.3	70.65	141.6	70.809	+3
7	22	312	w-m	149.3	74.65	149.7	74.836	+4
8	26	510	w	164.9	82.45	165.4	82.687	+5
9	28	501	m	172.6	86.30	173.1	86.551	+5
10	28	103	m	172.6	86.30	173.1	86.548	+5
11	30	332	w	179.9	90.05	179.2	90.398	-.7
12	32	440	st	171.0	94.50	171.5	94.250	+5
13	32	213	st	171.0	94.50	171.5	94.246	+5
14	34	530	m-w	163.5	98.25	163.8	98.119	+3

^aNumber of reflections used in lattice refinement program. ¹³

^b $d = 2x2\theta$, $2\theta < 90^\circ$; $2x(180-2\theta)$, $2\theta > 90^\circ$.

^c $\Delta = d_{\text{calc}} - d_{\text{obs}}$. Note that the sense of Δ changes at $2\theta = 90^\circ$. Numbers in parentheses are for reflections not used in lattice refinement.

Table IV.7. Continued

h^a	$h^2+k^2+3l^2$	hkl	I_{obs}	d_{obs}^b	$2\theta_{\text{obs}}$	d_{calc}	$2\theta_{\text{calc}}$	Δ^c
15	36	600	m	155.4	102.30	155.9	102.027	+ .5
16	36	303	m	155.4	102.30	156.0	102.023	+ .6
17	38	512	m-w	147.8	106.10	148.0	105.990	+ .2
18	40	620	vst	139.8	110.10	139.9	110.037	+ .1
19	40	323	vst	139.8	110.10	139.9	110.034	+ .1
	44	541	unobs	-	-	123.0	118.482	-
	44	413	unobs	-	-	123.0	118.479	-
20	46	532	m	114.6	122.70	114.1	122.956	- .5
21	48	631	vvst	103.4	128.30	104.7	127.673	(+1.3) ^d
22	48	004	vvst	103.4	128.30	104.7	127.666	(+1.3) ^d
23	50	550	w	95.1	132.45	94.6	132.710	- .5
24	50	114	w	95.1	132.45	94.6	132.702	- .5
25	52	640	m	83.5	138.25	83.6	138.196	+ .1
26	52	204	m	83.5	138.25	83.6	138.186	+ .1
27	56	721	st	56.5	151.75	56.8	151.604	+ .3
28	56	224	st	56.5	151.75	56.8	151.592	+ .3
29	58	730	m	36.8	161.60	37.5	161.231	+ .7
30	58	314	m	36.8	161.60	37.6	161.212	+ .8

^dReflection rejected by the lattice refinement program.

was this extraneous phase a problem in either the neutron diffraction or magnetic susceptibility experiments.

Table IV.8 lists all lattice parameters for selected RM_4Al_8 alloys. Figures IV.9 and IV.10 present this information pictorially: Figure IV.9 plots the observed a and c parameters against the rare earth atomic radii given by Cotton and Wilkinson;⁴⁴ Figure IV.10 plots the observed unit cell volume against the cubes of those atomic radii. It can be seen that the RM_4Al_8 alloys obey the well-known lanthanide contraction rule. However, it should be noted that values for the ionic radii of manganese, iron, or copper cannot be used as predictors of unit cell dimensions. Cotton and Wilkinson give values of 0.80, 0.76, and 0.72 Å, respectively, for those elements,⁴⁴ that is, manganese is largest, followed by iron and then copper. Reference to Table IV.8 and Figures IV.9 and IV.10 show this order to be followed for the a parameters, whereas the order $Cu > Mn > Fe$ is followed for the c parameters, and the order $Mn > Cu > Fe$ is followed for the unit cell volumes. This behavior implies such things as Jahn-Teller distortions of the transition metals, that is, that they can no longer simply be thought of as spherical atoms.

The RM_4Al_8 alloys are isostructural with $ThMn_{12}$, as mentioned previously. Referring to Table IV.3, the values of x and y are 0.351 and 0.291, respectively, for $DyCu_4Al_8$, and these values are virtually identical for all alloys considered; indeed, when calculating intensities for powder pattern identification, these parameters were used in

Table IV.8.a. Lattice parameters for RMn_4Al_8 compounds

Rare Earth	$_a$	$a(\text{\AA})$	$c(\text{\AA})$	$(a/c)^2$	$V(\text{\AA}^3)$	$\rho(\text{g/cm}^3)$
Y	28	8.8431(24)	5.1070(17)	2.9982 ^b	399.37(20)	4.3614(22)
Y	$_c$	8.856	5.103		400.24	
La	$_c$	9.031	5.166		421.30	
Ce	$_d$	8.89	5.17		409	
Ce	$_c$	8.947	5.133		410.89	
Pr	$_c$	8.962	5.143		413.01	
Gd	28	8.8703(13)	5.1210(9)	3.0003	402.94(11)	4.8861(13)
Gd	$_c$	8.887	5.119		404.31	
Tb	28	8.842(3)	5.1050(21)	2.9999	399.10(24)	4.947(3)
Er	$_c$	8.829	5.096		397.30	
Yb	$_c$	8.819	5.084		395.35	

^aNumber of reflections used/Citation.

^bDeviation of these values from 3.00 for the manganese and iron compounds is an artifact of the lattice constant refinement procedure.

^cFrom Buschow et al.⁶⁹

^dFrom Zarechnyuk and Kripyakevich.⁶³

Table IV.8.b. Lattice parameters for RFe_4Al_8 compounds

Rare Earth	\bar{a}	$a(\text{Å})$	$c(\text{Å})$	$(a/c)^2$	$V(\text{Å}^3)$	$\rho(\text{g/cm}^3)$
Y	27	8.7301(10)	5.0410(7)	2.9993 ^b	384.21(8)	4.5650(10)
Y	\bar{c}	8.740	5.045		384.92	
La	\bar{c}	8.900	5.075		401.98	
Ce	\bar{d}	8.86	5.08		399	
Ce	\bar{c}	8.805	5.048		391.34	
Pr	\bar{c}	8.834	5.058		394.67	
Nd	\bar{c}	8.813	5.058		392.86	
Sm	\bar{c}	8.773	5.051		388.08	
Gd	$\bar{24}$	8.7498(11)	5.0515(8)	3.0002	386.74(9)	5.1220(12)
Gd	\bar{c}	8.758	5.048		387.18	
Tb	$\bar{28}$	8.7355(14)	5.0439(10)	2.9995	384.89(11)	5.1610(15)
Tb	\bar{c}	8.749	5.043		386.02	
Dy	$\bar{29}$	8.723(3)	5.0370(24)	2.9991	383.3(3)	5.213(4)
Dy	\bar{c}	8.715	5.037		382.59	
Ho	$\bar{30}$	8.706(3)	5.0286(22)	2.9974	381.14(25)	5.264(3)
Ho	\bar{c}	8.720	5.035		382.84	
Er	$\bar{17}$	8.7223(5)	5.0358(3)	3.0000	383.01(4)	5.2586(5)
Er	\bar{c}	8.704	5.037		381.64	
Tm	\bar{c}	8.697	5.034		380.78	
Yb	\bar{c}	8.714	5.026		381.63	
Lu	\bar{c}	8.689	5.036		380.20	

^aNumber of reflections used/Citation.

^bDeviation of these values from 3.00 for the manganese and iron compounds is an artifact of the lattice constant refinement procedure.

^cFrom Buschow et al.⁶⁹

^dFrom Zarechnyuk and Kripyakevich.⁶³

Table IV.8.c. Lattice parameters for RCu_4Al_8 compounds

Rare Earth	$_a$	$a(\text{\AA})$	$c(\text{\AA})$	$(a/c)^2$	$V(\text{\AA}^3)$	$\rho(\text{g/cm}^3)$
Y	29	8.709(7)	5.132(7)	2.8798 ^b	389.2(7)	4.769(9)
Y	$_c$	8.721	5.139		390.85	
Ce	$_d$	8.84	5.17	2.92	404	5.02
Ce	$_c$	8.829	5.157		402.03	
Pr	$_c$	8.806	5.157		399.92	
Gd	26	8.735(3)	5.1429(24)	2.8848	392.40(25)	5.308(3)
Gd	$_c$	8.748	5.146		393.84	
Tb	30	8.715(9)	5.132(8)	2.8838	389.8(8)	5.358(11)
Dy	26	8.7081(22)	5.1327(18)	2.8784	389.23(19)	5.396(3)
Ho	29	8.6819(25)	5.1240(19)	2.8709	386.22(21)	5.459(3)
Er	24	8.6728(24)	5.1159(19)	2.8739	384.81(19)	5.550(3)
Er	$_c$	8.691	5.119		386.70	
Tm	28	8.6726(24)	5.1145(16)	2.8754	384.69(19)	5.516(3)
Yb	$_c$	8.710	5.110		387.74	

^aNumber of reflections used/Citation.

^bDeviation of these values from 3.00 for the manganese and iron compounds is an artifact of the lattice constant refinement procedure.

^cFrom Buschow et al.⁶⁹

^dFrom Zarechnyuk and Kripyakevich.⁶³

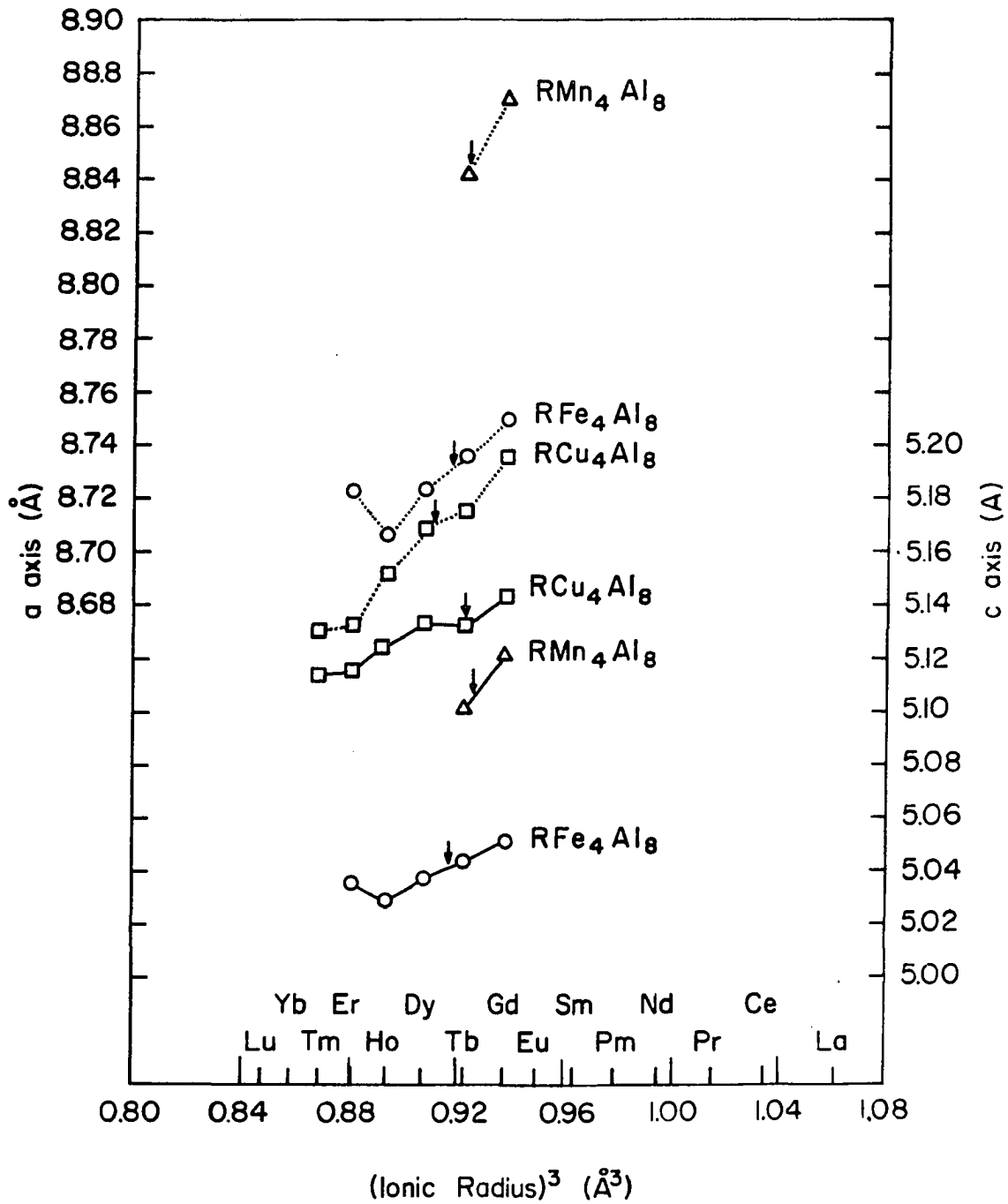


Figure IV.9. Unit cell parameters

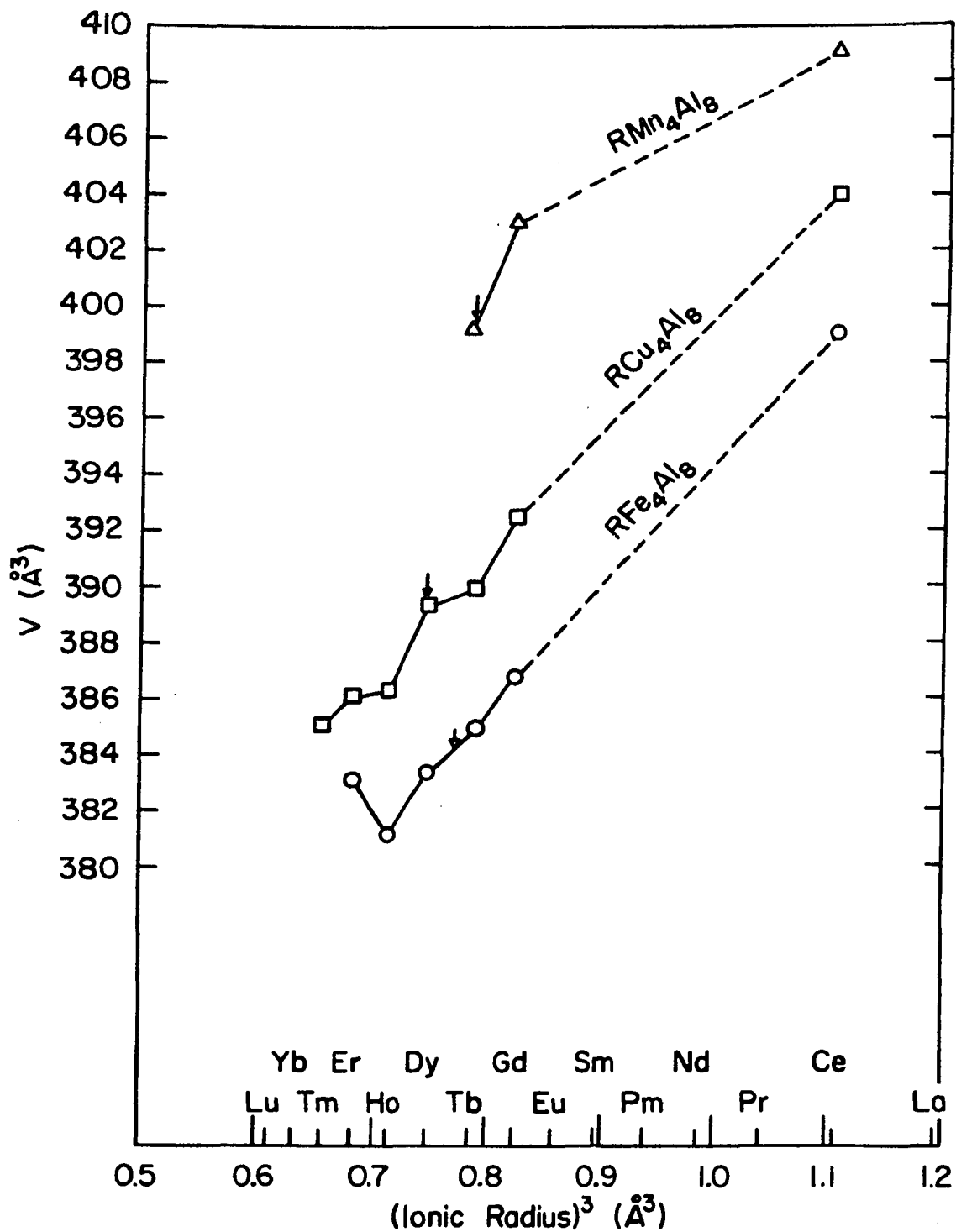


Figure IV.10. Unit cell volumes

all cases. It should be emphasized that the RM_4Al_8 alloys are completely ordered: the M atoms occur exclusively in the 8f crystallographic sites; the aluminum atoms occur exclusively in the 8i and 8j sites. (As a counterexample in a related compound, in $Ce_2Mn_7Al_{10}$, one site has 2/3 occupancy Mn, 1/3 occupancy Al.⁶³) A listing of intensity data for $DyCu_4Al_8$ is given in Table IV.9. Using the expression $R = |\Sigma I_{obs} - \Sigma I_{calc}| / \Sigma I_{obs}$ as a measure of goodness of fit, this data has a value of $R = 8\%$.⁶⁶

Magnetic Susceptibility:

Theoretical

Following Kittel,⁷⁴ one can treat a medium containing N atoms per unit volume, each bearing a magnetic moment μ , in the following manner. Magnetization results from the orientation of the magnetic moments in an applied field, H. An expression for this magnetization can be given by the Langevin equation

$$M = N\mu L(x)$$

where $x = \mu H / k_B T$, and the Langevin function $L(x)$ is

$$L(x) = \text{ctnh}(x) - 1/x.$$

The magnetization can also be given by the equation

$$M = N\mu \tanh(x)$$

Table IV.9. X-ray intensity data for DyCu₄Al₈

hkl	I _{obs}	I _{calc}	
110	2.1	3.7	
200	1.8	1.2	
101	2.8	5.9	
220	15	19	
211	17	17	
310	9.4	9	
002	-	0.9	
301	23.8	22.8	
112	5	4.8	
202	74.1	74	
321	100	50.5	95.5
400		45	
330	8.1	5.1	
222	22.5	17.7	
411	13.9	14	
420			
312	11.6	12.2	
510	10.5	9	
103	-	-	
402	-	-	
501	11.2	12	
437			
332	6.5	6	
213	6.0	4	
422	43.5	48.5	
521	32.3	34	
440			
530	11.5	10.1	
303	10.6	11.7	
600	-	-	
512	13	13.3	
323	28	27.3	
620	43.8	39	
611			

This equation can be seen as a special case (with $J = 1/2$) of the equation

$$M = Ng_J\mu_B B_J(x), \quad (x = g_J\mu_B H/k_B T),$$

where the Brillouin function B_J is defined by

$$B_J(x) = ((2J+1)/2J) \operatorname{ctnh}((2J+1)x/2J) - (1/2J) \operatorname{ctnh}(x/2J),$$

where J is the total angular momentum, g_J is the spectroscopic splitting factor, μ_B is the Bohr magneton, and k_B is the Boltzmann constant.

The two equations $M = N\mu L(x)$ and $M = N\mu \tanh(x)$ are different in that the former is based on a classical model (continuous orientation of magnetic moments), whereas the latter uses a quantum mechanical model (quantized orientation).

For an electron $\mu \sim 10^{-20}$ erg/gauss; at room temperature and a field of 10^4 gauss we have $x = \mu H/k_B T = 2 \times 10^{-3}$. In the limit $x \ll 1$, we see that both equations given above for B reduce to

$$\chi = M/H = N\mu^2/3k_B T = C/T,$$

where the Curie constant $C = N\mu^2/3k_B$. The above equation is known as the Curie Law. From these equations it is obvious that judicious experimental design can give information about M (and hence, χ and μ) as a function of H and T .

It should be noted that an excellent description of the development of the science of magnetism may be found in the Nobel lectures given by Van Vleck, Anderson, and Mott in 1977. These lectures, reproduced in *Science*, cover the topics of quantum mechanics and magnetism,⁷⁵ local moments and localized states,⁷⁶ and electronic structure.⁷⁷

Experimental

Measurements of the magnetization of all samples were made using the extraction technique, and were performed either at the Service de Mesures d'Aimentation, (SMA), (Magnetization Measurement Service), or the Service National des Champs Intenses, (SNCI), (National Intense Field Service), both of the CNRS in Grenoble, France. This technique, described by Cullity,⁷⁸ is based on the flux change in a search coil when the specimen is removed from the coil. Two important advantages of this technique are that it can be used to measure M directly at a particular field strength, rather than a change of M due to a change in field, and that the flux change in the search coil does not involve the applied field H . This latter fact is of importance when M is small compared to H , as it is for weakly magnetic materials.

At both facilities in Grenoble, the experimental apparatus was basically of the type described by Cullity. Here morsels of the sample are placed in a small plastic cylinder of approximate dimension 2mmx1cm. (Morsels are used, rather than a fine, monocrystalline powder, so that individual particles of the sample are not free to

rotate in the applied field.) The cylinder containing the sample is attached to the end of a rod which is inserted into some manner of temperature controlling device. In the case of the SMA facility, this took the form of a demountable cryostat system, which was a liquid helium dewar and column nested inside of a similar liquid nitrogen system; in the case of the SSCI facility this cryostat system was not demountable. The rod allowed the rapid extraction necessary for the technique, as well as accurate positioning of the sample between the pole pieces of the magnet; the cryostat systems were designed to allow all temperatures between room temperature and liquid helium temperature (4.2K, or even 1.4K, the "easy" limit of pumped helium) to be reached; the magnetic fields obtainable were variable over a range of 0-26kG at the SMA facility, 0-150kG at the SSCI.^{79,80}

To describe the magnetic behavior of a material, it is frequently desirable to measure the magnetization of that material at a variety of temperatures and applied fields. In the case of applied fields produced by superconducting magnets, it is difficult to rapidly change the applied field. Thus, in that case, the temperature of the sample is changed over the desired range at a particular applied field, and upon completion of measurements at that field, the field is changed and the experiment is repeated. In the case of classical magnets, however, it is often easier to hold the temperature constant as one varies the applied field from 0 to the desired maximum. As both the

SMA and SNCI facilities used in this study used classical magnets, this latter regimen was followed.

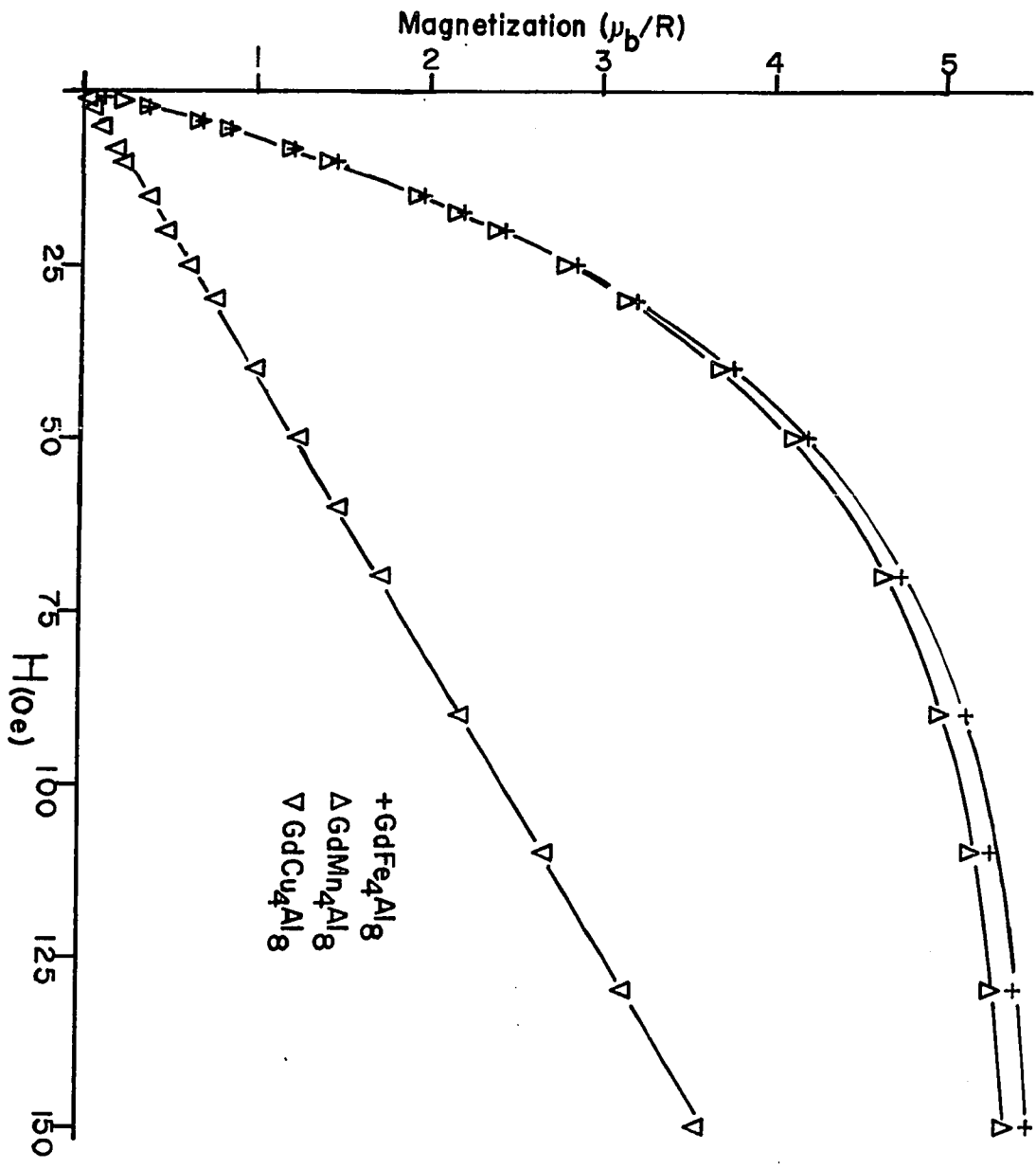
Results

Figure IV.11 plots magnetization, M (in units of Bohr magnetons per rare earth atom), versus the applied field, H (in kOe), for the three gadolinium compounds $GdFe_4Al_8$, $GdMn_4Al_8$, and $GdCu_4Al_8$. This data, taken at 4.2K, is typical of all such data, and there are two comments that should be made concerning it.

As the hyperbolic tangent of x ($\tanh(x)$) is defined as $(e^x - e^{-x}) / (e^x + e^{-x})$, and the limit of this expression as $x \rightarrow \infty$ is 1, one can see that whereas for small x the equation $M = N\mu \tanh(x)$ can be approximated as the linear equation $M = N\mu x$ (that is, $M = N\mu 2H / k_B T$), as H/T increases there is a levelling off of the magnetization curve near the value $N\mu$. This is indeed the behavior seen for $GdFe_4Al_8$ and $GdMn_4Al_8$ in Figure IV.12. The fact that the curve for $GdCu_4Al_8$ appears to be a straight line is not a contradiction of this phenomenon: saturation simply has not yet been reached, even at the high applied field of 150kOe.

It should also be noted that it is the behavior of $GdCu_4Al_8$ that is different from the other two materials. In that case, the transition temperature from an unordered to an ordered state lies above 4.2K, and the transition metal atoms (copper atoms) are not magnetic. In the case of the manganese and iron compounds, the ordering

Figure IV.11. Magnetization versus applied field for GdM_4Al_8 compounds



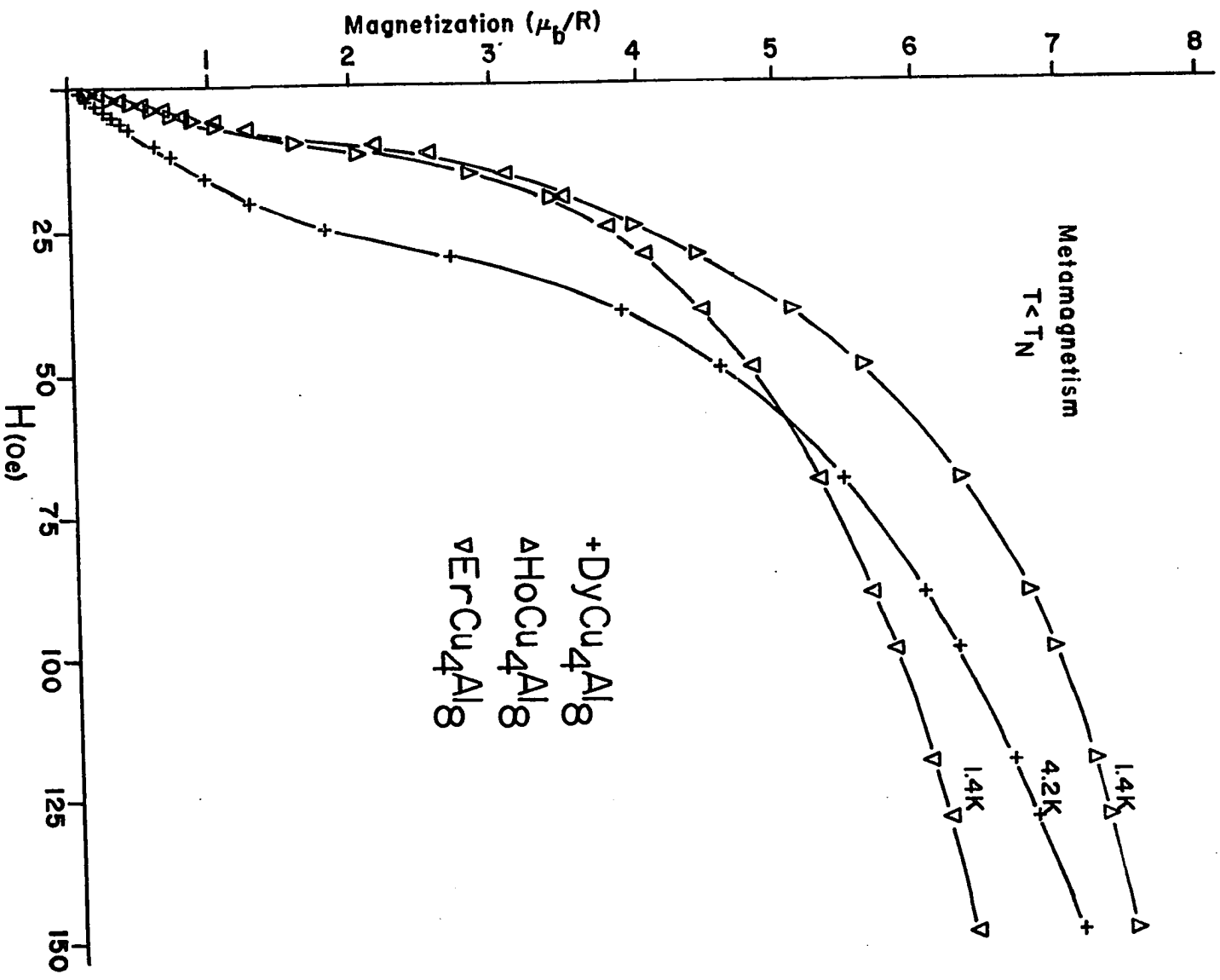
temperature lies below the temperature at which this data was taken, and the 3d elements are magnetic. It is for these reasons that we see the difference in the magnetization curves.

Figure IV.12 plots magnetization against applied field, as in Figure IV.11. This time, low temperature curves for the three copper compounds DyCu_4Al_8 , HoCu_4Al_8 , and ErCu_4Al_8 are shown. All three curves demonstrate the phenomenon of metamagnetism. At zero field the rare earth atoms show antiferromagnetic ordering, as will be mentioned in the discussion of the neutron diffraction data. An applied field can introduce a change in the magnetic structure, however, a change shown schematically in Figure IV.13. Here, a field applied at a right angle to the directions of the moments induces a metastable change in the magnetic structure. In Figure IV.12 the effects of this change are shown: above some critical field H_c the curves deviate upwards from straight line behavior.

Figure IV.14 shows a different sort of plot, this being of the reciprocal susceptibility ($1/\chi$) versus temperature. The values of χ used in this illustration were calculated from the equation $\chi = M/H$, and are based on data such as that depicted in Figures IV.11 and IV.12, actually, instead of $\chi = M/H$, the expression $\chi = \lim_{H \rightarrow 0} (M/H)$ was used.

The Curie law $\chi = C/T$ ($C = N\mu^2/3k_B$) can be rewritten as $1/\chi = T/C$, an expression linear in T . This is the genesis of the plot shown

Figure IV.12. Magnetization versus applied field for RCu_4Al_8 compounds



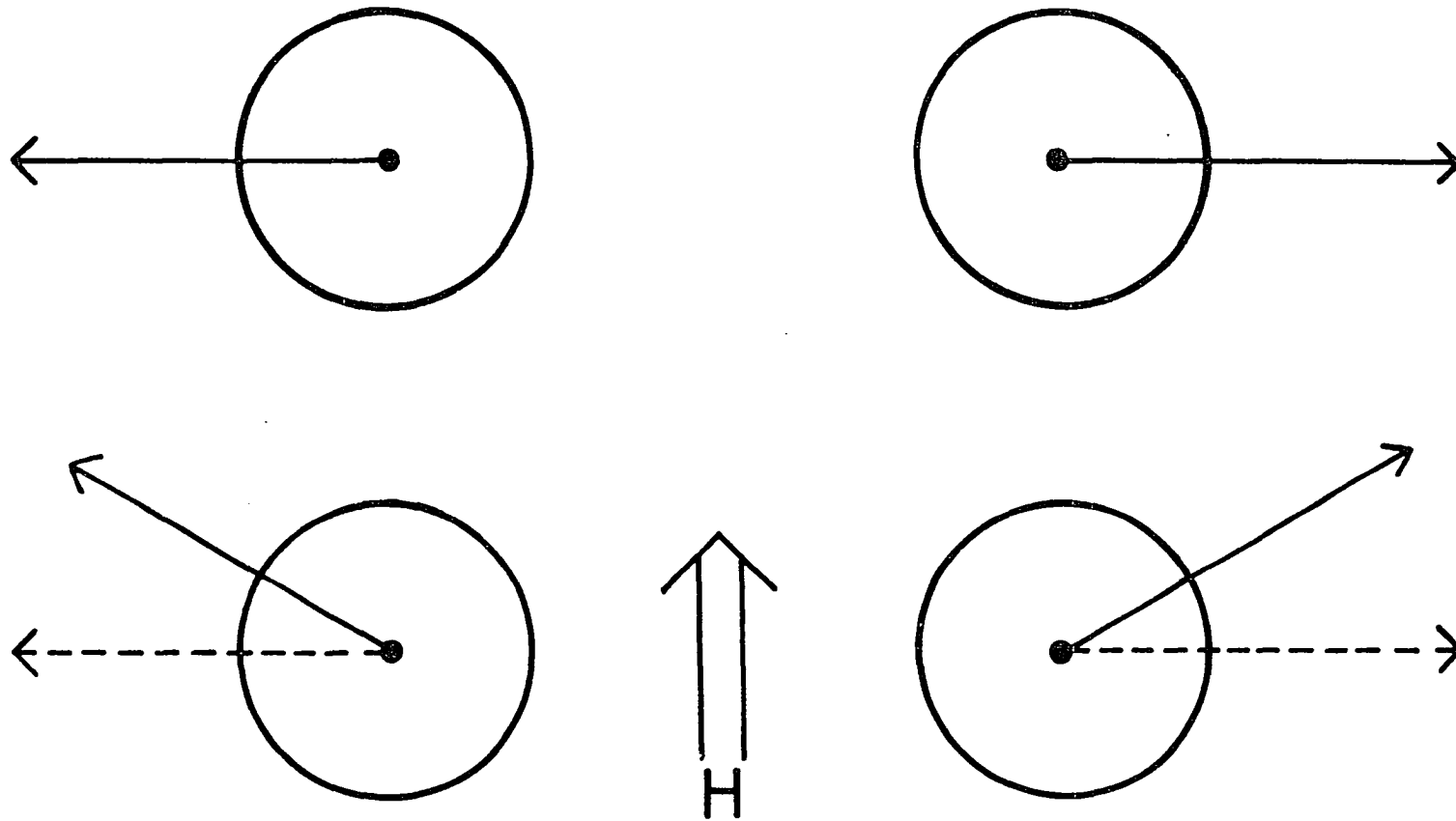


Figure IV.13. Induced metastable magnetic structure

Figure IV.14. Reciprocal susceptibility versus temperature

in Figure IV.15. This figure, after Kittel,⁷⁴ shows the temperature dependence of the magnetic susceptibility in paramagnets, ferromagnets, and antiferromagnets. It can be seen that for paramagnetism the Curie law ($\chi = C/T$) applies; for ferromagnetism the Curie-Weiss law ($\chi = C/(T-T_c)$) applies for temperatures above the ordering (i.e., Curie) temperature, ($T > T_c$); for antiferromagnetism an additional law $\chi = C/(T+\theta)$ holds when the temperature is above the ordering (i.e., Néel) temperature ($T > T_N$). This last equation may be written as $1/\chi = (T+\theta)/C$. The quantity designated by the symbol θ_p is known as the paramagnetic Curie temperature. These quantities need not be positive; if the negative magnetic interactions dominate (i.e., forces which tend towards antiparallel arrangements of moments), θ_p will be a negative number.

The insert of Figure IV.14 shows the low temperature behavior of DyCu_4Al_8 and GdFe_4Al_8 . The lowest temperature measured (4.2K) is above the ordering temperature of the iron compound, and its curve shows the straight line behavior of a paramagnet. However, this temperature of 4.2K is below the ordering temperature of the copper compound, which can be deduced from the well-defined kink in the curve of $1/\chi$ versus T . It should be noted that this transition is also marked by peaks in the heat capacity and thermal expansion coefficient, but measurement of these values lies outside of the scope of this thesis.

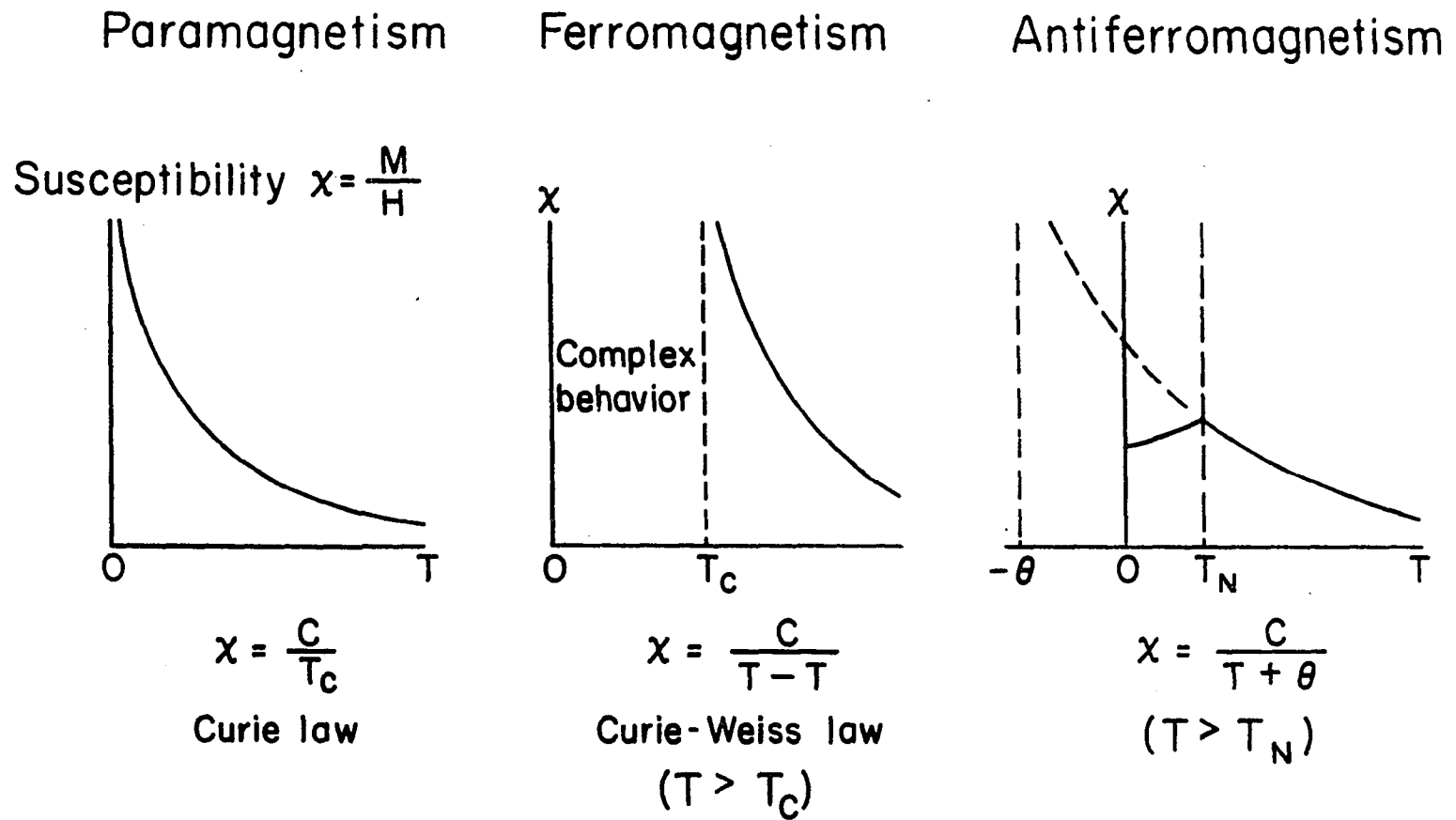


Figure IV.15. Behavior of susceptibility for various types of magnetism

The effective magnetic moment of the material being considered can also be gained from analysis of such curves as shown in Figure IV.15. As $1/\chi = (T+\theta)/C = (T+\theta)3k_B/N\mu_{\text{eff}}^2$, it is easy to see that the slope of such a curve may be used to calculate μ_{eff} . Information such as T_N , θ_P , and μ_{eff} are tabulated in Table IV.10 for all materials herein considered. As shown in that table, the susceptibility experiments showed negative paramagnetic Curie temperatures for all compounds studied, with the onset of the paramagnetic state occurring from about 2K up to 20K, depending upon the compound. Effective magnetic moments, calculated from the relationship between reciprocal susceptibility and temperature, proved to be those of the free ion rare earths.

Neutron Diffraction Data

Powder neutron diffraction data were taken at the Laboratoire de Diffraction Neutronique du Departement de Recherche Fondamentale au Commissariat a l'Energie Atomique de Grenoble (Neutron Diffraction Laboratory, Department of Fundamental Research, Atomic Energy Commission of Grenoble, France). Thermal neutrons were monochromated via the $|200|$ reflection of a copper crystal, giving a wavelength of 1.14 Å. The neutron beam was then diffracted by the sample, and the diffracted neutrons were detected by a BF_3 counter. 30' collimation was provided by cadmium Soller slits. In general, counting was continued at a particular 2θ setting until 375,000 (or 750,000) monitor counts were recorded. Typically this would result in peak heights of

Table IV.10. Magnetic properties of RM_4Al_8 compounds

Compound	Ordering Temp. (K)	θ_P (K)	μ_{eff} (μ_B/R)	μ_{the} (μ_B/R) ⁷⁴
GdMn ₄ Al ₈	<4.2	-8	7.93	7.94
TbMn ₄ Al ₈ ^a	6.2	~0	9.84	9.72
DyMn ₄ Al ₈ ^a	2.4	~0	10.69	10.63
HoMn ₄ Al ₈ ^a	3.4	~0	11.03	10.60
GdFe ₄ Al ₈	<4.2	-7	7.92	7.94
TbFe ₄ Al ₈ ^a	<20, >4.2	-15	9.64	9.72
HoFe ₄ Al ₈ ^a	<4.2	-24	12	10.63
ErFe ₄ Al ₈ ^a	<4.2	-7	11.5	10.60
GdCu ₄ Al ₈	15	-18	7.77	7.94
TbCu ₄ Al ₈	26	-5.5	9.65	9.72
DyCu ₄ Al ₈	21	-12	10.86	10.6
HoCu ₄ Al ₈	3.0	-6	9.80	10.6
ErCu ₄ Al ₈	2.8	-8	9.34	9.6
TmCu ₄ Al ₈	<2.6	0.5	7.64	7.56

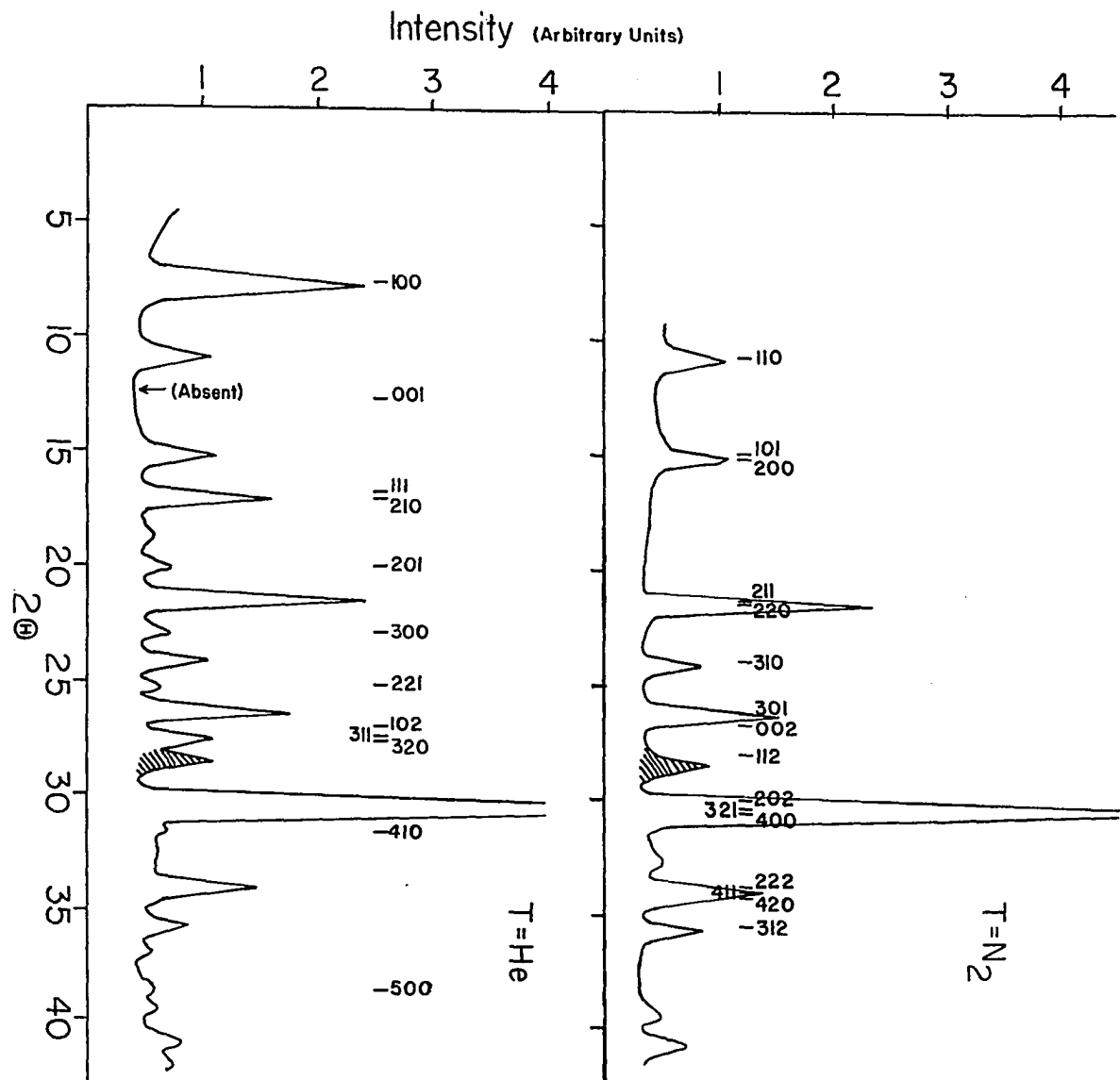
^aPrivate communication from Baye Kebe, CNRS Laboratories, Grenoble, France.

the order of 10^3 - 5×10^4 counts being superimposed upon a background of some 5000 counts. Data were taken at temperatures of 300, 77, 4.2, and 1.4K.

Figures IV.16 and IV.18 show typical neutron diffraction patterns for the compounds considered. Figure IV.16 shows the scattering patterns for DyCu_4Al_8 taken at 77 and 4.2K. As the Néel temperature for this compound is 21K, it can be seen that the upper pattern shows only nuclear (nonmagnetic) peaks, whereas the lower pattern also shows contributions from magnetic scattering which results from the magnetic structure of the material.

Analysis of these patterns is as follows. At 77K, the pattern obeys the selection rule $h+k+l=2n+1$, extinct, in keeping with the fact that DyCu_4Al_8 crystallizes in the body centered tetragonal space group $I4/mmm$. At 4.2K, however, new lines have appeared, lines which obey the selection rule $h+k+l=2n+1$, present. The intensities of the $h+k+l=2n$ lines remain unchanged from 77K to 4.2K, and the 001 reflection is absent at the lower temperature. Analysis of the extinction condition behavior shows the magnetic structure of DyCu_4Al_8 to be an antiferromagnetic one; the absence of the 001 reflection fixes the direction of the moments as being parallel to the c axis. A representation of the magnetic structure of DyCu_4Al_8 is given in Figure IV.17; a listing of intensity data is given for the nuclear contributions (77K) and the magnetic ones (4.2K) in Table IV.10. It should be noted

Figure IV.16. Neutron diffraction patterns for DyCu_4Al_8 :
above, 77K; below, 4.2K



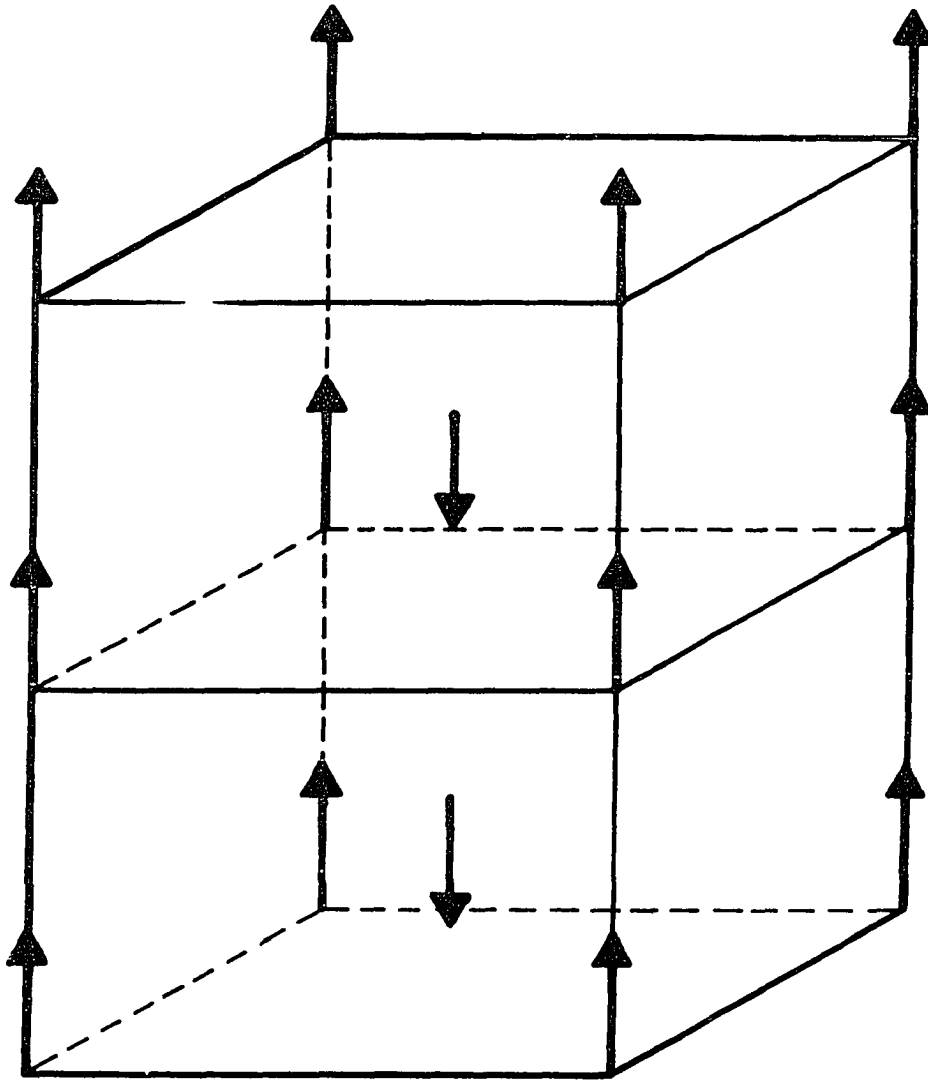


Figure IV.17. Magnetic structure of DyCu_4Al_8

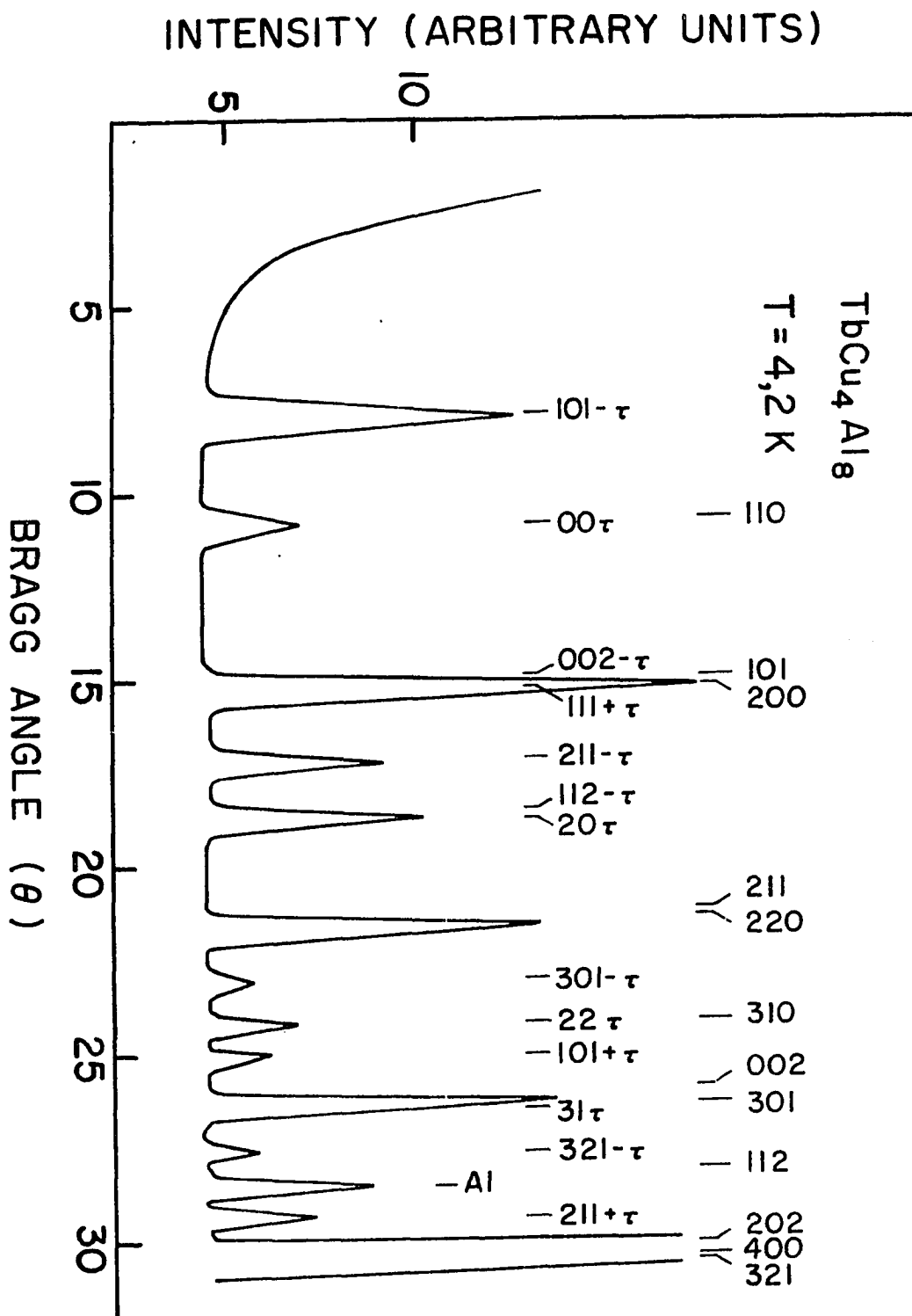


Figure IV.18. Neutron diffraction pattern for TbCu₄Al₈

Table IV.11.a. Nuclear intensities for DyCu_4Al_8 (77K)

hkl	I_{calc}	I_{obs}
200	8.8	45.2
101	37.4	
220	158.2	301.9
211	142	
310	81.9	84
002	16.8	261.6
301	259.9	
112	47.6	-
202	912.5	
321	742	2162
400	550.4	
330	62.7	-
420	185.1	
411	1.5	499.5
222	274.7	

Table IV.11.b. Magnetic intensities for DyCu_4Al_8 (4.2K)

hkl	I_{calc}	I_{obs}
100	92.4	118
111	66.1	256.8
210	165.6	
201	91	79.4
300	76.1	82
221	104.4	91
102	10.2	
311	204.8	379
320	133.2	

that DyCu_4Al_8 , HoCu_4Al_8 , and ErCu_4Al_8 behave in substantially the same manner.

Figure IV.19 shows the scattering pattern for TbCu_4Al_8 taken at 4.2K, and the intensity data is tabulated in Table IV.18.⁶⁶ Here analysis is more complicated, for the magnetic peaks are of the type $(h,k,\ell+\tau)$, where $\tau = 0.84$. The intensity of the reflection $(301-\tau)$, associated with a direction nearly in the basal plane, is much weaker than that for the $101+\tau$ reflection, associated with a direction more nearly parallel with the c axis. This is in contrast with the 300 and 102 magnetic reflections for DyCu_4Al_8 , the former of which is nearly an order of magnitude larger than the latter. From this information one can conclude that the magnetic moments of the terbium atoms of TbCu_4Al_8 lie in the basal plane of the crystallographic structure.

Solution of the structure shows that a model consistent with the data (and resulting in an R factor of 7%) is that the terbium atoms are ordered ferromagnetically in each plane perpendicular to the c direction, and have a mean magnetic moment $\sigma_\mu = 6.5\mu_B/\text{Tb}$. The component $(0,0,0.84)$ defines a modulation of moments or moment direction along the c direction, but without single crystal data it is impossible to distinguish a structure in which the terbium atoms show a helimagnetic structure with a constant moment $\sigma = \sigma_\mu$, from a structure in which the terbium atoms show a modulated structure with a maximum moment of $(\pi/2)\sigma_\mu$, a value equal to $10.2\mu_B/\text{Tb}$. However, as that

Table IV.12.a. Nuclear intensities for TbCu_4Al_8 ($T = 77\text{K}$)

hkl	I_{calc}	I_{obs}
110	1.2	0.5
101	0.8	46.4
200	45.6	
220	76.2	
211	20.8	97.0
310	15.2	
002	2.2	118.4
301	116.2	
202	617.1	
321	343	1249.7
400	289.6	

Table IV.12.b. Magnetic intensities for TbCu_4Al_8 ($T = 4.2\text{K}$)

hkl	I_{calc}	I_{obs}
101- τ	25.2	24
00 τ	11	12
002- τ	10.6	44.9
11 τ	34.5	
211- τ	40.6	55.4
112- τ	26.5	
20 τ	28.9	
202- τ	28.1	34.8
301- τ	18.5	16.1
22 τ	21.4	23.8
101+ τ	32.6	26.5
31 τ	40	4.1
321+ τ	33.3	34.6
211+ τ	52.3	60

value of $10.2 \mu_B/\text{Tb}$ is very close to the value of $9.72 \mu_B/\text{Tb}$, the free ion value of terbium,⁷⁴ and μ_{eff} measured for TbCu_4Al_8 is $9.65 \mu_B/\text{Tb}$ (cf. Table IV.10), it seems that the modulated structure is most likely. This conclusion is consistent with the structure derived for TbZn_{12} ; in both compounds only the Tb is magnetic, and in TbZn_{12} the structure is modulated along the c direction.⁶⁶

Analysis of the neutron diffraction patterns for the RMn_4Al_8 and RFe_4Al_8 compounds is significantly more difficult than analysis of the RCu_4Al_8 data, since the manganese and iron atoms both have localized magnetic moments, just as the behavior of the RMn_{12} compounds⁵⁷ is much more complicated than that of the RZn_{12} compounds.⁶⁶ At present no definitive solution of the structures of these ternary alloys has been obtained. However, based on the results of susceptibility and Mössbauer experiments, van der Kraan and Buschow⁷⁰ draw several conclusions about the RFe_4Al_8 alloys. The Fe atoms order antiferromagnetically at about 165K (from Mössbauer data, $T_N = 184.7\text{K}$ for YFe_4Al_8 and $T_N = 165\text{K}$ for TbFe_4Al_8), but the rare earth atoms do not order until temperatures of 30K or less are reached, at which temperature they assume a ferromagnetic structure. This is in substantial agreement with results of our own magnetic susceptibility experiments, our preliminary neutron structural studies, and the phenomenon of Deportes' two ordering temperatures for the RMn_{12} compounds,⁶⁴ shown pictorially in Figure IV.6, and described in Table IV.4.

Conclusion and Future Work

These studies show ferromagnetic behavior of the manganese and iron compounds, and antiferromagnetic behavior for the copper ones. Unfortunately, just as in the case of the previous RMn_{12} studies, the magnetocrystalline structures of the two ferromagnetic classes proved too difficult for rapid solution. However, the work done on the RCu_4Al_8 compounds represents an important step, a step which helps to bridge the gap between understanding the structure and behavior of the simpler RZn_{12} compounds and the more complex RMn_{12} compounds. The lack of definitive results for the RFe_4Al_8 and RMn_4Al_8 compounds at present is undoubtedly temporary: work continues using not only the neutron diffraction and susceptibility measurements experiments described above, but also Mössbauer experiments using small amounts of iron 57 in both compounds.

In addition, it is believed that the series of pseudobinary compounds $\text{R}(\text{Co}_x\text{Mn}_{1-x})_{12}$ is stable up to about $x = 0.8$ (i.e., $\text{RCo}_{10}\text{Mn}_2$). If so, these compounds should be of considerable importance, for they should share many of the properties of the RCo_5 parent compounds: high Curie temperatures, great anisotropy, and, for certain of the rare earths, ferromagnetism; in short, they have great promise as permanent magnets.

Research into the structures and properties of the rare earth intermetallics is presently at a tantalizing stage. One is frequently

able to predict behavior even before a compound is made, and thus one can custom design compounds. Unfortunately, or fortunately perhaps, this does not always work, and thus there is still large amounts of basic research to be done in this field.

CHAPTER V.

USE OF RADIAL DISTRIBUTION FUNCTIONS
IN STRUCTURAL ANALYSIS

Introduction

The technique of producing a Patterson function from diffraction data has long been used to help resolve crystalline structures when the structure is unknown, for this technique does not require presupposed structural knowledge, other than rudimentary lattice information. In an exactly analogous manner, radial distribution function (RDF) analysis has been used to describe the structure of liquids and other amorphous materials. In this chapter, a combination of these two techniques will be considered and applied to the RDFs calculated from neutron diffraction data collected for polycrystalline metal hydrides.

Theoretical

As discussed in Stout and Jensen,⁸³ A. L. Patterson⁸⁴ showed in 1935 that one may use a Fourier transform of diffraction intensity data as a tool in crystal structure determination. That transform given by Patterson and today bearing his name, may be written as

$$P(u,v,w) = \frac{1}{V} \sum_{h=-\infty}^{\infty} \sum_{k=-\infty}^{\infty} \sum_{l=-\infty}^{\infty} |F_{hkl}|^2 \cos 2\pi(hu + kv + lw), \quad (5.1)$$

where $P(u,v,w)$ is the Patterson function, V is the unit cell volume, h , k , and l take on their usual meaning as crystallographic indices, the terms $|F_{hkl}|^2$ are the intensity data gathered by some manner of diffraction experiment, and u , v , and w are defined as $u = x_1 - x_2$, $v = y_1 - y_2$, and $w = z_1 - z_2$ ((x_1, y_1, z_1) and (x_2, y_2, z_2) being the parameters describing the positions in the unit cell of atoms 1 and 2, respectively). The function $P(u,v,w)$ is of great use in crystallographic analysis since its calculation does not require any description of the crystal structure to be given. That is, the phases of the individual F_{hkl} terms need not be known, for the terms $|F_{hkl}|^2$, rather than F_{hkl} , are used. The Patterson function is of especial utility when the diffraction experiment is performed on single crystals of so-called "heavy-atom" compounds. The interested reader is urged to consult both Stout and Jensen⁸³ and Lipscomb and Jacobson⁸⁵ for further description of Patterson functions and their uses.

For noncrystalline materials, the problem of structural deduction changes, due in greatest part to the lack of long range order and the isotropic character of the scattering. However, in 1915 Peter Debye laid the groundwork for an important technique for the analysis of such data,⁸⁶ the technique of radial distribution function (RDF) analysis. Exhaustive description of RDFs and their calculation may be found in Klug and Alexander,⁸⁷ Ergun,⁸⁸ Karnicky and

Ping,⁸⁹ Blum and Narten,⁹⁰ and Kruh,⁹¹⁻⁹² as well as many, many references found in those papers.

In general, the articles cited above concern themselves with the structural description of liquids and amorphous solids, frequently using an experiment very similar to the standard powder diffraction experiment. As many substances do not exist in crystalline form, and indeed the very noncrystallinity itself of other materials is frequently of interest, these experiments are of great value today. However, as will be discussed below, there is no absolute requirement that amorphous substances be studied; polycrystalline samples (powders) may also be studied using these techniques.

As a complete development of the mathematics of RDF analysis is given in many of the references already cited, only a sketch of that development will be presented here, a sketch which follows Kruh.⁹¹⁻⁹² A glossary of terms is given in Table V.1.

We can write an expression for $I(\theta)$, the observed intensity at angle θ :

$$I(\theta) = N(I_{\text{coh}}(\theta) + I_{\text{inc}}(\theta))P(\theta)L(\theta)A(\theta)G(\theta) \quad (\text{V.2})$$

where symbols are defined in Table V.1.

It should be noted that for neutron diffraction $P(\theta) = 1$ for all θ , and $A(\theta)$ is very nearly a constant; for all practical purposes we can rewrite equation V.2 as

Table V.1. Glossary of terms

N	= number of atoms
θ	= scattering angle
$I_{\text{coh}}(\theta)$	= coherent intensity
$I_{\text{inc}}(\theta)$	= incoherent intensity
$P(\theta)$	= polarization correction = 1 for neutron diffraction
$L(\theta)$	= Lorentz correction = $1/2(1 + \cos^2 2\theta)$
$A(\theta)$	= absorption correction
$G(\theta)$	= a geometric factor, generally = 1
K	= $NP(\theta)A(\theta)G(\theta)$, approximately a constant in θ for neutron diffraction
$B(\theta)$	= background expression
f_m, f_n	= atomic form factor for $m^{\text{th}}, n^{\text{th}}$ atoms
b_m, b_n	= nuclear form factor for $m^{\text{th}}, n^{\text{th}}$ atoms
s	= $(4\pi \sin \theta)/\lambda$
λ	= radiation wavelength
r_{mn}	= separation of $m^{\text{th}}, n^{\text{th}}$ atoms

$$I(\theta) = K(I_{\text{coh}}(\theta) + I_{\text{inc}}(\theta))L(\theta) \quad (\text{V.3})$$

It is with the term $I_{\text{coh}}(\theta)$ that our interest ultimately lies, and thus the term $I_{\text{inc}}(\theta)$ must be accounted for. Although elaborate analytical techniques for description of $I_{\text{inc}}(\theta)$ exist, in the case of most neutron diffraction experiments it seems that the background may be "eye-balled" out, taking with it $I_{\text{inc}}(\theta)$ and all spurious contributions to the observed powder pattern. Equation V.3 can thus be rewritten as

$$I(\theta) = KI_{\text{coh}}(\theta) + B(\theta), \quad (\text{V.4})$$

where $B(\theta)$ is the total background contribution from all sources, and the Lorentz correction has been applied to the data.

It may be shown that (for x-ray diffraction)

$$I_{\text{coh}_X}(s) = N^{-1} \sum_m \sum_n f_m(s) f_n(s) \frac{\sin(sr_{mn})}{sr_{mn}}. \quad (\text{V.5})$$

where symbols are defined in Table V.1.

Description of the intensity data in terms of s , rather than θ , has the advantage that two experiments performed upon the same sample, but at different radiation wavelengths, yield the same spacing of diffraction maxima.

For neutron diffraction, Equation V.5 becomes

$$I_{\text{coh}_N}(s) = N^{-1} \sum_m \sum_n b_m b_n \frac{\sin(sr_{mn})}{sr_{mn}}, \quad (\text{V.6})$$

where the b parameters, the atomic nuclear scattering amplitudes, are constant in all s .

In the case of x-ray diffraction, Equation V.5 may be approximated as

$$I_{\text{coh}_X}(s) = N^{-1} f^2(s) \sum_m \sum_n \frac{\sin(sr_{mn})}{sr_{mn}}, \quad (\text{V.7})$$

where $f^2(s)$ is a term used to simplify calculation by representing aggregate scattering. In analogous fashion, we may rewrite Equation V.6 as

$$I_{\text{coh}_N}(s) = N^{-1} b^2 \sum_m \sum_n \frac{\sin(sr_{mn})}{sr_{mn}} \quad (\text{V.8})$$

The approximations introduced in Equations V.7 and V.8 enable us to rewrite those equations as

$$I_{\text{coh}_X}(s) = f^2(s) + N^{-1} f^2 \sum_{m \neq n} \frac{\sin(sr_{mn})}{sr_{mn}} \quad (\text{V.9})$$

$$I_{\text{coh}_N}(s) = b^2 + N^{-1} b^2 \sum_{m \neq n} \frac{\sin(sr_{mn})}{sr_{mn}}. \quad (\text{V.10})$$

Noting that we may consider $4\pi r^2 \rho(r) dr$ to be a continuous function with which we can express the number density of atoms lying at a distance between r and $r+dr$ from a given atom, for N total atoms we may write this as $N \cdot 4\pi r^2 \rho(r) dr$. This permits conversion of Equations V.9 and V.10:

$$i_X(s) = \frac{I_{\text{coh}_X}(s) - f^2(s)}{f^2(s)} = \int_0^{\infty} 4\pi r^2 \rho(r) \frac{\sin(sr)}{sr} dr \quad (\text{V.11})$$

$$i_N(s) = \frac{I_{\text{coh}_N}(s) - b^2}{b^2} = \int_0^{\infty} 4\pi r^2 \rho(r) \frac{\sin(sr)}{sr} dr \quad (\text{V.12})$$

(As the second halves ^{of these} of these equations are of the same form, the subscripts X and N will now be dropped.)

Equations V.11 and V.12 may be rewritten as

$$si(s) = \int_0^{\infty} 4\pi r \rho(r) \sin(sr) dr. \quad (\text{V.13})$$

The integral in Equation V.13 does not converge; however, the equation may be rewritten as

$$si(s) = \int_0^{\infty} 4\pi r [\rho(r) - \rho_0] \sin(sr) dr + \int_0^{\infty} 4\pi r \rho_0 \sin(sr) dr \quad (\text{V.14})$$

where ρ_0 represents the average density.

As the additive part of this equation is practically zero, except for small s (an area generally avoided), it may be ignored. Now, as the intensity function $si(s)$ is the Fourier sine transform of $4\pi r(\rho(r) - \rho_0)$, we can write the inverse relationship

$$4\pi r(\rho(r) - \rho_0) = \frac{2}{\pi} \int_0^{\infty} si(s) \sin(sr) ds. \quad (\text{V.15})$$

Multiplying both sides by r , and rearranging, we get

$$4\pi r^2 \rho(r) = 4\pi r^2 \rho_0 + \frac{2r}{\pi} \int_0^{\infty} si(s) \sin(sr) ds. \quad (\text{V.16})$$

The term $4\pi r^2 \rho_0$ describes a parabola in r , a parabola which represents the RDF, assuming a homogeneous sample, i.e. exhibiting no structure. Those fluctuations resulting from the inhomogeneous nature of real matter are introduced by the integral term of Equation V.16.

However, Equation V.16 must be altered to describe experimental data, for an infinite set of data cannot be collected. As $s \equiv 4\pi \sin\theta/\lambda$, it can be seen that $0 \leq s \leq 4\pi/\lambda$ are the absolute limits of integration. In practice, however, some s_{\min} is chosen to avoid problems with the direct beam, and/or the aforementioned problems with the additive part of Equation V.14. Likewise, an $s_{\max} \leq 4\pi/\lambda$ is generally necessitated by experimental design. As an example, in the diffraction experiment for lutetium hydride described below, $\lambda = 1.293 \text{ \AA}$, $\theta_{\min} = 11^\circ$, and $\theta_{\max} = 47.5^\circ$, values which give $s_{\min} = 1.85 \text{ \AA}^{-1}$, $s_{\max} = 7.17 \text{ \AA}^{-1}$.

Were Equation V.16 to be evaluated as

$$4\pi r^2 \rho(r) = 4\pi r^2 \rho_0 + \frac{2r}{\pi} \int_{s_{\min}}^{s_{\max}} \text{si}(s) \sin(sr) ds, \quad (\text{V.17})$$

severe termination errors would occur, errors that would manifest themselves as extreme rippling of the resultant RDF. These errors may be substantially reduced by application of a suitable damping factor, vis

$$4\pi r^2 \rho(r) = 4\pi r^2 \rho_0 + \frac{2r}{\pi} \int_{s_{\min}}^{s_{\max}} \text{si}(s) \sin(sr) e^{-\delta^2 s^2} ds \quad (\text{V.18})$$

Experience has shown that if $\exp\{-\delta^2 s_{\max}^2\} \sim 0.05$, good RDFs result. It should be noted⁸⁸ that the value chosen for δ is directly related to the peak width at half intensity for a given peak in the resultant RDF, namely that

$$\text{fwhm} = 4\delta(1\ln 2)^{1/2} \sim 3.33\delta. \quad (\text{V.19})$$

Using the above cited example, where $s_{\max} = 7.17 \text{ \AA}^{-1}$, we see that $\text{fwhm} = 0.19 \text{ \AA}$, a value small enough to give satisfactory results for the purposes needed therein.

The value $\rho(r)$ calculated by Equation V.18 may be seen to be exactly analogous to the Patterson function $P(u,v,w)$, given by Equation 5.1; the RDF $\rho(r)$ is a one-dimensional Patterson function. For materials which lack three-dimensional long range order, such as liquids, liquid crystals, amorphous materials, and the like, the RDF frequently represents a useful way of deducing structural information. However, as will be seen below, use of RDFs, need not be limited to just the study of noncrystalline materials.

There are a broad range of compounds which exist in the crystalline state, but for one reason or another defy the experimentalist who desires single crystals of sufficient size to gather data by standard four-circle or film single crystal techniques. For x-ray studies, one is generally required to use a crystal of the order of half a millimeter on a side; for neutron diffraction, single crystals up to a centimeter on a side might be required. For these crystalline

materials, powder diffraction is the only suitable diffraction experiment available.

Powder diffraction experiments are doomed to give poorer results than are obtainable from single crystal work, due to the problem of multiple or overlapping reflections. Techniques to deal with this problem have been developed, most notably by Rietveld,⁹³ but many assumptions and simplifications must be made before the data can profitably be used. It is, however, possible to do RDF work on powder data, thus gaining considerable structural information with no assumptions as to peak shape, width, and so on.

To produce a one-dimensional RDF, one need only follow the scheme described above. To stop at that point, however, throws out all knowledge of the lattice nature of the material being considered; if one already knows that the compound crystallizes in a cubic system with a unit cell size of 7.3 \AA , for example, one should be able to use that information itself in further analysis of the structure using the RDF. A technique to do that will be described below.

A three-dimensional Patterson map may be constructed from a one-dimensional RDF very simply. As the RDF function $\rho(r)$ carries units of weighted interactions per unit volume, one may construct a three-dimensional Patterson map with the same units by assigning to the Patterson function $P(u,v,w)$ at point (u,v,w) that value of the RDF, $\rho(r)$, at the radius appropriate for the distance of point (u,v,w)

from the origin (0,0,0) of Patterson space. By so doing, a three-dimensional Patterson function with spherical symmetry results.

Analysis of single crystal Patterson maps by using superposition techniques has been described by Stout and Jensen⁸³ and Lipscomb and Jacobson.⁸⁵ These are the techniques which can be used in this analysis, as well: one can perform Patterson superpositions on all lattice points with no knowledge of the unit cell contents whatsoever. If other knowledge is available (e.g., that the cell is I-centered, that heavy atoms exist at points (x,y,z) and (x',y',z'), etc.), even further use of the superposition technique may be made.

The RDF-Patterson superposition technique is ideally suited to the study of metal hydride structures. The materials exist as polycrystalline samples, only; the lattice type and description is well known; and some prior knowledge of the metal atom positions is also usually known. Using RDF-Patterson superposition techniques, direct information can be obtained regarding the hydrogen or deuterium positions. They could then be refined using the techniques of Rietveld.⁹³

The compounds MH_x are isostructural with the compounds MD_x , and thus the technique of isomorphous replacement can also be used as a tool in structural elucidation (neutron diffraction). This is especially useful, for whereas the scattering lengths for most nuclei are positive, and in particular deuterium has a positive scattering length of 0.710, hydrogen (protium) has a negative scattering length of -0.374. Comparison of diffraction results of a deuteride and a

hydride of the same material thus can give additional direct information on the structure of the material in question.

The remainder of this chapter will describe the analysis of the radial distribution functions of four compounds, namely $\text{NbH}_{.730}$, $\text{NbD}_{.718}$, $\text{LuH}_{.208}$, and $\text{LuD}_{.205}$. The structure of NbH has been described by DeHaven.⁹⁴ This information will be used to verify that the analysis of the $\text{NbH}_x/\text{NbD}_x$ system is correct. Then, the system $\text{LuH}_x/\text{LuD}_x$ will be considered, that being a system whose structure has been the subject of some debate.

Experimental

Sample Preparation

Samples of niobium hydride and deuteride were kindly provided by Dr. David Peterson of this laboratory. These samples were prepared by bathing pieces of niobium metal which had been heated to 850° C in high pressure (~ 1300 lbs/psi) hydrogen or deuterium gas, some of the gas being subsequently taken up by the niobium metal. Analysis of the samples showed their composition to be $\text{NbH}_{.730}$ and $\text{NbD}_{.718}$. As these samples were quite brittle, they were easily fractured into fine (400 mesh) powder for use in neutron diffraction experiments.

Lutetium hydride and deuteride samples were supplied with equal kindness by Mr. Bernard Beaudry, also of this laboratory, using a technique substantially the same as that used for the niobium compounds. The lutetium samples were in the form of solid metal rods,

approximately 6 mm in diameter and 35 mm in length. As they existed as polycrystalline solids, it was not deemed necessary to break the samples into a fine powder for use in neutron diffraction experiments. Analysis of the two compounds showed their composition to be $\text{LuH}_{.208}$ and $\text{LuD}_{.205}$.

Diffraction Experiments

Neutron diffraction data were taken for the niobium hydride and lutetium deuteride samples at the Ames Laboratory Research Reactor (ALRR) by Patrick DeHaven of this laboratory. As was discussed in his thesis, the experimental design of the neutron diffractometer used was such that in addition to major contribution to diffraction by 2.00 \AA wavelength radiation, considerable ($\sim 14\%$) contribution came from 1.00 \AA radiation, with small ($\sim 1\%$) contribution from 0.67 \AA radiation. This multiwavelength radiation source generates certain difficulties in production and analysis of the RDFs deriving from the neutron diffraction data, as will be discussed below.

For the niobium deuteride and lutetium hydride samples neutron diffraction data were taken by the author at the Missouri University Research Reactor (MURR), located at the Columbia Campus of the University of Missouri. Unlike the data collected in Iowa, the Missouri data were taken using monochromatic radiation of wavelength 1.293 \AA . As mentioned in the acknowledgements of this thesis, the

author is extremely indebted to Dr. William Yelon of the MURR for the high quality of both his assistance and his facility.

Analysis of Diffraction Data

All four data sets were manipulated by the program RDF, written by the author, and available upon request from him or R. A. Jacobson. Results from that program are shown in Figures V.1 through V.8.

The radial distribution functions shown in Figures V.4 and V.8 exhibit three types of interactions: metal-metal; metal-hydrogen (deuterium); and hydrogen-hydrogen (deuterium-deuterium). If one assumes that the structure of a particular metal hydride is the same as its deuteride, and then subtracts the metal hydride RDF from the metal deuteride RDF, the result would be a curve which showed only the metal hydrogen (deuterium) and hydrogen-hydrogen (deuterium-deuterium) interactions. Figure V.9 shows the curve resulting when the RDF for NbH_{0.730} was subtracted from that for NbD_{0.718}, and Figure V.10 shows a similar curve for LuH_{0.208} and LuD_{0.205}.

As mentioned previously, in neutron diffraction, this kind of analysis works particularly well, for the scattering length of hydrogen (protium) is opposite in sign to that for deuterium. The effect of that may be seen in Tables V.2 and V.3.

It should be noted that, for the niobium compounds, the magnitude of the (Nb•D) - (Nb•H) interaction is 6.90 times that of the (D•D) - (H•H) interaction, and that, for the lutetium compounds this

Figure V.1. Neutron diffraction pattern for niobium deuteride: above, raw data; below, with background removed

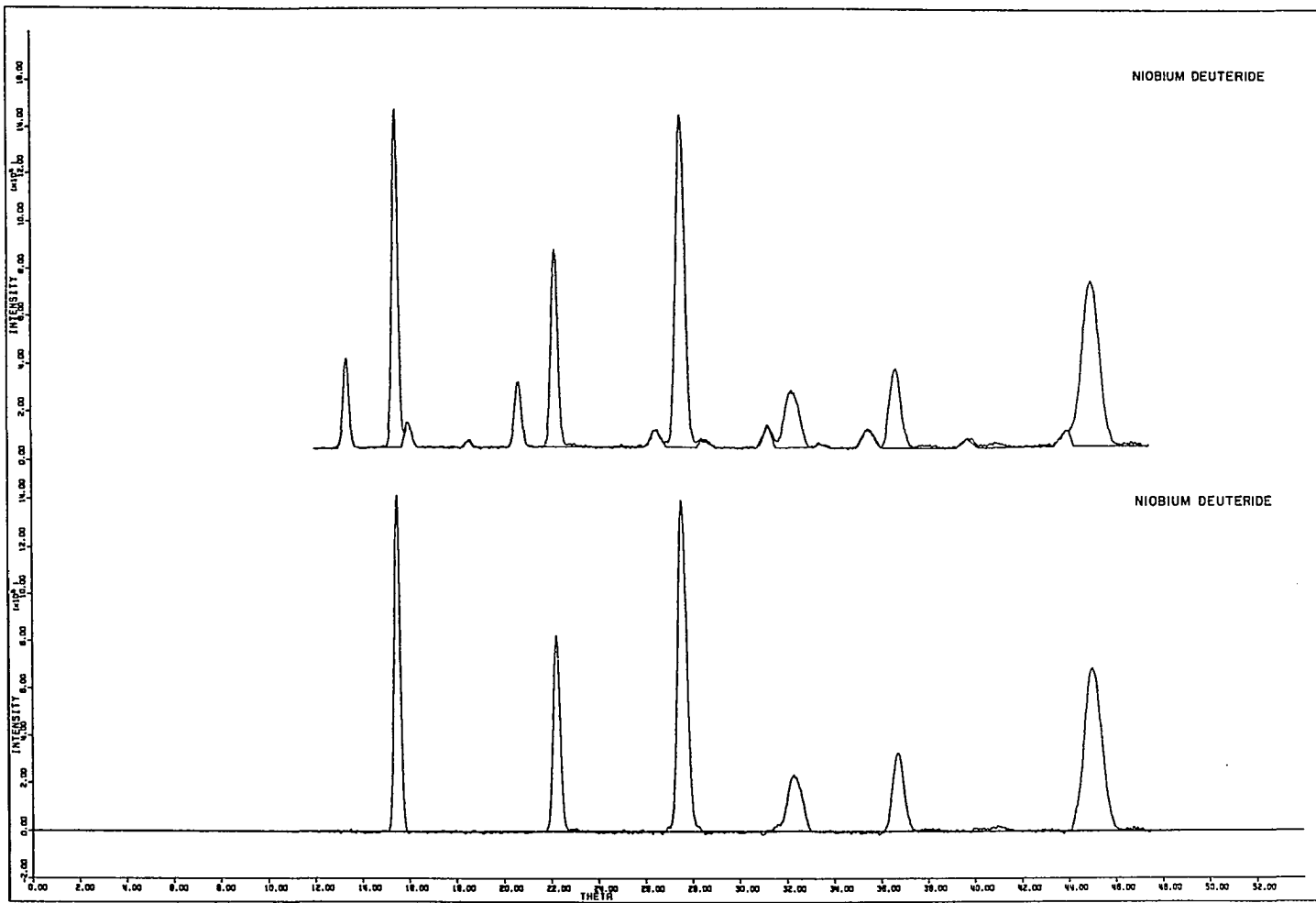


Figure V.2. Neutron diffraction patterns for niobium hydride: above, raw data; below, with background removed

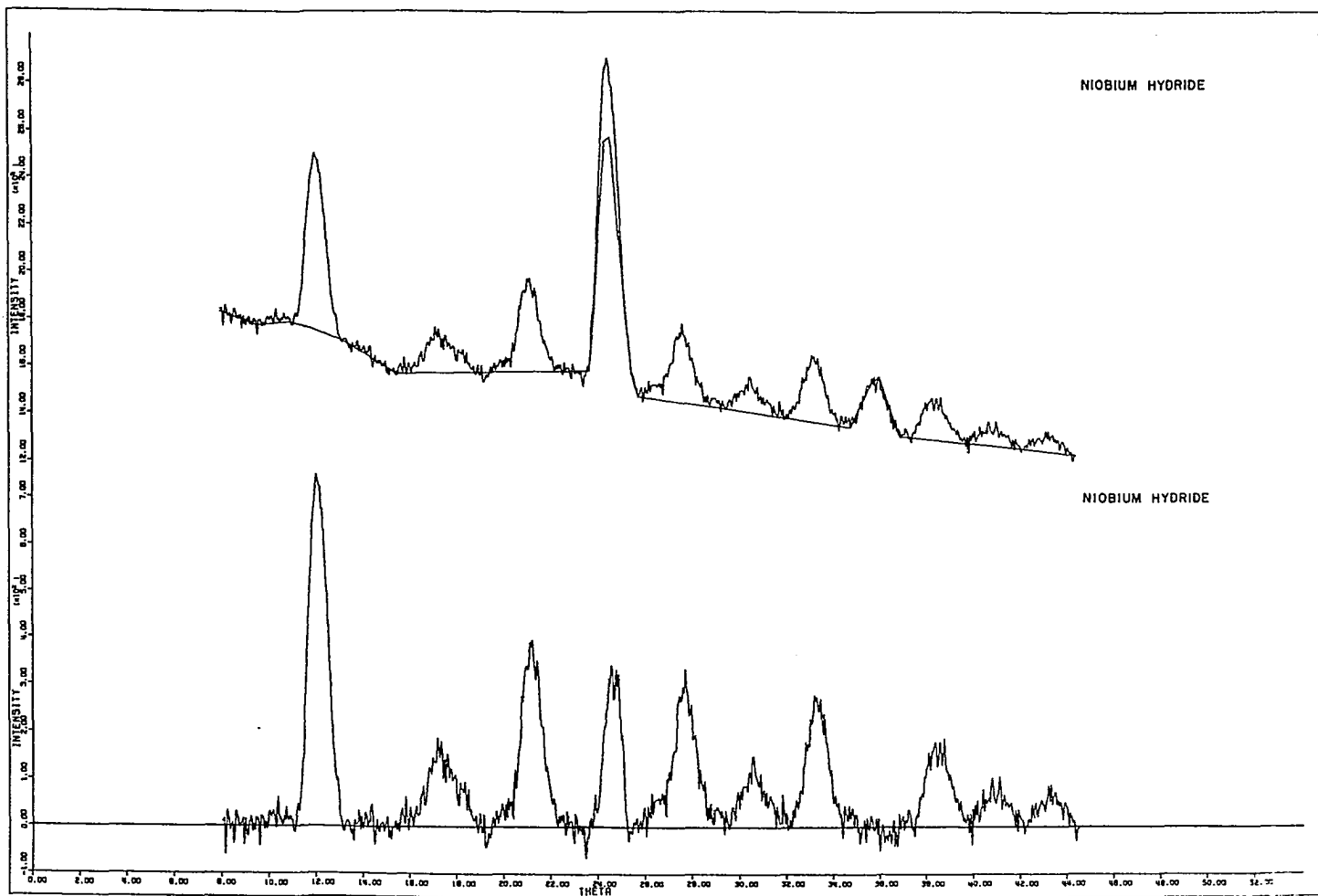


Figure V.3. Curves showing $s \cdot i(s)$ vs. s for niobium deuteride and hydride

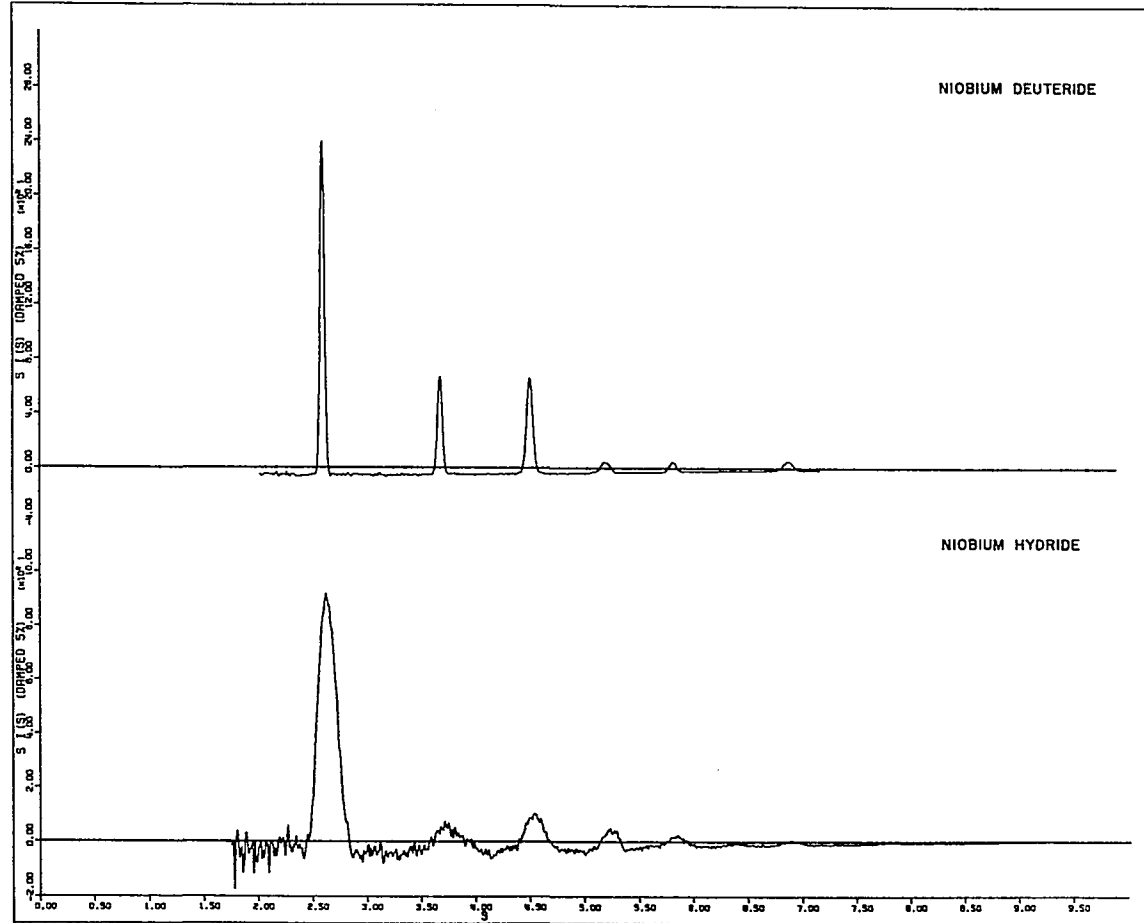


Figure V.4. Radial distribution functions for niobium deuteride and hydride

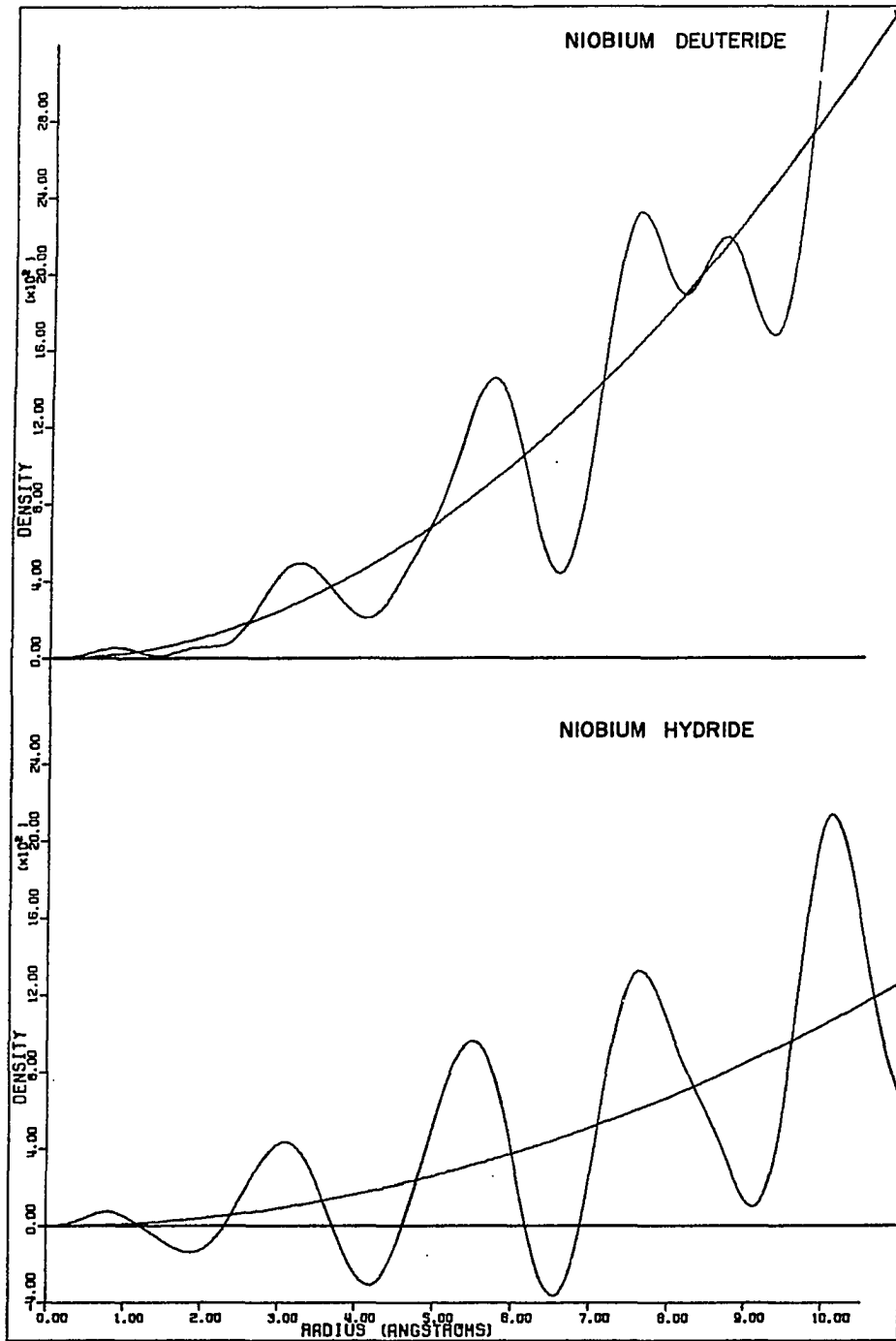


Figure V.5. Neutron diffraction pattern for lutetium deuteride: above, raw data; below, background removed

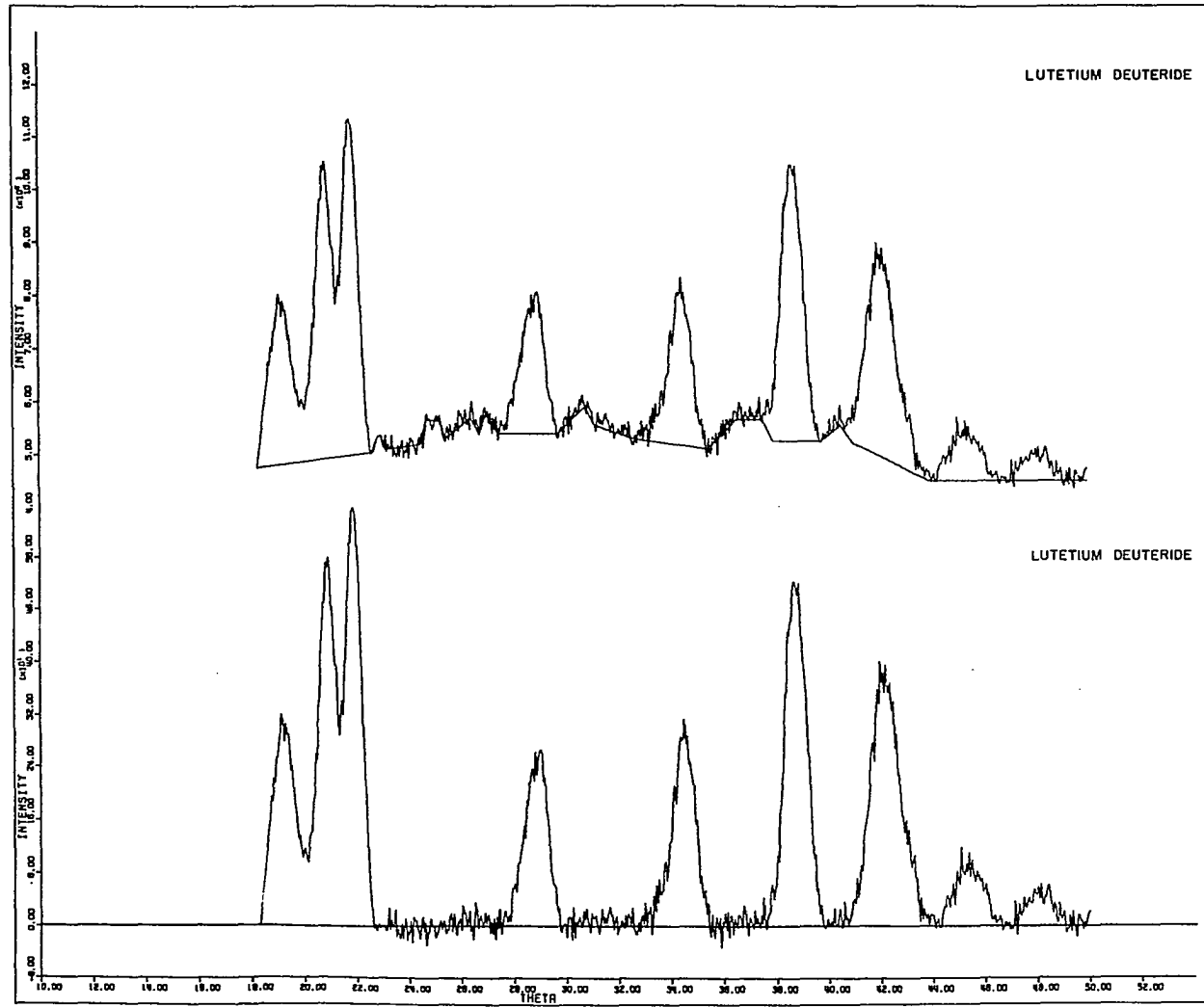


Figure V.6. Neutron diffraction pattern for lutetium hydride: above, raw data; below, with background removed

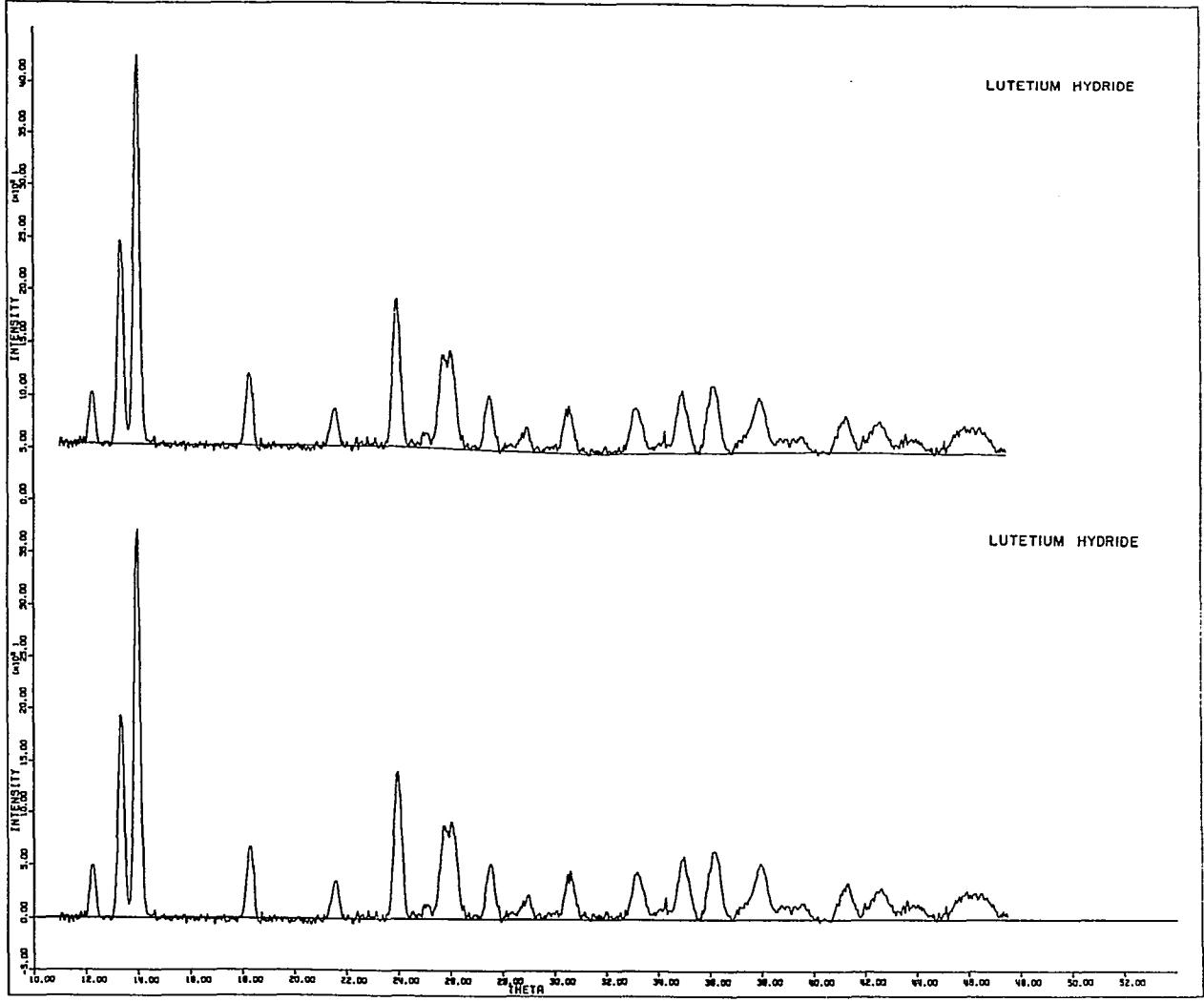


Figure V.7. Curves showing $s \cdot i(s)$ vs. s for lutetium deuteride and hydride

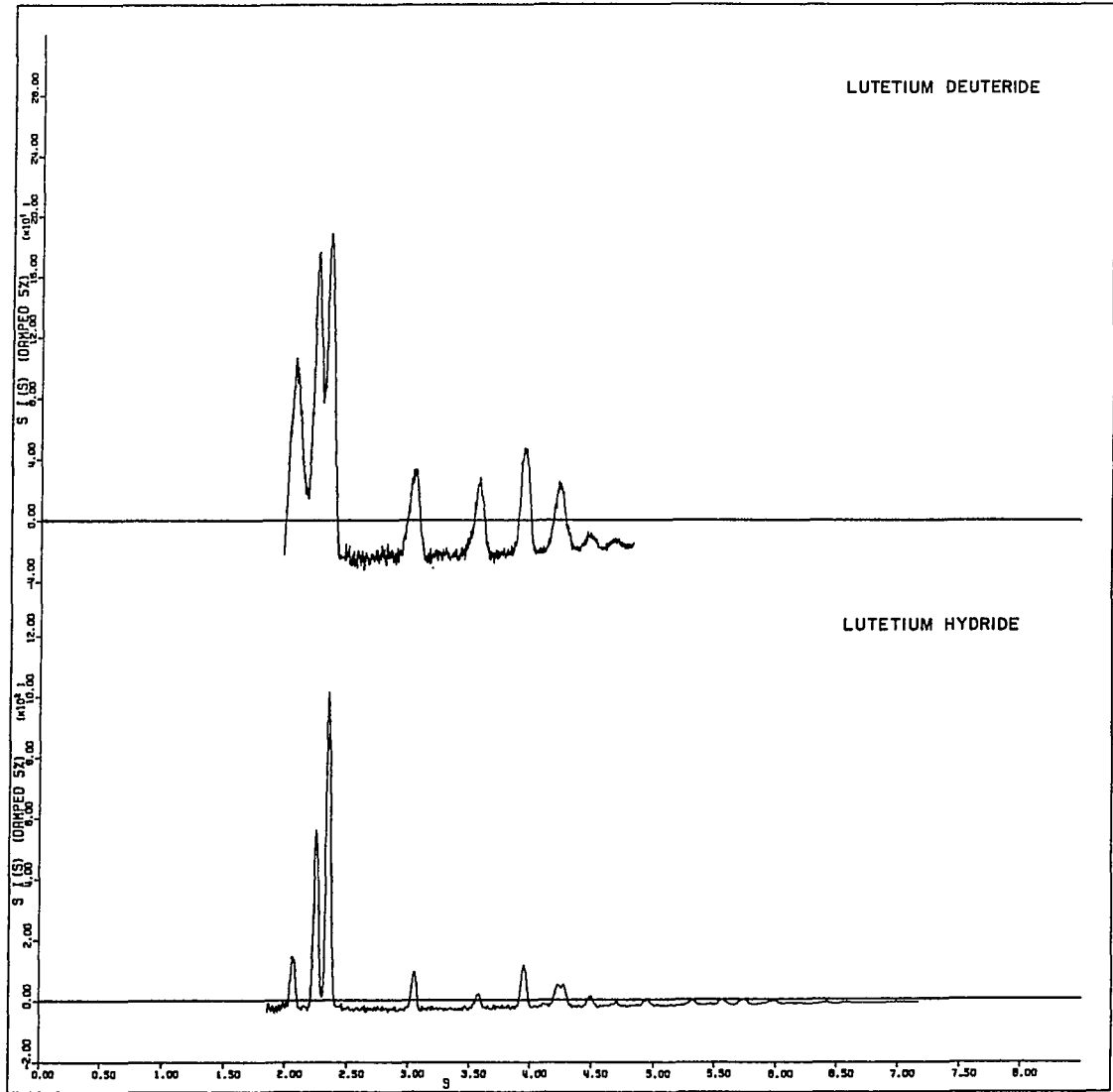


Figure V.8. Radial distribution functions for lutetium deuteride and hydride

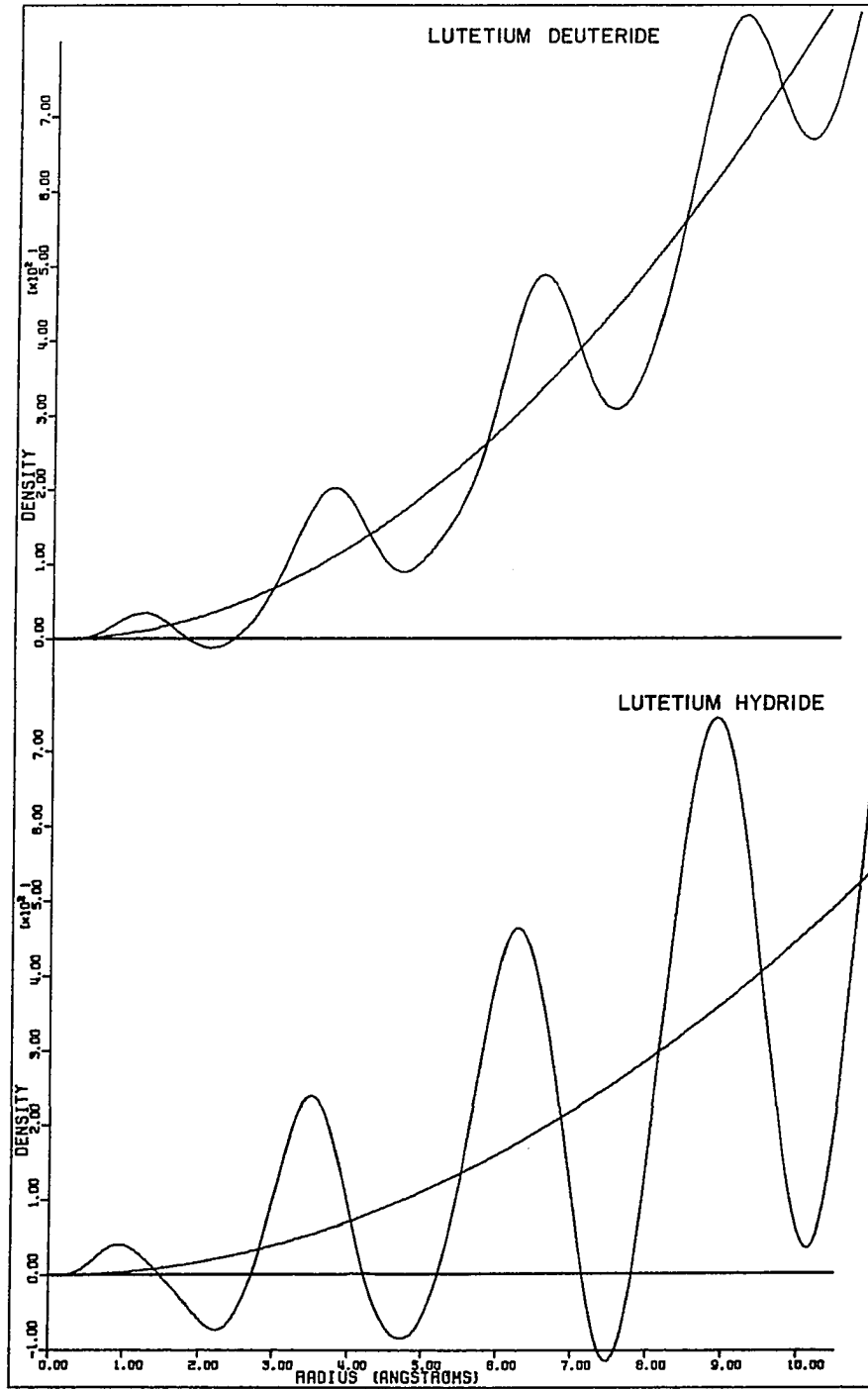


Figure V.9. Difference RDFs for niobium compounds

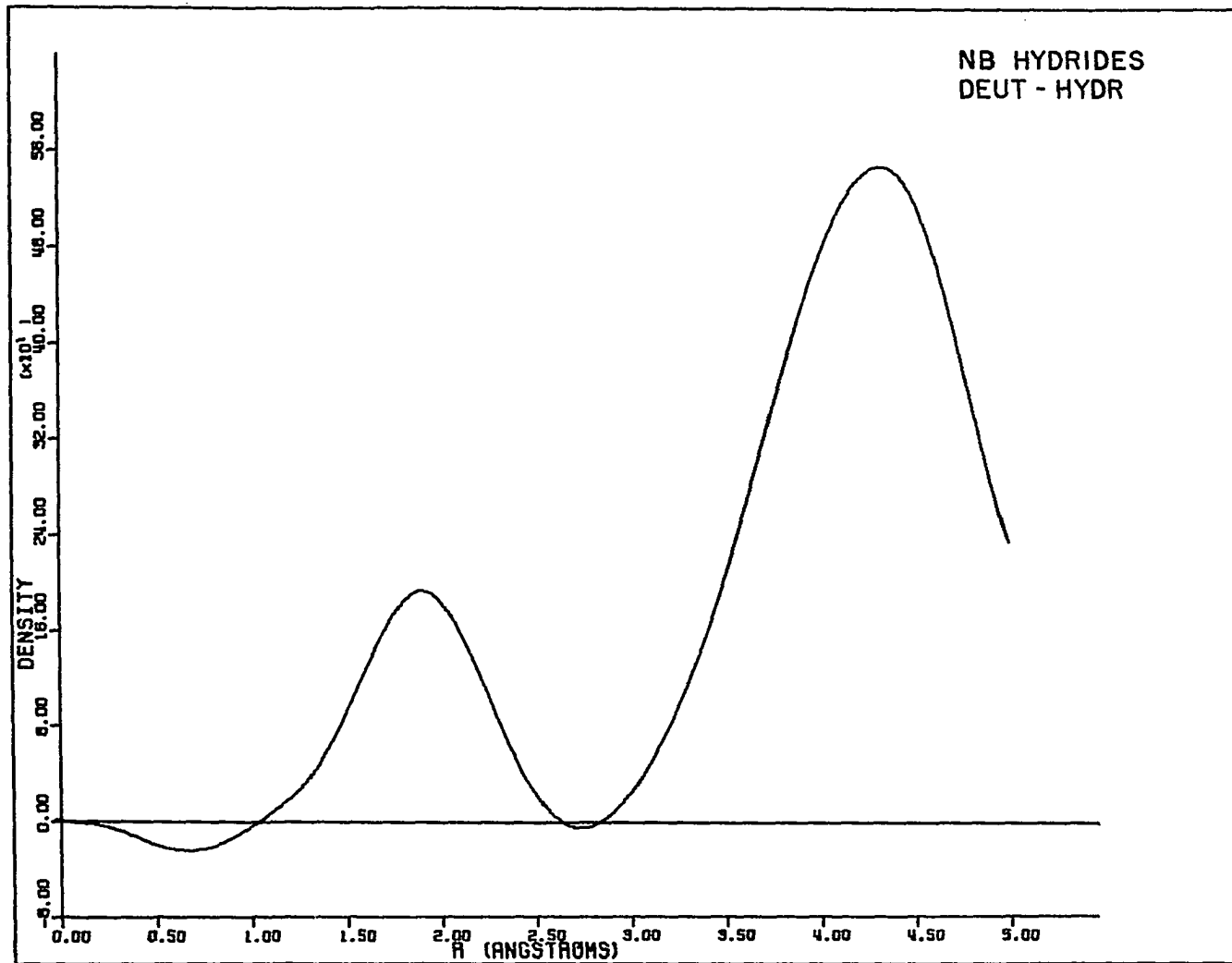


Figure V.10. Difference RDFs for lutetium compounds

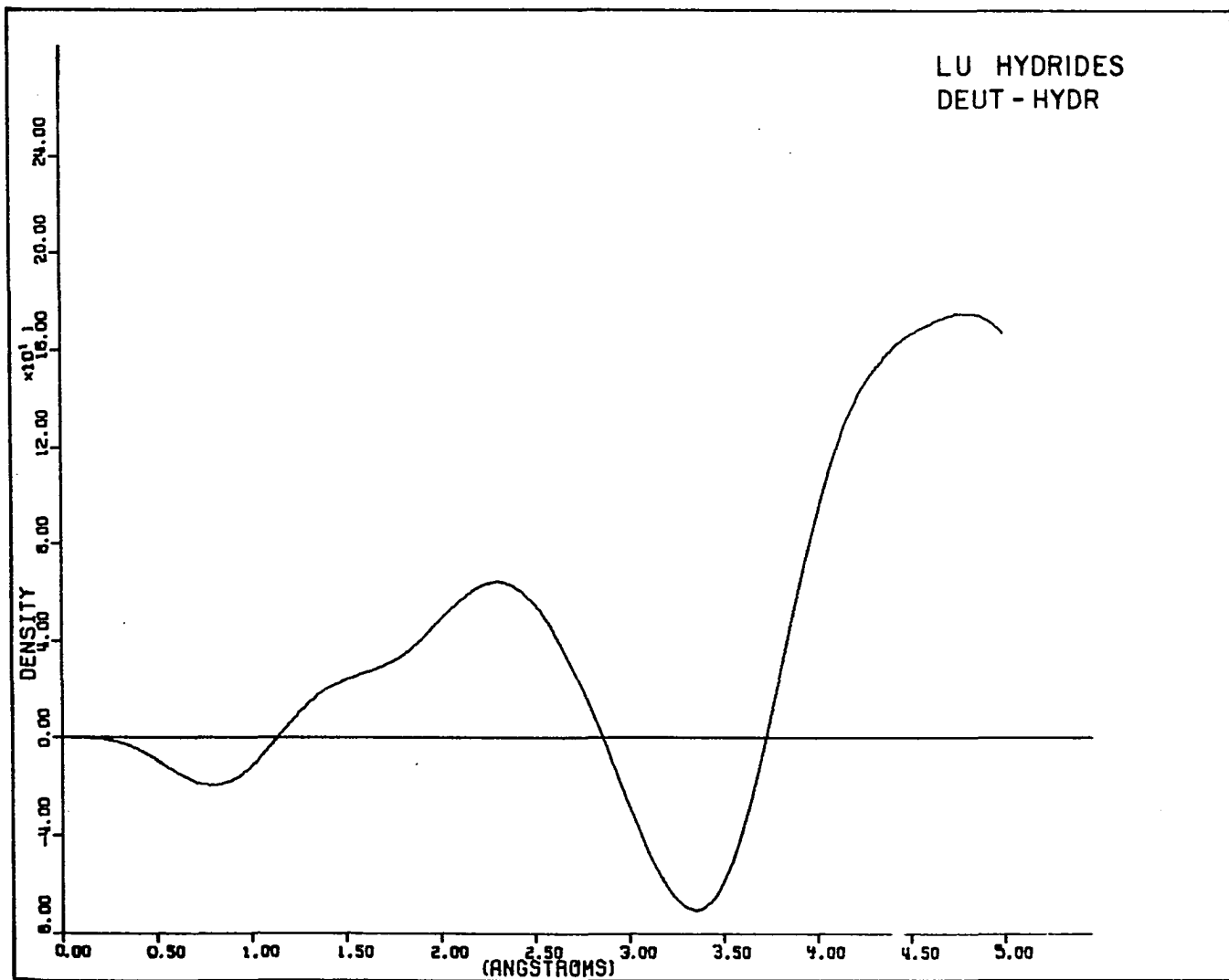


Table V.2. Difference RDF information for NbD_{0.718}/NbH_{0.730}

Niobium: $b = 0.710$

Deuterium: $b = 0.667$

$x = \text{stoichiometric factor}$

$$= 0.718/2 = 0.359$$

Hydrogen $b = -0.374$

$$x = 0.730/2 = 0.365$$

Interactions:

$$\text{Nb} \cdot \text{Nb} = (1.000 \cdot 0.710) \cdot (1.000 \cdot 0.710) = 0.504100$$

$$\text{Nb} \cdot \text{D} = (1.000 \cdot 0.710) \cdot (0.359 \cdot 0.667) = 0.170012$$

$$\text{Nb} \cdot \text{H} = (1.000 \cdot 0.710) \cdot (0.365 \cdot (-0.374)) = -0.096922$$

$$\text{D} \cdot \text{D} = (0.359 \cdot 0.667) \cdot (0.359 \cdot 0.667) = 0.057338$$

$$\text{H} \cdot \text{H} = (0.365 \cdot (-0.374)) \cdot (0.365 \cdot (-0.374)) = 0.018635$$

$$(\text{Nb} \cdot \text{Nb}) - (\text{Nb} \cdot \text{Nb}) \equiv 0$$

$$(\text{Nb} \cdot \text{D}) - (\text{Nb} \cdot \text{H}) = 0.266934$$

$$(\text{D} \cdot \text{D}) - (\text{H} \cdot \text{H}) = 0.038703$$

Table V.3. Difference RDF information for LuD_{.205}/LuH_{.208}

Lutetium: b = 0.730

Deuterium: b = 0.667

$$x = 0.305/2 = 0.1025$$

Hydrogen: b = -0.374

$$x = 0.208/2 = 0.104$$

Interactions:

$$\text{Lu}\cdot\text{Lu} = (1.000*0.730)*(1.000*0.730) = 0.532900$$

$$\text{Lu}\cdot\text{D} = (1.000*0.730)*(0.1025*0.667) = 0.049908$$

$$\text{Lu}\cdot\text{H} = (1.000*0.730)*(0.104*(-0.374)) = -0.028394$$

$$\text{D}\cdot\text{D} = (0.1025*0.667)*(0.1025*0.667) = 0.004674$$

$$\text{H}\cdot\text{H} = (0.104*(-0.374))*(0.104*(-0.374)) = 0.001513$$

$$(\text{Lu}\cdot\text{Lu}) - (\text{Lu}\cdot\text{Lu}) \equiv 0$$

$$(\text{Lu}\cdot\text{D}) - (\text{Lu}\cdot\text{H}) = 0.078302$$

$$(\text{D}\cdot\text{D}) - (\text{H}\cdot\text{H}) = 0.003161$$

ratio is 24.8. Thus, to a great extent the curve arising from subtracting a metal hydride RDF from the corresponding metal deuteride RDF may be thought of as showing the metal-hydrogen (deuterium) interaction alone.

Analysis of Results

Table V.4 shows a tabulation of all interactions expected for the niobium compounds, following DeHaven.⁹⁴ It can be seen from this table that the technique of radial distribution difference function analysis works well in predicting M-H(D) interaction distances; the peak occurring at 1.85 Å in Figure V.9 agrees well with the distance of 1.909 Å expected for the niobium-hydrogen (deuterium) interaction, that distance being the one appropriate for the tetrahedral site.

The success of the radial distribution function analysis technique in the treatment of the problem of hydrogen (deuterium) location in the niobium system inspired extension to the lutetium system. Bonnet⁹⁵ had suggested that in the α phase lutetium-hydrogen (deuterium) system there was some question as to whether the hydrogen (deuterium) resided in the tetrahedral or octahedral site. These two positions ((1/3, 2/3, 3/8) and (0,0,0), respectively) lead to 2.14 and 2.45 Å metal to hydrogen distances, respectively. Inspection of Figure V.10 shows a broad maximum centered more about the former than the latter distance, indicating the tetrahedral site as the one occupied. This verifies the conclusion reached by Bonnet: x-ray

Table V.4. Tabulation of interaction information for the niobium system

Radius (Angstroms)	Type	N	Deuteride	Hydride	Difference
1.706	H•H	4	0.23	0.07	0.15
1.909	Nb•H	8	1.36	-0.78	2.14
2.957	Nb•Nb	8	4.03	4.03	0.00
3.077	Nb•H	8	1.36	-0.78	2.14
3.414	Nb•Nb	12	6.05	6.05	0.00
3.414	H•H	8	0.46	0.15	0.31
3.818	H•H	8	0.46	0.15	0.31
3.913	Nb•H	16	2.72	-1.55	4.27
4.596	Nb•H	24	4.08	-2.33	6.41
4.828	Nb•Nb	24	12.10	12.10	0.00
4.828	H•H	16	0.92	0.30	0.62

diffraction peak broadening upon addition of hydrogen, thermal expansion behavior, and neutron diffraction studies all favor the tetrahedral site over the octahedral site as the one occupied. Table V.5 gives the pertinent results for the lutetium compounds.

It is obvious from Figures V.9 and V.10 that the metal-hydrogen (deuterium) interaction is more pronounced for the niobium system than for the lutetium system. This is not surprising in view of Tables V.2 and V.3. The ratio of the magnitude of the Nb•Nb interaction to that of the difference interaction (Nb•D) - (Nb•H) is $0.504100/0.266934 = 1.888$; for the lutetium system, the ratio of the Lu•Lu interaction to the difference interaction (Lu•D) - (Lu•H) is $0.532900/0.078302 = 6.806$. Thus, the metal-hydrogen (deuterium) interactions are only about a third as visible above the metal-metal interaction "background" in the lutetium system as for the niobium system. That the metal-hydrogen (deuterium) interaction is as visible as it is for the lutetium system is testimony to the power of this technique.

RDF-Patterson Superposition Studies

As mentioned above, it is possible to create a three-dimensional Patterson map with spherical symmetry from the difference RDFs shown in Figures V.9 and V.10, and then perform successive superpositions on unit cell repeats, or where atoms are located in the cell. To use the RDF-Patterson superposition technique as a tool for choosing

Table V.5. Tabulation of interaction information for the lutetium system (tetrahedral hole model used)

Radius ° (Angstroms)	Type	N	Deuteride	Hydride	Difference
1.40	H•H	1	0.005	0.002	0.003
2.14	Lu•H	8	0.399	-0.227	0.626
2.47	H•H	6	0.028	0.009	0.019
3.46	Lu•Lu	6	3.197	3.197	0.000
3.46	H•H	6	0.028	0.009	0.019
3.50	Lu•H	2	0.100	-0.057	0.157
3.52	Lu•Lu	6	3.197	3.197	0.000
3.52	H•H	12	0.056	0.018	0.038
3.79	H•H	6	0.028	0.009	0.019
4.11	Lu•H	18	0.898	-0.511	1.409
4.20	H•H	1	0.005	0.002	0.003
4.30	H•H	6	0.028	0.009	0.019
4.67	H•H	6	0.028	0.009	0.019
4.94	Lu•Lu	6	3.197	3.197	0.000
4.94	H•H	6	0.028	0.009	0.019
4.96	Lu•H	12	0.599	-0.341	0.940

between the tetrahedral or octahedral sites for the hydrogen (deuterium) positions, the best positions to choose for superposition are those describing the particular octahedral or tetrahedral site in question. Tables V.6 and V.7 list such positions for both the niobium and lutetium compounds, respectively. Upon performing the successive superpositions, the tetrahedral site was indicated for both classes of compounds: for the tetrahedral sites, a significant peak occurred at the target position in each case; for the octahedral sites, a non-descript flat region was found.

Conclusions

The technique of radial distribution function analysis has been shown to be useful in the study of materials which occur only as polycrystalline (powder) samples. Radial distribution difference function analysis has been shown to be particularly useful in elucidation of the structure of metal hydride (deuteride) systems, and the extension of that technique to include Patterson superposition techniques has also been shown to be valuable. For both niobium and lutetium metal hydride (deuteride) systems, tetrahedral (as opposed to octahedral) hydrogen (deuterium) sites have been shown to be favored.

Table V.6. Superposition sites for the niobium hydride (deuteride) system

Tetrahedral site at (0,0,0.250)

Niobium Positions	Superposition Sites
(-0.250,-0.250,0.000)	(0.000,0.000,0.000)
(-0.250,0.250,0.500)	(0.000,0.500,0.500)
(0.250,-0.250,0.500)	(0.500,0.000,0.500)
(0.250,0.250,0.000)	(0.500,0.500,0.000)

Octahedral Site at (0.500,0.500,0.000)

(0.250,0.250,0.000)	(0.000,0.000,0.000)
(0.250,0.750,-0.500)	(0.000,0.500,-0.500)
(0.250,0.750,0.500)	(0.000,0.500,0.500)
(0.750,0.250,-0.500)	(0.500,0.000,-0.500)
(0.750,0.250,0.500)	(0.500,0.000,0.500)
(0.750,0.750,0.000)	(0.500,0.500,0.000)

Table V.7. Superposition sites for the lutetium hydride (deuteride) system

Tetrahedral site at (0.333,0.667,0.375)

Lutetium Positions	Superposition Sites
(-0.333,0.333,0.250)	(0.000,0.000,0.000)
(0.333,0.667,0.750)	(0.667,0.333,0.500)
(0.667,0.333,0.250)	(1.000,0.000,0.000)
(0.667,1.333,0.250)	(1.000,1.000,0.000)

Octahedral Site at (0.000,0.000,0.500)

Lutetium Positions	Superposition Sites
(-0.333,0.333,0.250)	(0.000,0.000,0.000)
(-0.667,-0.333,0.750)	(-0.333,-0.667,0.500)
(-0.333,-0.667,0.250)	(0.000,-1.000,0.000)
(0.333,-0.333,0.750)	(0.667,-0.667,0.500)
(0.333,0.667,0.750)	(0.667,0.333,0.500)
(0.667,0.333,0.250)	(1.000,0.000,0.000)

BIBLIOGRAPHY

1. T. Moeller, D. F. Martin, L. C. Thompson, R. Ferrus, G. R. Feistel, and W. J. Randall, Chem. Revs., 65, 1 (1965).
2. J. E. Powell and H. R. Burkholder, J. Chromatog., 36, 99 (1968).
3. C. C. Fuller, D. K. Molzahn, and R. A. Jacobson, Inorg. Chem., 17, 2138 (1978).
4. C. C. Fuller, P. D. Murphy, and R. A. Jacobson, Cryst. Struct. Comm., accepted for publication.
5. J. E. Benson and R. A. Jacobson, Chemistry Department, Iowa State University, to be published.
6. W. J. Rohrbaugh and R. A. Jacobson, Inorg. Chem., 13, 2535 (1974).
7. S. L. Lawton and R. A. Jacobson, Inorg. Chem., 7, 2124 (1968).
8. W. R. Busing, K. O. Martin, and H. A. Levy, USAEC Report ORNL-TM-305, 1962.
9. C. R. Hubbard, C. O. Quicksall, and R. A. Jacobson, USAEC Report IS-2625, 1971.
10. H. P. Hanson, F. Herman, J. D. Lea, and S. Skillman, Acta Cryst., 17, 1040 (1960).
11. D. H. Templeton, in "International Tables for X-Ray Crystallography," Vol. III, Table 3.3.2c, The Kynoch Press, Birmingham, England, 1962, pp. 215-216.
12. R. F. Stewart, E. R. Davidson, and W. T. Simpson, J. Chem. Phys., 42, 3175 (1965).
13. F. Takusagawa, Brookhaven National Laboratory, private communication.
14. C. K. Johnson, USAEC Report ORNL-3794 (second Revision with Supplemental Instructions), 1971.
15. M. D. Lind, B. Lee, and J. L. Hoard, J. Amer. Chem. Soc., 87, 1611 (1965).
16. T. Moeller and E. P. Horwitz, J. Inorg. Nucl. Chem., 12, 49 (1967).

17. B. Lee, Inorg. Chem., 11, 1072 (1972).
18. E. L. Muetterties and L. J. Guggenberger, J. Amer. Chem. Soc., 96, 1748 (1974).
19. W. G. O'Brien and R. G. Bautista, USAEC Report IS-3259, 1974.
20. G. F. Volodina, I. M. Rumanova, and N. V. Belov, Sov. Physics-Cryst., 6, 741 (1961), see also Sov. Physics-Cryst., 9, 545 (1965).
21. C. C. Fuller and R. A. Jacobson, Cryst. Struct. Comm., 5, 349 (1976).
22. W. R. Busing, K. O. Martin, and H. A. Levy, USAEC Report ORNL-TM-306, 1964.
- 23-24. S. P. Sinha, in "Structure and Bonding," Vol. 25, J. D. Dunitz, et al., Eds., Springer-Verlag, 1976.
25. E. L. Muetterties and C. M. Wright, Q. Rev., 21, 109 (1976).
26. D. G. Karraker, J. Chem. Ed., 47, 424 (1970).
27. A. R. Al-Karaghoulis and J. S. Wood, Inorg. Chem., 11, 2293 (1972).
28. R. B. King, J. Amer. Chem. Soc., 92, 6460 (1970).
29. Y. C. Lin and D. E. Williams, Can. J. Chem., 51, 312 (1973).
30. I. Jelenic, D. Grdenic, and A. Bezjak, Acta Cryst., 17, 758 (1964).
31. M. N. Akhtar and A. J. Smith, J. C. S. Chem. Comm., 705 (1969).
32. K. K. Bhandary and E. Manohar, Acta Cryst., B29, 1093 (1973).
33. D. B. Shinn and H. A. Eick, Inorg. Chem., 7, 1340 (1968).
34. A. R. Al-Karaghoulis and J. S. Wood, J. Amer. Chem. Soc., 90, 6548 (1968).
35. D. S. Moss and S. P. Sinha, Z. P. Chem. (N.F.), 63, 190 (1969).

36. J. L. Hoard and J. V. Silverton, Inorg. Chem., 2, 235 (1963).
37. A. R. Al-Kharaghoulfi and J. S. Wood, J. C. S. Chem. Comm., 135 (1970).
38. G. D. Smith, C. N. Caughlan, Mazhar-ul-Hague, and F. A. Hart, Inorg. Chem., 12, 2654 (1973).
39. Mazhar-ul-Hague, C. N. Caughlan, F. A. Hart, and R. Van Nice, Inorg. Chem., 10, 115 (1971).
40. R. Wang, R. Bodnar, and H. Steinfink, Inorg. Chem., 5, 1468 (1966).
41. N. L. Morrow and L. Katz, Acta Cryst., B24, 1466 (1966).
42. Mazhar-ul-Hague, F. A. Hart, and C. N. Caughlan, J. C. S. Chem. Comm., 1240 (1970).
43. A. Al-Karaghoulfi and J. S. Wood, J. C. S. Dalton, 2318 (1973).
44. F. A. Cotton and G. Wilkinson, "Advanced Inorganic Chemistry," Third Edition, Interscience Publishers, New York 1972, p. 246.
45. B. Barbara, D. Gignoux, D. Givord, F. Givord, and R. Lemaire, Int. J. Magn., 4, 77 (1973).
46. A. R. Mackintosh, Physics Today, 30, 23 (1977).
47. R. Lemaire, Courier du C.N.R.S., 16, 52 (1975).
48. R. Lemaire, Cobalt, 32, 132 (1966); and Cobalt, 33, 201 (1966).
49. W. Haucke, Z. Anorg. Chem., 244, 17 (1940).
50. W. E. Wallace, R. S. Craig, V. U. S. Rao, and R. A. Butera, 7th Russian Conference on Rare Earth Metals, Moscow (1972).
51. C. Shull and T. Yomada, J. Phys. Soc. Japan, 17, BIII, 1 (1972).
52. R. M. Moon, Phys. Rev., 136, A195 (1964).
53. H. A. Mook and C. G. Shull, J. Appl. Phys., 37, 1034 (1966).
54. E. Kren, J. Schweizer, and F. Tasset, Phys. Rev., 186, 479 (1969).

55. R. Lemaire, D. Paccard, R. Pauthenet, and J. Schweizer, J. Appl. Phys., 39, 1092 (1968).
56. K. J. Strnat, Cobalt, 36, 133 (1967).
57. J. Deportes, Ph.D. Thesis, Universite Scientifique et Medicale et l'Institute National Polytechnique de Grenoble, Grenoble, France, 1977.
58. J. V. Florio, R. E. Rundle, and A. I. Snow, Acta Cryst., 5, 449 (1952).
59. J. Deportes, D. Givord, R. Lemaire, and H. Nagai, J. Less-Common Metals, 40, 299 (1975).
60. Q. Johnson and G. S. Smith, Acta Cryst., 23, 327 (1967).
61. Q. C. Johnson, G. S. Smith, D. H. Wood, and E. M. Cramer, Nature, 201, 600 (1964).
62. J. Deportes and D. Givord, Solid State Comm., 19, 845 (1976).
63. O. S. Zarechnyuk and P. I. Kripyakevich, Soviet Physics-Cryst., 7, 436 (1963).
64. J. Deportes, D. Givord, R. Lemaire, and H. Nagai, Physica, 86-88B, 69 (1977).
65. J. Deportes, D. Givord, and B. Kebe, in "Rare Earths and Actinides, 1977," Inst. Phys. Conf. Ser. No. 37., 1978, p. 278.
66. B. Kebe, Ph.D. Thesis, Universite Scientifique et Medicale et l'Institute National Polytechnique de Grenoble, Grenoble, France, 1978.
67. J. Deportes, D. Givord, B. Kebe, and C. Fuller, CNRS Laboratories, Grenoble, France, to be published.
68. O. S. Zarechnyuk, I. F. Kolobnev, and M. Yu. Teslyuk, Russian J. Inorg. Chem., 8, 868 (1963).
69. K. H. J. Buschow, J. H. N. van Vucht, and W. W. van den Hoogenhof, J. Less-Common Metals, 50, 145 (1976).
70. A. M. van der Kraan and K. H. J. Buschow, Physica B & C, 86-88, 93 (1977).

- 71-73. E. S. Makarov and S. I. Vinogradov, Sov. Physics-Cryst., 1, 499 (1956).
74. C. Kittel, "Introduction to Solid State Physics," Third Edition, John Wiley and Sons, New York, 1966.
75. J. H. Van Vleck, Science, 201, 113 (1978).
76. P. W. Anderson, Science, 201, 307 (1978).
77. N. F. Mott, Science, 201, 871 (1978).
78. B. D. Cullity, "Introduction to Magnetic Materials," Addison-Wesley Publishing Co., New York, 1972, p. 65.
79. A. Barlet, Report from the Service de Mesures d'Aimentation, CNRS, Grenoble, France, 1977.
- 80-82. P. Rub, J. C. Picoche, and H. I. Schneider-Muntau, Coloques Internationaux CNRS, 242, 149 (1974).
83. G. H. Stout and L. H. Jensen, "X-Ray Structure Determination," Macmillan Publishing Co., New York, 1968, pp. 270 ff.
84. A. L. Patterson, Z. Krist., A90, 517 (1935).
85. W. N. Lipscomb and R. A. Jacobson, in "Physical Methods of Chemistry," Vol. I, Part IIID, A. Weissberger and B. W. Rossler, Eds., John Wiley and Sons, New York, 1972, pp. 1 ff.
86. P. Debye, Ann. Phys., 46, 809 (1915).
87. H. P. Klug and L. E. Alexander, "X-Ray Diffraction Procedures," John Wiley and Sons, New York 1974, pp. 791 ff.
88. S. Ergun, "Chemistry and Physics of Carbon," Vol. 3, P. L. Walker, Jr., Ed., Marcel Dekker, New York, 1968, pp. 250 ff.
89. J. F. Karnicky and C. J. Ping, Adv. Chem. Phys., 34, 157 (1976).
90. L. Blum and A. H. Narten, Adv. Chem. Phys., 34, 203 (1976).
- 91-92. R. F. Kruh, Chem. Rev., 62, 319 (1962).

93. H. M. Rietveld, Acta Cryst., 22, 151 (1967), see also H. M. Rietveld, J. Appl. Cryst., 2, 65 (1969).
94. P. W. DeHaven, Ph.D. Thesis, Iowa State University, (1977).
95. J. E. Bonnet, J. Less-Common Metals, 49, 451 (1976).
96. J. E. Johnson and R. A. Jacobson, Acta Crystallogr., B29, 1669 (1973).
97. J. E. Johnson, T. A. Beineke, and R. A. Jacobson, J. Chem. Soc. (A), 1371 (1971).
98. J. E. Johnson and R. A. Jacobson, J. Chem. Soc. (A), 580 (1973).
99. J. Rodgers, and R. A. Jacobson, J. Chem. Soc. (A), 1826 (1970).
100. C. C. Fuller and R. A. Jacobson, to be published.
101. E. R. Howells, D. C. Phillips, and D. Rogers, Acta Crystallogr., 3, 210 (1950).
102. "International Tables for X-Ray Crystallography," Vol. III, p. 260, Table 4.1.1, The Knoch Press, Birmingham, England, 1962.
103. H. C. Freeman and M. R. Snow, Acta Crystallogr., 18, 843 (1965).
104. J. Bernstein and A. T. Hagler, J. Amer. Chem. Soc., 100, 673 (1978).
105. J. Page and R. Plant, from "Stairway to Heaven," Superhype Music, Inc. ASCAP, Atlantic Recording Corp., New York, New York, 1975.

ACKNOWLEDGEMENTS

I would like to express my great appreciation of Robert Jacobson for his years of guidance through the wilds of reciprocal space. Through thick and thin, he has been a source of help and friendship. One owes a lot to his major professor; I owe a lot to Dr. Jacobson. To him I say a hearty thanks.

William James introduced me to laboratory science in general, and diffraction and magnetism in particular. It was at his suggestion that I braved the frozen winters of central Iowa; it was by his arrangement that I went to France. For all these things and many others I am greatly indebted.

Remy Lemaire provided more than excellent scientific guidance when I was in France. His warm humanity and continual encouragement of me to indulge in things French made my stay in France better than excellent.

Likewise, my French coworkers (Baye Kebé, Jacques Deportes, Dominique Givord, and Albert Barlet) did much to make those months profitable and the fourth chapter of this thesis possible. To them and all my French friends I say "Merci."

Another Francophile, William Yelon, should likewise be remembered for allowing me to use the facilities of the Missouri University Research Reactor, and for aiding me in that use. His assistance has always been of the highest quality.

My many friends from Ames must be remembered, as well. I firmly believe that one's friendships are of the greatest importance. I am glad to have found so many friends in my years in Ames.

And, finally, my greatest indebtedness lies with my family. Their love and encouragement has meant more to me than all else. This thesis and my life stand in testimony to them.

APPENDIX.

THE CRYSTAL AND MOLECULAR STRUCTURE OF THE COMPOUND

BIS(O-TRICYANOETHYLENEOATE)BIS

(2',2',N,N'BISPYRIDYLAMINE)

COPPER(II)

Abstract

The crystal and molecular structure of bis(O-tricyanoethyleneoate)bis(2,2',N,N'-bispyridylamine)copper(II), (triclinic, $\bar{P}1$, $a = 10.075(2)$, $b = 10.911(2)$, $c = 7.841(2)$ Å, $\alpha = 107.98(2)$, $\beta = 104.78(2)$, $\gamma = 108.40(2)^\circ$, $V = 716.19$ Å³, $Z = 1$, Mo K α radiation), has been determined by three dimensional x-ray analysis. The structure was solved by conventional Patterson and Fourier techniques, and refined by a full matrix least-squares procedure to a final conventional residual index, $R = \Sigma ||F_o| - |F_c|| / \Sigma |F_o|$, of 7.2% for 1984 unique observed reflections ($F_o > 3\sigma_{F_o}$). The copper atom is hexacoordinate (D_{4h} symmetry), with the four equatorial sites occupied by an oxygen atom of a tricyanoethylenol moiety. The molecule itself has a center of inversion.

Introduction

Considerable attention has been given recently to the products formed when tetracyanoethylene (TCNE) and its derivatives are reacted with a wide variety of other compounds. As some of these complexes

have interesting charge transfer properties, we have recently embarked on a program of preparation and study of products obtained from reaction mixtures containing TCNE and a variety of organometallic complexes.

In addition, extensive structural studies of complexes containing the bispyridylamine ligand have been carried out in this laboratory. In particular, the structure of bispyridylamine itself was reported by Johnson and Jacobson in 1973,⁹⁶ and two copper complexes with that ligand were also reported,^{97,98} as was a related bispyridylmethyl compound.⁹⁹

Combining these two areas of interest, this appendix reports the results of reacting tricyanoethylene with the square planar copper complex bispyridylaminecopper(II) dichloride.¹⁰⁰

Experimental Section

Crystal Data

The title compound was prepared by mixing stoichiometric amounts of copper(II) bispyridylamine dichloride in aqueous solution with tetracyanoethylene (TCNE) in butyl alcohol solution, and allowing this mixture to go to dryness at room temperature. Well-formed golden brown single crystals were thus formed and used without further purification. A crystal of approximate dimensions 0.2x0.2x0.2mm was mounted on a glass fiber using Duco cement, and preliminary oscillation

photographs indicated that the compound crystallizes in the triclinic system. A Howells, Phillips, and Rogers test¹⁰¹ did not unambiguously resolve the question of the presence or absence of a crystallographic center of symmetry, but subsequent structure refinement showed that such a center does exist, thus fixing the space group as $\bar{P}1$. Final unit cell parameters, obtained from a least squares fit of $\pm 2\theta$ values ($2\theta > 25^\circ$) for twenty-eight independent reflections (Mo $K\alpha$ radiation, $\lambda = 0.70954 \text{ \AA}$) at 27° yielded $a = 10.075(2)$, $b = 10.911(2)$, $c = 7.841(2) \text{ \AA}$, $\alpha = 107.98(2)$, $\beta = 104.78(2)$, $\gamma = 108.40(2)^\circ$, $v = 716.19 \text{ \AA}^3$, $D_{\text{calc}} = 1.489 \text{ g}\cdot\text{cm}^{-3}$.

Collection and Reduction of X-ray Intensity Data

Data were collected at room temperature using a technique and apparatus described by Rohrbaugh and Jacobson.⁶ Within a 2θ sphere of 50° ($\sin\theta/\lambda = 0.596 \text{ \AA}^{-1}$) all data in the hkl , $hk\bar{l}$, $h\bar{k}l$, and $h\bar{k}\bar{l}$ octants were measured. As a general check on crystal and electronic stability, the intensities of six standards were remeasured periodically (after every 75 reflections) during the data collection period of 56.8 hours for the 3317 reflections. No significant decrease in intensity was detected during the data collection period for these standards, and therefore no correction was made for crystal decomposition.

The intensity data were corrected for Lorentz and polarization effects, but as the crystal was small and the linear absorption

coefficient was low ($\mu = 5.70 \text{ cm}^{-1}$), no absorption correction was made. The estimated error in each intensity was calculated by

$$\sigma_I^2 = C_T + K_t C_B + (0.03C_T)^2 + (0.03C_B)^2$$

where C_T , K_t , and C_B are the total count, counting time factor, and background count, respectively, and the factor 0.03 represents an estimate of nonstatistical errors. The estimated deviations in the structure factors were calculated by the finite difference method.⁷ Of the 3317 reflections measured, 2378 were considered observed ($> 3\sigma_{F_o}$), and of these, 1984 were unique, and thus used in subsequent calculations.

Solution and Refinement of Structure

The position of the copper atom was fixed by symmetry arguments to be at a center of symmetry. (The position (1/2,1/2,1/2) was chosen for convenience.) The remaining nonhydrogen atoms were found by successive structure factor⁸ and density map calculations.⁹ The positional and isotropic thermal parameters of all nonhydrogen atoms were refined, via minimization of the function $\sum \omega (|F_o| - |F_c|)^2$, where $\omega = 1/\sigma_{F_o}^2$, resulting in a conventional discrepancy factor $R = \sum ||F_o| - |F_c|| / \sum |F_o| = 12.5\%$. After conversion to anisotropic temperature factors and subsequent refinement, an R factor of 8.3% resulted. The hydrogen positions in the bispyridylamine group were

then calculated, and also allowed to refine, although the isotropic thermal parameters for the hydrogen atoms were fixed at 4.0 \AA^2 . A final R factor of 7.2% resulted. An examination of the large $|F_o|s$ indicated the absence of any appreciable secondary extinction effect. The scattering factors for the nonhydrogen atoms were those of Hanson et al.,¹⁰ modified for the real and imaginary parts of anomalous dispersion.¹¹ For hydrogen, the scattering factors of Stewart et al. were used.¹²

The final positional parameters are listed in Table A.I.a; the anisotropic temperature factors are listed in Table A.I.b. Bond lengths and bond angles are listed in Tables A.II and A.III, respectively, with a tabulation of least squares planes information being given in Table A.IV. A listing of structure factor amplitudes is given elsewhere.¹⁰⁰

Description and Discussion

Although the two starting compounds in this study were TCNE and the square planar copper complex bispyridylaminecopper(II) dichloride, solution of the crystal structure showed that the TCNE had undergone a reaction, losing one CN group which was subsequently replaced with an oxygen. This reaction took place via a Michael addition, as

Table A.I.a. Final positional^a parameters

Atom	X	Y	Z	Atom	X	Y	Z
Cu	5000	5000	5000	N1	-1333(7)	126(6)	-3175(11)
NA	6623(6) ^b	3064(5)	3890(8)	N2	2672(8)	-718(8)	-1665(11)
NPA	5578(5)	3753(5)	6190(7)	N3	730(7)	3894(7)	1037(10)
CPA1	6160(6)	2898(6)	5360(9)	C1	1447(7)	989(6)	-946(9)
CPA2	6371(7)	1878(7)	5979(11)	C2	2237(7)	2337(7)	535(10)
CPA3	6009(8)	1765(8)	7492(12)	C3	-107(8)	515(7)	-2166(11)
CPA4	5466(8)	2695(8)	8438(11)	C4	2150(7)	57(7)	-1339(10)
CPA5	5277(7)	3660(7)	7746(9)	C5	1361(7)	3199(7)	781(10)
NPB	6911(5)	5395(5)	4534(7)	HA	691(9)	242(8)	330(12)
CPB1	7310(6)	4352(6)	3825(9)	HPA2	688(9)	123(8)	533(12)
CPB2	8421(7)	4518(7)	3027(10)	HPA3	622(8)	117(8)	819(12)
CPB3	9212(7)	5827(8)	3130(10)	HPA4	525(9)	275(9)	941(13)
CPB4	8934(7)	6974(7)	4079(10)	HPA5	481(9)	435(8)	838(12)
CPB5	7772(7)	6718(6)	4721(9)	HPB2	857(9)	367(8)	235(12)
O	3606(5)	2910(5)	1700(7)	HPB3	1003(9)	600(8)	252(11)
				HPB4	946(9)	795(8)	423(12)
				HPB5	744(9)	741(8)	533(12)

^aThe positional parameters are presented in fractional coordinates ($\times 10^4$ for the nonhydrogen atoms, $\times 10^3$ for the hydrogen atoms).

^bIn this and succeeding tables, estimated standard deviations are given in parentheses for the least significant figures.

Table A.I.b. Thermal parameters^{a,b}

Atom	β_{11}	β_{22}	β_{33}	β_{12}	β_{13}	β_{23}
Cu	109(2)	83(1)	233(3)	59(1)	97(2)	66(2)
NA	122(8)	86(6)	247(15)	64(6)	97(9)	65(8)
NPA	103(7)	82(6)	204(13)	39(5)	74(9)	59(7)
CPA1	97(8)	78(7)	202(15)	35(6)	63(9)	48(9)
CPA2	139(10)	104(8)	277(20)	64(8)	76(12)	87(11)
CPA3	160(11)	118(9)	293(22)	60(8)	58(13)	105(12)
CPA4	138(10)	143(10)	211(18)	50(8)	76(11)	98(12)
CPA5	122(9)	117(9)	185(16)	43(7)	61(10)	61(10)
NPB	110(7)	71(5)	172(12)	45(5)	75(8)	42(7)
CPB1	98(8)	100(7)	170(14)	49(6)	64(9)	54(9)
CPB2	112(9)	122(9)	217(17)	64(7)	91(10)	69(10)
CPB3	121(9)	164(11)	240(18)	78(8)	108(11)	117(12)
CPB4	124(9)	124(9)	255(19)	49(8)	106(11)	98(11)
CPB5	122(9)	95(8)	207(16)	40(7)	85(10)	62(9)
O	113(6)	120(6)	248(12)	51(5)	51(7)	16(7)
N1	147(10)	116(8)	457(24)	48(8)	30(13)	84(12)
N2	235(12)	141(9)	394(22)	124(9)	123(13)	72(12)
N3	190(10)	174(10)	342(20)	124(9)	122(12)	90(12)
C1	117(9)	91(7)	208(16)	53(7)	62(10)	56(9)
C2	124(10)	121(9)	200(16)	64(7)	88(11)	57(10)
C3	138(11)	84(8)	283(20)	45(8)	70(12)	60(10)
C4	145(10)	98(8)	233(18)	59(8)	74(11)	54(10)
C5	129(10)	108(8)	224(17)	62(8)	68(11)	44(10)

^aThe β_{ij} are defined by: $T = \exp -(h^2\beta_{11} + k^2\beta_{22} + l^2\beta_{33} + 2hk\beta_{12} + 2hl\beta_{13} + 2kl\beta_{23})$. Isotropic temperature factors of 4.0 \AA^2 were assumed for all hydrogen atoms.

^bNumbers shown are $\times 10^4$.

Table A.II.a. Selected intramolecular interatomic distances (Å)

Cu-NPA	2.016(6)	O-C2	1.260(7)
Cu-NPB	1.989(6)	C1-C2	1.372(7)
Cu-O	2.520(4)	C1-C3	1.433(9)
NPA-CPA1	1.342(9)	C1-C4	1.414(11)
CPA1-CPA2	1.396(12)	C2-C5	1.483(12)
CPA2-CPA3	1.356(14)	N1-C3	1.138(10)
CPA3-CPA4	1.404(13)	N2-C4	1.128(12)
CPA4-CPA5	1.365(13)	N3-C5	1.138(12)
CPA5-NPA	1.356(10)	NA-Ha	0.88(10)
NPB-CPB1	1.334(9)	CPA2-HPA2	1.08(10)
CPB1-CPB2	1.406(10)	CPA3-HPA3	1.00(11)
CPB2-CPB3	1.364(11)	CPA4-HPA4	0.84(11)
CPB3-CPB4	1.396(12)	CPA5-HPA5	1.07(10)
CPB4-CPB5	1.373(11)	CPB2-HPB2	1.00(9)
CPB5-NPB	1.367(18)	CPB3-HPB3	1.05(10)
NA-CPA1	1.388(10)	CPB4-HPB4	0.98(9)
NA-CPB1	1.379(9)	CPB5-HPB5	0.96(10)

Table A.II.b. Selected intermolecular interatomic distances (Å)

N2-HA(2) ^a	2.14(9)
N1-HPB5(1)	2.55(8)
N3-HPB2(1)	2.61(10)
N3-HPB3(1)	2.64(9)
N1-HPA2(1)	2.69(10)
C3-HPB4(2)	2.71(10)
O-HPA4(1)	2.74(11)
N3-HPB3(2)	2.75(9)
N1-HPB4(2)	2.83(10)
N2-HPB2(2)	2.87(9)
N2-HPA3(2)	2.93(10)
N2-HPA2(2)	2.93(10)

^aExplanation of symmetry operations: (1) Position related to (x,y,z) by unit cell translations; (2) Position related to (-x,-y,-z) by unit cell translations.

Table A.III. Selected bond angles (degrees)

N1-C3-C1	178.3(11)	CPB2-CPB3-CPB4	119.3(8)
N2-C4-C1	178.0(8)	CPB3-CPB4-CPB5	118.6(7)
N3-C5-C2	177.4(6)	CPB4-CPB5-NPB	122.7(7)
C3-C1-C2	120.0(7)	NA-CPA1-NPA	119.3(7)
C4-C1-C2	121.2(6)	NA-CPB1-NPB	119.1(6)
C5-C2-C1	115.5(6)	NA-CPA1-CPA2	118.6(7)
C3-C1-C4	118.7(5)	NA-CPB1-CPB2	118.5(6)
C5-C2-O	117.2(5)	CPA1-NA-CPB1	125.1(5)
C1-C2-O	127.3(8)	CPA1-CPA2-HPA2	121(6)
O-Cu-NPA	90.26(17)	CPA3-CPA2-HPA2	121(6)
O-Cu-NPB	89.30(16)	CPA2-CPA3-HPA3	127(6)
NPA-Cu-NPB	86.28(23)	CPA4-CPA3-HPA3	112(6)
Cu-NPA-CPA1	120.6(5)	CPA3-CPA4-HPA4	128(7)
Cu-NPB-CPB1	121.3(4)	CPA5-CPA4-HPA4	114(7)
Cu-NPA-CPA5	121.3(5)	CPA4-CPA5-HPA5	120(6)
Cu-NPB-CPB5	120.9(5)	NPA-CPA5-HPA5	116(6)
Cu-O-C2	130.8(5)	CPB1-CPB2-HPB2	119(5)
CPA1-NPA-CPA5	117.8(6)	CPB3-CPB2-HPB2	122(5)
CPB1-NPB-CPB5	117.4(6)	CPB2-CPB3-HPB3	122(5)
NPA-CPA1-CPA2	122.0(7)	CPB4-CPB3-HPB3	119(5)
CPA1-CPA2-CPA3	119.2(8)	CPB3-CPB4-HPB4	124(6)
CPA2-CPA3-CPA4	119.6(9)	CPB5-CPB4-HPB4	117(6)
CPA3-CPA4-CPA5	118.1(8)	CPB4-CPB5-HPB5	126(5)
CPA4-CPA5-NPA	123.2(7)	NPB-CPB5-HPB5	111(5)
NPB-CPB1-CPB2	122.4(6)	CPA1-NA-HA	116(7)
CPB1-CPB2-CPB3	118.8(7)	CPB1-NA-HA	112(6)

Table A.IV.a. Equations of least squares planes^{a,b}

Plane A.		Plane B.	
Fitting O,N1,N2,N3,C1,C2,C3,C4,C5		Fitting Cu,NPA,NPB	
0.38108X + 0.68934Y - 0.61610Z = 1.82530		0.01964X + 0.44587Y + 0.89487Z = 4.70888	
Atom	Distance	Atom	Distance
O	0.0279	Cu	0.0000
N1	0.0249	NPA	0.0000
N2	-0.0171	NPB	0.0000
N3	-0.0242	NA	-1.3666
C1	-0.0116		
C2	0.0091		
C3	-0.0046		
C4	-0.0015		
C5	-0.0026		
Cu	-0.5976		

^aPlanes are defined as $c_1X + c_2Y + c_3Z = d$, where X, Y, and Z are cartesian coordinates which are related to the triclinic cell coordinates (x,y,z) by the transformations

$$X = xa \sin\gamma + zc (\cos\beta - \cos\alpha \cos\gamma) / \sin\gamma$$

$$Y = xa \cos\gamma + yb + zc \cos\alpha$$

$$Z = zc(1.0 - \cos^2\alpha - \cos^2\beta - \cos^2\gamma + 2\cos\alpha\cos\beta\cos\gamma)^{1/2} / \sin\gamma$$

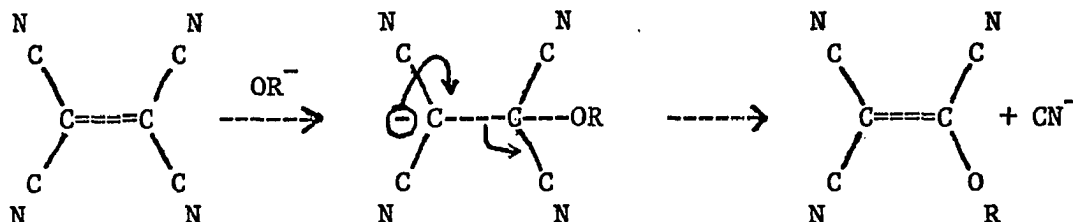
^bDistances given in Angstroms.

Table A.IV.a. Continued

Plane C. Fitting NPA,CPA1,CPA2,CPA3,CPA4, CPA5 $0.63947X + 0.44538Y + 0.62665Z = 5.50474$		Plane D. Fitting NPB,CPB1,CPB2,CPB3,CPB4, CPB5 $0.41809X - 0.1752Y + 0.89206Z = 3.86811$	
Atom	Distance	Atom	Distance
NPA	-0.0216	NPB	-0.0438
CPA1	0.0153	CPB1	0.0459
CPA2	0.0035	CPB2	-0.0061
CPA3	-0.0155	CPB3	-0.0335
CPA4	0.0089	CPB4	0.0348
CPA5	0.0094	CPB5	0.0026
Cu	-0.2830	Cu	-0.4496
NA	0.1195	NA	0.2082
HPA2	0.0712	HPB2	-0.0653
HPA3	0.0897	HPB3	-0.1013
HPA4	0.0375	HPB4	0.0301
HPA5	-0.0257	HPB5	-0.0004

Table A.IV.b. Inter-plane angles (degrees)

Plane	Plane	Angle
A	B	76.32
B	C	39.47
B	D	43.11
C	D	41.41



where $R = H$.

Two of these enol compounds subsequently lose one hydrogen each and react with the copper complex, which itself loses both Cl^- ions, thus producing the title compound.

As can be seen in Tables A.II.a and A.III, distances and angles in this compound are in keeping with those found in similar molecules. In particular, it might be noted that the copper-(pyridyl ring) nitrogen distances (2.016(6) and 1.989(6) Å), are comparable to similar distances found in other copper bispyridylamine compounds of 1.94–2.09 Å;^{96,97} likewise the copper oxygen distance of 2.520(4) Å is quite similar to the distance of 2.46 Å given as typical for axial oxygens in D_{4h} copper compounds.¹⁰²

The copper atom has approximate D_{4h} symmetry, although the bispyridylamine group's bite of 86.28° is slightly smaller than 90° due to steric reasons. Indeed, similar steric reasons account for a puckering of the bispyridylamine group of 41.41° (cf. Table IVb), an effect that can be seen in Figure A.I. As noted by Johnson and Jacobson,⁹⁶ the bispyridylamine ligand is more flexible than the bispyridyl ligand, allowing it to assume a great variety of geometric

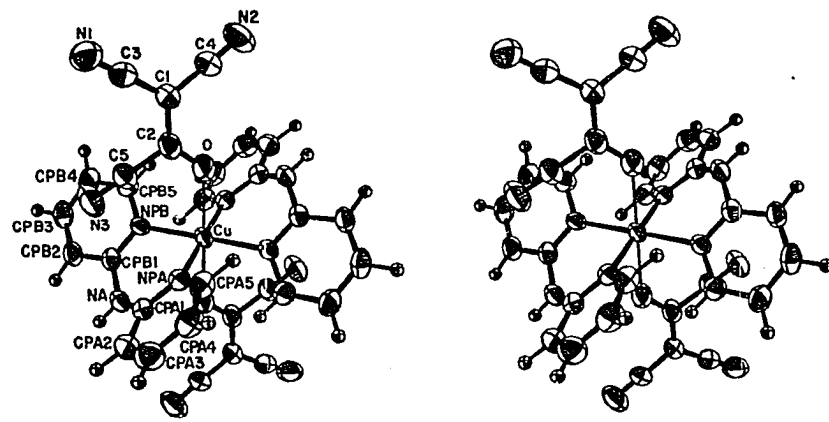


Figure A.I. OR TEP picture of copper complex

and bonding configurations. For example, in the copper complexes $\text{CuL}_2(\text{ClO}_4)_2$ ⁹⁷ and $(\text{CuL}_2\text{I})_2\text{I}(\text{ClO}_4)$,⁹⁸ (L = bispyridylamine), the interplanar angles between the pyridyl groups are 9.6° , and 33 and 37° (for two groups), respectively; in the palladium complex (PdL_2) reported by Freeman and Snow the interplanar angle is 38.2° ,¹⁰³ in the related nickel complex $\text{NiL}'\text{Br}_2$, (L' = dimethyl-di(2-pyridylmethylamine), reported by Rodgers and Jacobson, the group is tridentate and planar, and the pyridyl nitrogens are axially bound to a trigonal bipyramidal nickel. The small value of 9.6° for $\text{CuL}_2(\text{ClO}_4)_2$ is consistent with the fact that the N-Cu-N angle has opened from 90° to 95.6° in this case and that the copper atom has a more tetrahedral than square planar environment; the angles of 30° or more being for approximate square planar metal atom geometries.

Figure A.II demonstrates why the bispyridylamine ligand is found to have a puckered geometry in those complexes. In that figure, representative Cu-N and N-C distances of 2.00 and 1.34 Å, respectively, were assumed, and for ease of calculation, an N-Cu-N angle of 90° and Cu-N-C and N-C-N angles of 120° were used. Assuming that the bispyridylamine ligand lies in a plane forces the angle about the amine nitrogen to open to 150° , while giving carbon to amine nitrogen distances of only 1.11 Å. Both of these values are chemically unrealistic, but if the amine nitrogen is allowed to move out of the plane, more normal values can result.

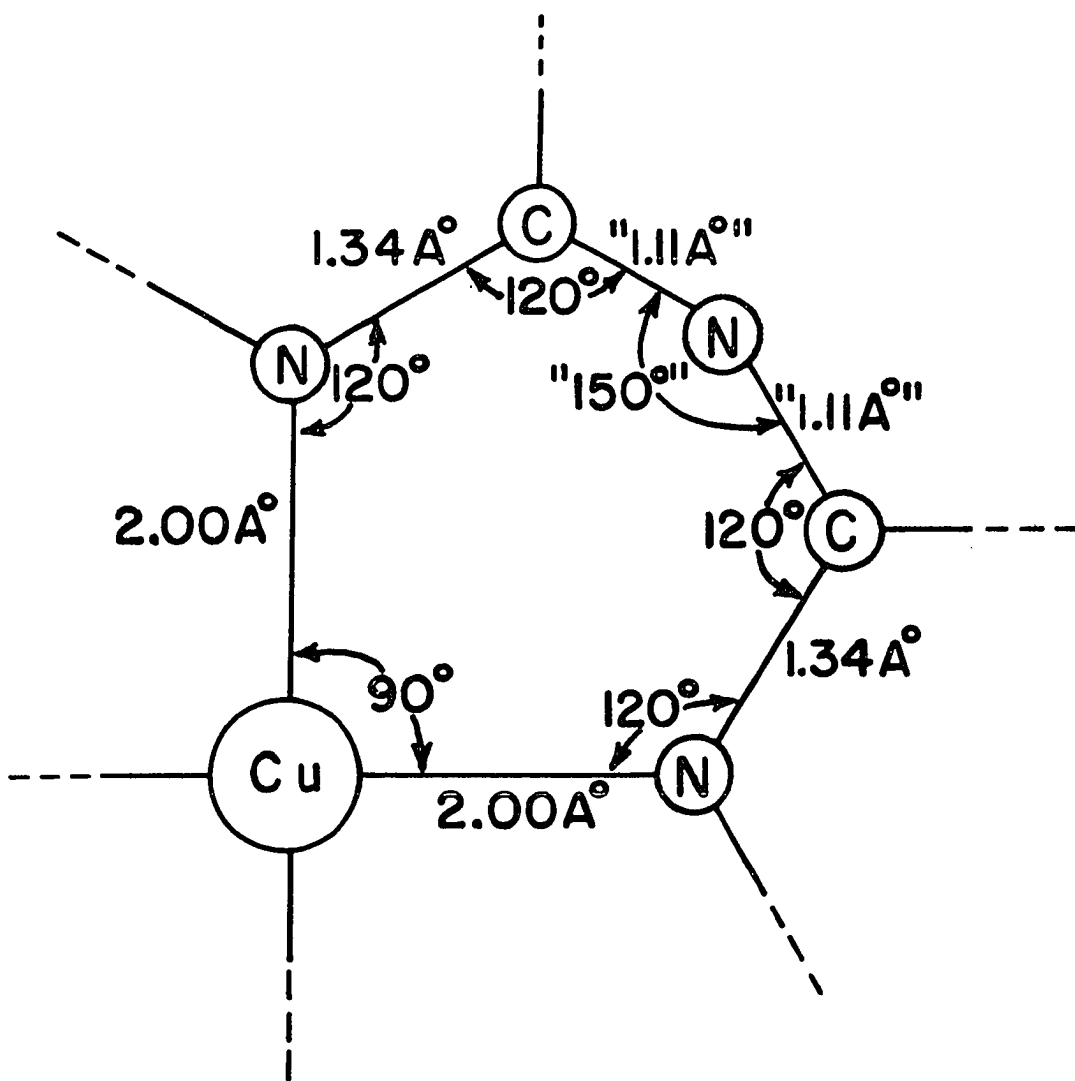


Figure A.II. Idealized ligand geometry

The angle Cu-O-C2 is $130.8(5)^\circ$, indicating considerable sp^2 character for the oxygen. This is in keeping with the extensive pi character of the tetra- (or, in this case, tri-) cyanoethylene molecule. One might also expect a certain amount of d-pi bonding between the oxygen and copper atoms. However, the torsional angle C2-O-Cu-NPB is 28.18° , rather than the 0° angle to be expected. Such a twist might still be indicative of appreciable d-pi bonding if considerable steric or hydrogen bonding effects are operative. Table A.II.b lists all such intermolecular interatomic distances less than 3.00 \AA , and Figure A.III, in which all atoms within 7.5 \AA of the copper atom are shown, shows the packing of the crystalline structure. Neither Table A.II.b nor Figure A.III make very convincing arguments in favor of hydrogen bonding sufficient enough to force a d-pi bond to twist by almost 30° .

In Figure A.IV, the interatomic distances from the ethylene moiety atoms to atoms in bispyridylamine moieties adjacent to this group are shown as a function of the departure of the torsional angle about the Cu-O bond from the measured value of 28.18° . To make this illustration, the ethylene moiety was rotated about an axis defined by the Cu-O bond, and the interatomic distances were followed for those dozen intermolecular atomic pairs separated by less than 3.0 \AA in the actual crystalline structure. It might be noted at the outset that although this illustration shows calculated values over a range of $\pm 20^\circ$, in fact it is unlikely that a rotation of anything like 20°

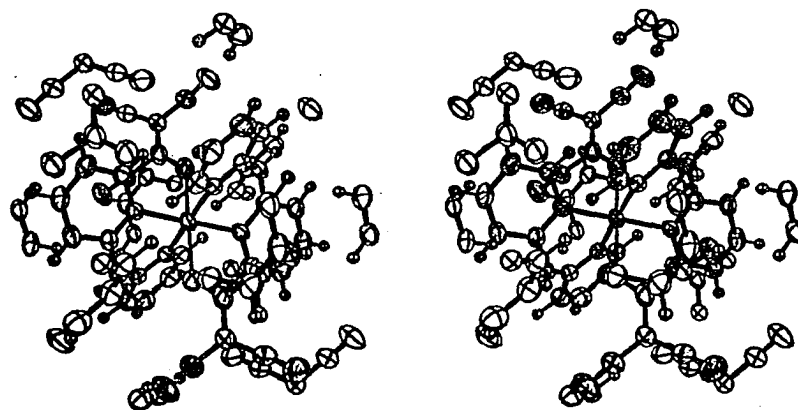
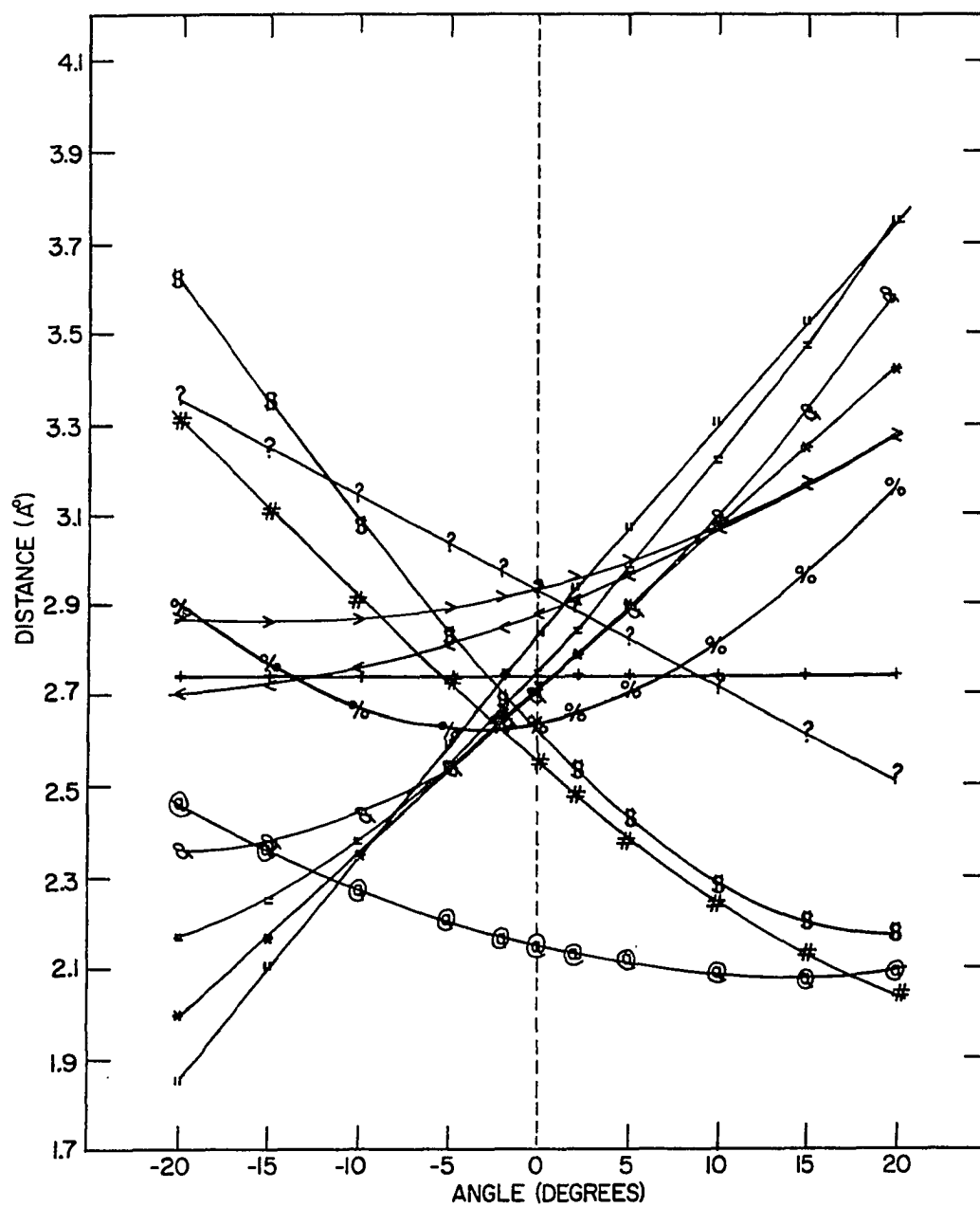


Figure A.III. OR TEP picture of copper complex showing all atoms within 7.5 Å of central copper atom

Figure A.IV. Plot of selected intermolecular interatomic distances as a function of the departure of the torsional angle $C_2-O-Cu-NPB$ from the observed value of 28.18° .
Legend: @ N2-HA(2); # N1-HPB5(1); \$ N3-HPB2(1);
% N3-HPB3(1); & N1-HPA2(1); * C3-HPB4(2); + O-HPA4(1);
= N3-HPB3(2); " N1-HPB4(2); < N2-HPB2(2); > N2-HPA3(2);
? N2-HPA2(2). Explanation of symmetry operations given in Table IIb.



could occur without gross morphological changes occurring in the overall crystalline structure. Indeed, in the case of a simpler molecule reported by Bernstein and Hagler, rotations of greater than 7.5° seem impossible without changing the crystalline structure.¹⁰⁴

Examination of the figure shows that rotation from the observed case in either direction decreases some distances representative of repulsive interactions while, of course, increasing other distances. This appears to account for the observed geometry, since increasing the torsional angle would rapidly decrease two distances (N1-HPB5(1) and N3-HPB2(1)); decreasing the torsional angle would rapidly decrease four others (N1-HPA2(1), N3-HPB3(2), C3-HPB4(2), and N1-HPB4(2)). The actual torsional angle of 28.18° can be seen as one which avoids the van der Waals crowding which would otherwise occur with rotation. It should be noted that the only intermolecular interatomic distance less than 3.0 \AA that should properly be called a "hydrogen bond" (N2-HA(2)), is relatively insensitive to the torsional angle.

Thus, the observed C2-O-Cu-NPB torsional angle of 28.18° can be viewed as mostly resulting from steric sources, and less as resulting from hydrogen bonding. Hydrogen bonding itself hardly seems strong enough to account for such a large twist of a d-pi bonded system; even the steric crowding arguments just presented seem insufficient to do that. One must therefore conclude that the Cu-O bond is largely sigma in character.

There's a feeling I get when I look
to the west,
And my spirit is crying for
leaving.

In my thoughts I have seen rings of
smoke through the trees,
And the voices of those who stand
looking.

And it's whispered that soon if we
all call the tune,
Then the piper will lead us to
reason.

And a new day will dawn for those
who stand long,
And the forests will echo with
laughter.

And it makes me wonder.

J. Page and R. Plant¹⁰⁵